Theoretical Modelling of Grass Drying in Deep Beds

Winoi Dorai

Delft University of Technology
Report Number-2668

Theoretical Modelling of Grass Drying in Deep Beds

By

Winoi Dorai

Student Number: 4184785

in partial fulfilment of the requirements for the degree of

Master of Science

in Sustainable Energy Technology

at the Process and Energy Technology Department,

Faculty of Mechanical, Maritime and Materials Engineering,

Delft University of Technology

February 2015

Supervisor:	Dr. Ir. W. de Jong
Thesis committee:	Prof. Dr.ir. B. J. Boersma,
	Dr. ir. G. Korevaar,
	Ir. Y. Joshi, PhD Candidate, 3mE

TU Delft Delft University of Technology

ABSTRACT

Verge grass is being considered to replace expensive wood pellets (thus reducing imports) as potential bio-energy resources for use in co-firing. However, drying of these verge grass resources is very important because of its high moisture content (almost 60 % wt.) and also results in an increased heating value for the fuel. Drying is the first process which occurs before torrefaction of biomass (which serves as an important pre-treatment step before co-firing with coal).

Though fixed bed drying models have been studied in the past, development of drying models for drying verge grass have so far not been investigated. The drying of verge grass in fixed bed using a system of coupled differential equations in the gas phase and algebraic equations in the solid phase have been used to setup mass and energy balances has been investigated. The system of differential and algebraic equations has been solved by the Runge-Kutta method using ordinary differential equation solvers available in MATLAB® and by using finite difference techniques.

The behaviour of the process variables (air humidity, air temperature, solid moisture content and solid temperature) with time and height has been investigated. Further a sensitivity analysis has been performed to study the effect of the influence of varying process parameters such as inlet air flow rate and temperature on the drying process. To validate the model, data from experiments performed with grass on a lab-scale drying and torrefaction setup were used at the Energy Technology research group have been used.

With increase in the inlet air flow rate and the air temperature the drying time period was reduced due to an increase in the drying rate. Under certain conditions the model was insensitive with regard to increase in the number of grid points used in modelling in space and time. The simulation results however weren't in agreement with experimental results and need to be further to investigate the validity of the assumptions or correlations used in the process of modelling.

Contents

Nomenclature iv

List of Figures viii

1. Introduction 1

1.1. Motivation 1

1.1.1. Classification and Conversion Routes 1

1.2. Mathematical Modelling 6

1.3. State of the Art 6

1.4. Research Objective 7

1.5. Methodology and Approach 7

1.6. Outline 7

2. Theoretical Background 8

2.1. Biomass 8

2.1.1. Moisture Content and Drying of Biomass Fuels 8

2.2. Drying Fundamentals 10

2.2.1. Mechanism of Drying and Drying Periods 11

2.3. Fixed (Deep) Bed Drying 13

2.3.1. Deep Bed (Grain) Drying Model Theories 13

2.3.2. Constitutive Equations 17

2.3.3. Correlations for heat and mass transfer coefficients 18

2.3.4. Deep Bed Drying Mathematical Model 21

3. Discretization and Simulation Strategy 27

3.1. Discretization and Finite Difference Scheme 27

3.1.1. Mass balance for water in the solid phase 27

3.1.2. Energy balance in the solid phase 28

3.2. Numerical Scheme 29

3.3. Algorithm Flow Description 30

4. Experimental Setup 32

5. Results and Discussion 34

5.1. Model Constants and Bed Properties 34

5.2. Parameter Analysis 35

5.2.1. Inlet Gas Temperature 36

5.2.2. Varying flow rates 39

5.2.3. Comparison of simulated and experimental results 42

5.2.4. Varying Inlet Gas Temperature 44

5.2.5. Sensitivity to grid points in space and time 45
6. Conclusion & Recommendations 47
6.1. Conclusions 47
6.2. Recommendations 47
References 49
APPENDIX 53
APPENDIX 1: (ODE45 Solver) 53
APPENDIX 2: (ODE23 Solver) 53
APPENDIX 3: Calculation Checks and Temperature Dependent Correlations 54
APPENDIX 4: Additional Plots generated 57

Nomenclature

A_{eff}	*Effective surface area of grass*[1]	$\frac{m^2}{kg_{drygrass}}$
a_V	*Characteristic Interfacial area per unit volume of dryer*	$\left(\frac{kg_{drygrass}}{m^3_{bed}}\right)$
c	*Specific heat capacity*	$\left(\frac{kJ}{kg-K}\right)$
D_{12}	*Water diffusivity in air*	$\left(\frac{m^2}{s}\right)$
d_p	*Particle diameter*	(m)
h_{av}	*Enthalpy of Steam emanating from the solid*	$\frac{kJ}{kg}$
h_H	*Heat transfer coefficient*	$\left(\frac{kW}{m^2_{bed}-K}\right)$
h_M	*Mass transfer coefficient*	$\left(\frac{kg}{m^2_{bed}-s}\right)$
Δh_v	*Latent Heat of vaporisation*	$\left(\frac{kJ}{kg}\right)$
i	*Location co-ordinate (finite difference grid)*	
j	*Time co-ordinate (finite difference grid)*	
j_H	*Heat transfer factor*	
j_M	*Mass transfer factor*	

k_B	*Thermal conductivity of air*	$\left(\frac{kW}{m-K}\right)$
k_Y	*Effective Mass Transfer Coefficient* $\left(k_Y = h_M . A_{eff}\right)$[1][2.23]	$\left(\frac{kg_{water}}{kg_{drygrass}-s}\right)$
M	*Molar Mass*	$\left(\frac{kg}{kmol}\right)$
n_h	*Number of grid points in space*	
n_t	*Number of grid points in time*	
p_o	*Pressure*	(Pa)
p^S	*Vapour Pressure at saturation*	(Pa)
Pr	*Prandtl number*	
q	*Heat flux* [2.26]	$\left(\frac{W}{kg}\right)$
R	*Universal gas constant*	$\left(\frac{kJ}{kmol-K}\right)$
R_c	*Constant rate of drying*	
Re	*Reynolds number*	
S	*Cross sectional area normal to flow direction*	(m^2)
Sc	*Schmidt number*	
St	*Stanton number*	
Δt	*Time step (finite difference method)*	*(s)*
T	*Absolute Temperature*	(K)

t_w	*Wet-bulb temperature*	(℃)
u_B	*Superficial air velocity*	$\left(\frac{m}{s}\right)$
W	*Mass flow rate*	$\left(\frac{kg}{S}\right)$
w_D	*Drying rate*	$\left(\frac{kg_{water}}{kg_{drygrass} - s}\right)$
X	*Moisture content (dry basis)*	$\left(\frac{kg_{water}}{kg_{drygrass}}\right)$
Y	*Absolute Humidity (dry basis)*	$\left(\frac{kg_{water}}{kg_{dryair}}\right)$
Y^S	*Saturation Humidity*	$\left(\frac{kg_{water}}{kg_{dryair}}\right)$
z	*Height of the dryer bed*	(m)
Greek Symbols		
α	*Effective Heat transfer Coefficient* $h_H . A_{eff}$ [2.26]	$\left(\frac{kW}{m^2 - K} . \frac{m^2}{kg_{drygrass}}\right)$
ε	*Porosity*	
μ_B	*Dynamic viscosity of air*	$\left(\frac{kg}{m - s}\right)$
ρ_S	*Density*	$\left(\frac{kg_{drygrass}}{m^3_{bed}}\right)$

τ	*Time*	(s)
ϕ	*Correction coefficient used in drying rate calculation*	
φ	*Relative Humidity*	
Subscripts		
S	*Dry solid*	
A	*Moisture in vapour phase*	
Al	*Moisture in liquid phase*	
B	*Dry gas*	
*	*In equilibrium*	
G	*Humid gas*	

List of Figures

Figure 1: Commercial and Developing routes for Biomass Conversion[9] 2
Figure 2: Relationship between higher heating value and moisture content[16] 4
Figure 3: Drying Curve for identifying four different types of water in sludges[34] 8
Figure 4: Thermal Drying[36,37] 10
Figure 5: Typical Drying Rate Curve of solid[18] 12
Figure 6: Deep Bed-Drying Schematic[26] 21
Figure 7: Sample Representation of Grid points in the Finite Difference Grid[45] 29
Figure 8: Lab-Scale Drying and Torrefaction Setup 33
Figure 9: Humidity Profile versus time 37
Figure 10: Air Temperature versus time 38
Figure 11: Grass Moisture Content versus time 38
Figure 12: Grass Temperature versus time 39
Figure 13: Humidity versus bed time 40
Figure 14: Gas Temperature versus time 40
Figure 15: Grass Moisture Content versus time 41
Figure 16: Grass Temperature versus time 41
Figure 17: Predicted and Experimental Temperature measured at the bottom of the column with time 43
Figure 18: Predicted and Experimental Temperature measured at the middle of the column with time 43
Figure 19: Predicted and Experimental Temperature measured at the top of the column with time 44
Figure 20: Grass Moisture Content versus time 45
Figure 21: Grass Moisture Content versus time (Ns=500, Nt = 2700) 46
Figure 22: Grass Moisture Content versus time (Ns = 1000, Nt = 3600) 46
Figure 23: Gas Temperature Profiles versus height and time 57
Figure 24: Solid Temperature profiles versus height and time 58
Figure 25: Moisture Content profiles versus height and time 59
Figure 26: Gas Humidity profiles versus height and time 60
Figure 27: Gas Temperature Profiles versus height and time 61
Figure 28: Solid Temperature Profiles versus height and time 62
Figure 29: Moisture Content Profiles versus height and time 63
Figure 30: Gas Humidity Profiles versus height and time 64
Figure 31: Gas Temperature Profiles versus height and time 65
Figure 32: Solid Temperature Profiles versus height and time 66
Figure 33: Moisture Content profiles versus height and time 67
Figure 34: Gas Humidity Profiles versus height and time 68
Figure 35: Gas Temperature Profiles versus height and time 69
Figure 36: Solid Temperature Profiles versus height and time 70
Figure 37: Moisture Content Profiles versus height and time 71
Figure 38: Gas Humidity Profiles versus height and time 72
Figure 39: Gas Temperature Profiles versus height and time 73
Figure 40: Solid Temperature Profiles versus height and time 74
Figure 41: Moisture Content Profiles versus height and time 75

Figure 42: Gas Humidity Profiles versus height and time 76

1. Introduction

1.1. Motivation

Energy, its generation and utilisation has occupied the heart of development of economic powers around the world. The dwindling of conventional fuel resources and the impending energy crisis has necessitated the need for non-conventional sources of energy to power the requirements of an ever increasing population. The concept of sustainable development puts forth the theory that "Meeting the needs of the present without compromising on the ability of future generations to meet their own"[2] as being one of the fundamental challenges in developing energy sources for the future.

Energy from biomass has long been touted to be one of the possible routes to develop a continuous, reliable power supply which could also contribute a significant amount to reduce dependence on imported conventional fuels.

1.1.1. Classification and Conversion Routes

Fuels derived from biomass can be classified into three generations depending on the source of the feedstock:

- The primary feed-stocks for first generation of biofuels are crops (such as sugarcane, corn and canola oil) which presently find use in food production. The usage of agricultural food crops has led to the classic food versus fuel debate (where some argue that one of the reasons for rising food prices is attributed to the increase in production of first generation of biofuels). The products produced by first generation biofuels are mainly ethanol (which is produced from corn or sugarcane) and biodiesel or FAME (fatty-acid methyl esters, which are produced from canola oil, soya-bean oil or palm oil)[3] The various conversion processes for first generation biofuels are: trans-esterification (homogenous or heterogeneous catalysis), ethanol conversion processes, fermentation and anaerobic digestion of biomass.

- Second generation biomass fuels are produced from ligno-cellulosic biomass (from the non-food, cheap and abundant materials available from plants). The products of second-generation biofuels include products such as ligno-cellulosic ethanol, butanol, mixed alcohols, hydro-treating oils, bio-oil and Fischer-Tropsch hydrocarbon fuels. They have the advantage of not competing with food production, being environmentally friendly and the technologies to reduce the conversion costs are still in development. The conversion of woody biomass into fermentable sugars requires costly pre-treatment technologies with special enzymes, due to which the production of second-generation biofuels is not yet economical on a large scale[4].

- Third generation biofuels are produced from microalgae (which are unicellular photosynthetic micro-organisms, living in saline or fresh water environments and convert sunlight, water and carbon dioxide to algal biomass) and also from macro-

algae or seaweeds[5]. The conversion routes to end fuels involve trans-esterification, catalytic conversion of biomass to produce gasoline and in some cases digestion through enzymes.

Biomass as a source of carbon-based fuels and chemicals broadly encompasses[6,7]:

- Agricultural food and feed crops,
- Dedicated energy crops (miscanthus) and trees,
- Agricultural residues (primary-straw, vineyard; secondary-nut shells, press cakes) forestry products (logs, chips) and residues (primary (e.g. stumps); secondary (bark, sawdust); tertiary (demolition wood)),
- Aquatic plants and aquatic species (micro-algae & macro-algae (seaweed)),
- Derivatives (e.g. from food industry)
- Animal, industrial & municipal organic wastes.

Some of the routes for the production of liquid biofuels from biomass are: biochemical processing and thermochemical processing. Biological conversion (trans-esterification, fermentation and anaerobic digestion) utilises biological organisms and a bio-catalyst for the conversion of the feedstock into suitable fuels[8]. On the other hand, thermochemical conversion (combustion, gasification and pyrolysis) mainly relies on high temperature and chemical catalysts to convert biomass chemical energy into other energy carriers including fuels[8]. Thermochemical conversion has much higher conversion efficiencies of biomass to energy when compared with biochemical conversion (because it has the advantage of converting all organic components of the biomass in comparison to biochemical processing which focuses mostly on the polysaccharides[3]) and the process is also much faster[8].

The commercially available and developing routes for the conversion of biomass feed-stocks to desired end-products has been described in the Special report of the intergovernmental panel on climate change published in 2011[9] and is shown in Figure 1:

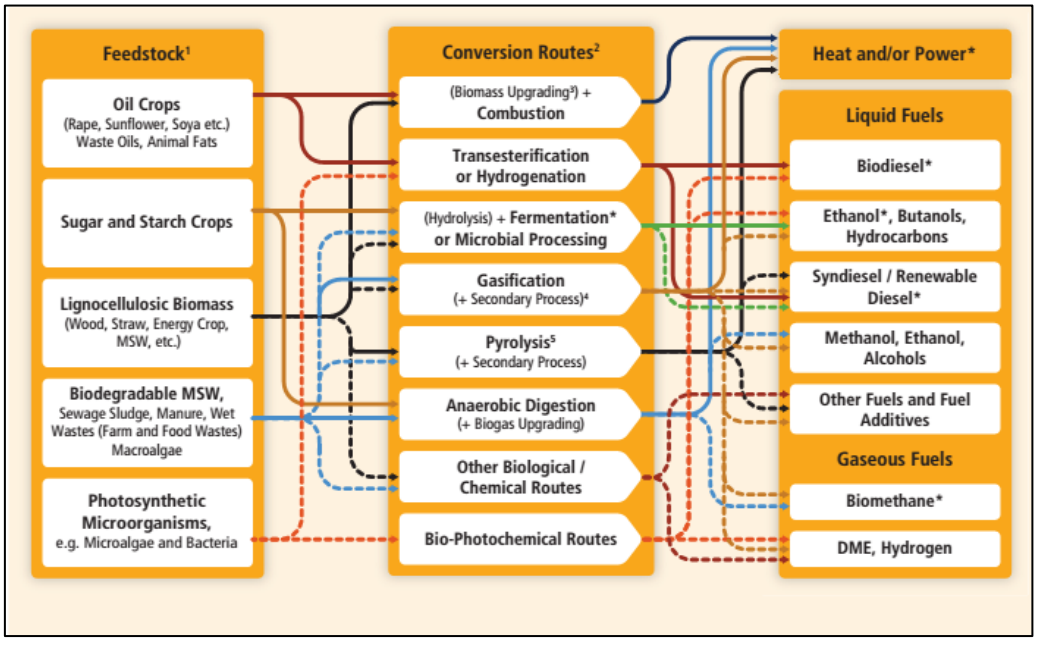

Figure 1: Commercial and Developing routes for Biomass Conversion[9]

Bio-energy is known to have all the possibilities to be an important alternative in a future with more sustainable and continuous energy supply[10]. Bio-energy supply is continuous in comparison to solar and wind energy sources because their availability depends on the availability of the sun and wind. Thus their intensity is highly variable and necessitates the provision of back-up power plant to account for the periods of low or zero generation[11]. Thus load levelling requires that the surplus generation during off-peak hours be stored to meet increased demand during the day. In grid connected systems, the supply from photovoltaic systems and wind turbines do not have large scale storage of energy that is economical at this moment in time. It is in these situations in small grid connected systems where bioenergy plays an important role. In stand-alone systems, though there is a need for storage of energy[11]. The growing interest in the field of bioenergy has been attributed to the following facts[10]:

- Contribution to the reduction of poverty in developing economies,
- Continuous supply of power without expensive conversion equipment and
- It can deliver any of the following forms of energy: solid, liquid, gaseous fuels, heat and electricity.

Bio-energy production in coal-fired plants by partial substitution of coal, as the main fuel with biomass feedstock is called co-firing and needs some changes to be made to existing infrastructure in power plants[12]. Three basic configurations[12] have been identified for co-firing of biomass with coal in power plants, namely:

- Direct co-firing where the fuel enters the boiler together with coal. Though this configuration requires minimum investments, it may face various shortcomings which arise due to the differences between the properties of mixed feedstocks (mainly herbaceous biomass feedstock which could cause problems during feeding and sizing).

- Parallel co-firing where the biomass is combusted in a separate boiler and supplying steam through a common header. The potential limiting factor in existing infrastructure could be the capacity of steam turbine. It should be made sure that there is sufficient overcapacity of the steam turbine to accommodate the extra power from biomass combustion. The investment in this case is significantly higher than in the direct option; however it has the advantage of using relatively different fuels with high alkali and chlorine contents.

- In-direct co-firing involves the gasification or combustion of biomass separately and the produced gas is injected and burned in the boiler. This technique has the advantage of allowing very high co-firing ratios and the drawback of having relatively high unit investment costs.

Biomass feedstocks vary significantly in physical, chemical and morphological characteristics. Biomass has relatively lower energy densities and higher moisture contents in its untreated form when compared to fossil fuels[8]. Wood pellets are expensive in comparison to coal on an energy basis, whereas herbaceous biomass residues or road/canal grass are interesting fuels in view of the local availability and short rotation times. These are land resources with considerable biomass potential and the removal of these resources seasonally

is part of the normal maintenance in these areas (Netherlands, Germany, Denmark and the UK) [13]. The conversion of the resources that have been removed towards potential bioenergy sources increases the economic efficiency of managing these areas. These could contributed significantly to increasing biomass potential, if sufficiently high financial incentives are in place, especially in countries (such as Netherlands, Denmark, Germany and the UK) where management of these resources is well organised[13]. Verge grass in the Netherlands is currently being investigated as a potential fuel to be co-fired along with coal in thermal power plants, but has the disadvantage of high moisture content (indicating highly energy intensive drying) [14].

Drying of bio-based fuels is therefore of high importance, because usage of a wet fuel could lead to lower combustion temperatures, lower process energy efficiencies and higher emissions of volatile compounds in comparison to a dry fuel[15]. The relationship between the moisture content of a fuel and the higher heating value[16] is shown in Figure 2 below:

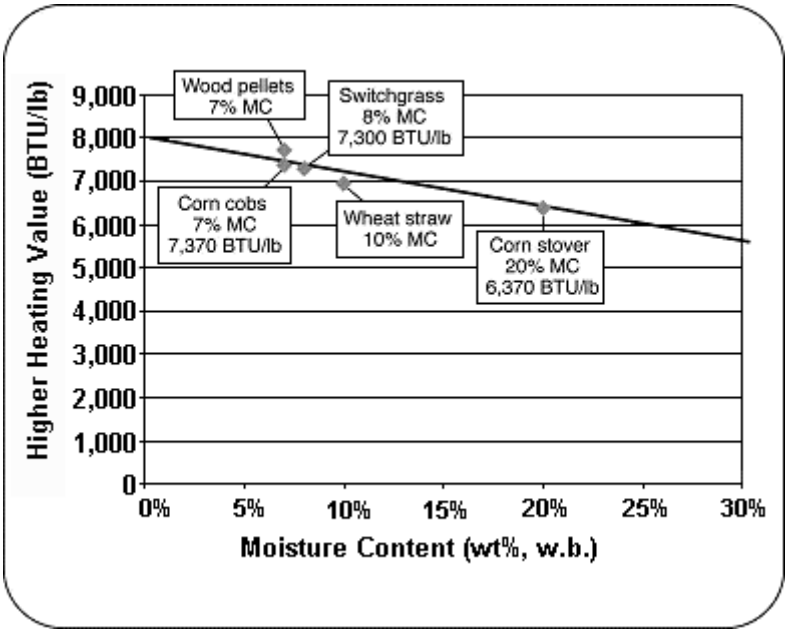

Figure 2: Relationship between higher heating value and moisture content[16]

The lower and higher heating values on an as received (a.r.) basis, d.b. (dry basis) and d.a.f. basis (dry ash free basis) for willow and verge grass obtained from the Phyllis database[14,17] are shown below.

Table 1-1: Willow and Grass Properties from the Phyllis Database[14,17]

	a.r. basis	d.b.	d.a.f
Willow[17]			
Moisture Content	43.50 % weight		
Lower Heating Value (MJ/kg)	8.68	17.25	17.53
Higher Heating Value (MJ/kg)	10.68	18.56	18.86
HHV_{Milne} *(MJ/kg)*	11.20	19.82	20.14
Verge Grass[14]			
Moisture Content	60 % weight		
Lower Heating Value (MJ/kg)	5.42	17.22	18.80
Higher Heating Value (MJ/kg)	7.40	18.50	20.20
HHV_{Milne} *(MJ/kg)*	7.19	17.98	19.62

Drying serves as an important thermal pre-treatment step before torrefaction, pyrolysis, combustion and gasification of biomass could be performed[8]. Drying is commonly used to describe a process of thermally removing moisture (by evaporation from a material) to yield a solid product[18] with improved heating value. Drying is a complex unit operation which involves transient heat and mass transfer along with several rate processes (such as physical (shrinkage, puffing, crystallization and glass transformations) or chemical(in some cases desirable or undesirable changes occur which result in change in colour, texture, odour or other properties of the solid product) transformations) which, in turn, may cause changes in product quality as well as with the mechanisms of heat and mass transfer[18].

Drying is the first process to occur before torrefaction[19] and a study carried out by Joshi et.al. to model a torrefaction process cycle concluded that the most energy intensive operation is the drying process[20].

Drying in fixed beds has been investigated in this study, the reason fixed beds were chosen is because models have been developed for the drying of foodstuffs in fixed beds and an attempt is made in this work to extend these models to non-food materials such as grass.

Therefore, the main focus of this work is to investigate the process of thermal drying of verge grass in fixed beds.

1.2. Mathematical Modelling

Mathematical models can serve the purpose of being powerful tools to help engineers to understand, design and analyse drying processes[21]. The advantage with the use of computer simulations is that they are adept at performing simulations that are capable of replacing experiments that are difficult, expensive and also time consuming[21,22]. It is also important to take into consideration the fact that the results from computer simulation are sometimes true only for the simulated model and might not hold true for empirical studies performed[22]. Therefore, it is highly important that a simulation tool be validated by comparison with experimental results before it can be used[23]. Mathematical modelling and computer simulation often indicate the need for conducting further experiments/research to calculate parameters which might have been neglected before[22]. Computer simulations also provide a reasonable view into the physics of the drying process and can be used to predict drying parameters which would aid in the design of high efficiency dryers or improving existing drying systems[24].

Since the effectiveness of the developed tool also depends on the computer program used to perform the simulations, this study makes use of the widely available MATLAB®[25] program. MATLAB® is chosen as the software tool for the process of modelling as the plethora of numerical (differential/partial differential) solvers that it offers significantly reduces the computational time required with systems of differential and/or algebraic equations[26].

The sections (subsequent chapters) that follow in the rest of this work describe: a literature review on drying which is followed by a review of the numerical modelling and evaluation of a simulation model for the prediction of drying parameters for the case of fixed bed drying.

1.3. State of the Art

Significant work exists in literature for the case of deep bed drying of malt[27], hazelnuts[23,28], paddy[24], grains[29] and ryegrass[30].

The foundation for the development of the models proposed for malt[27] and hazelnuts[23,28] is from the model proposed by Nellist[30]. The approach in their work uses partial differential equations for the mass balance, energy balance, heat transfer rate and a thin layer equation for the drying rate. In their work, the deep bed is considered to be made of a series of thin layers, with the outlet conditions of the drying medium for one layer being used as the inlet condition for the subsequent layer[23].

Other approaches proposed in literature by Srivatsava[29] and Herman et.al[31] present a model with coupled differential and partial differential equations . The differential balance equations proposed in the model[31] (Herman et.al) for the gas phase have been solved using the Runge-Kutta approach (in the direction of flow of the drying medium). The solid phase balance equations have been expressed in terms of the variation along the height in the gas phase for a fixed time step. The algebraic equations thus proposed for the solid phase have been solved using a finite difference approach (for the stationary solid phase). The mathematical model suggested by Srivastava[29] however does not present validation with experimental data. The

mathematical model suggested by Herman et. al[31] uses heat and mass transfer properties for both the air and product and provides validation with experimental data using carrots.

The work carried out in this study uses the approach suggested by Mujumdar[26], described in the next chapter and attempts to extend the same for the case of verge grass drying in deep beds.

1.4. Research Objective

The primary objective of this work is to develop a model of the drying process in a static bed dryer for verge grass and validate (test) it with available experiments.

The research questions that this work aims to address are:

- What are influences of varying process parameters (inlet gas flow rate and temperature) on the developed model?
- Do the results from the model show agreement with experimentally obtained profiles for the temperature distribution within the column?

1.5. Methodology and Approach

The mass and energy balances for the grass and the drying medium have been setup in such a manner that the coupled differential equations (gas phase) and algebraic equations (solid phase) could be solved by the use of Runge-Kutta and finite difference methods[29,31]. In the chapters that follow, a complete description of the approach followed in the design and development of a simulation model and a description of the structure of the algorithm developed have been shown.

1.6. Outline

The work presented in this report is *divided* into five chapters. ***Chapter 2*** presents a brief background on biomass feedstock, drying process fundamentals; the theoretical background behind the modelling of a fixed bed dryer. The chapter also describes the assumptions used in the development of the model. ***Chapter* 3** presents the discretization methodology and the simulation strategy used in MATLAB®. ***Chapter 4*** provides a brief description of the experimental setup housed in the Process and Energy Department. . ***Chapter 5*** analyses the results from the computer simulations and attempts to evaluate the simulated model against experimental results from a lab-scale dryer. The chapter also presents a parameter analysis to analyse the influence of varying input process parameters on drying. ***Chapter 6*** addresses the various conclusions from the work and provides some suggestions to improve the model before it is put into practice.

2. Theoretical Background

This chapter describes the fundamentals of the drying process and models available in literature to characterise the drying in fixed (which are deeper than 20 cm as is the case in this work (36 cm)) beds. Lastly, the chapter provides the fundamentals behind the developed model equations available from the work of Mujumdar[26], which is considered as the starting point for model development in this research.

2.1. Biomass

2.1.1. Moisture Content and Drying of Biomass Fuels

Biomass feed-stocks which have high moisture contents require more energy for drying, give much higher char yields during pyrolysis resulting in bio-oil with high moisture and have higher costs associated with their thermochemical conversion[32].

Drying and compression of biomass fuels to pellets or briquettes would lead to the fuel having a controlled moisture content, higher energy density and also be easier to transport[15].

The moisture contained in solid fuels[19,33] can be classified as shown in Figure 3[34] and in literature:

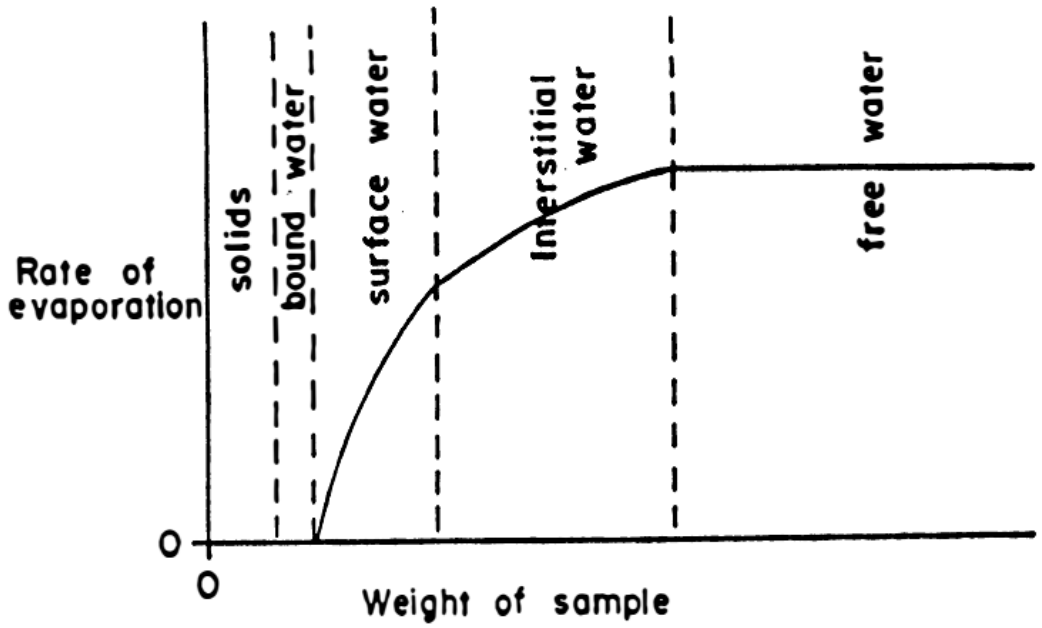

Figure 3: Drying Curve for identifying four different types of water in sludges[34]

- ***Free Moisture (or capillary moisture)***

This mainly represents the largest part of moisture in biomass that can be removed from the biomass by means of simple thickening or by the use of weak mechanical strains[33].

- ***Bound Moisture (or hygroscopic moisture)***

This mainly represents the moisture content that is held in combination, present as a liquid solution within the material or even trapped in the microstructure of the solid and exerts a vapour pressure that is less than that of pure water[18]. This moisture content can be removed by the application of auxiliary (thermal) treatments[33]. The bound moisture can be further sub-classified into[33]:

a) Chemically bound moisture

This represents the moisture that is bound to the solid by chemical bindings and can be removed by the application of thermal drying at 105℃.

b) Physically bound moisture

This represents the moisture that is fixed to the solid particles by adsorption and absorption. This fraction can also be eliminated by the use of thermal drying

c) Mechanically bound moisture

This represents the part that is mainly contained in the biomass capillaries and can be removed by the application of mechanical strain[33]. The biomass moisture content can be reduced to $50\%_{w.b.}$ with the application of mechanical de-watering (to the maximum extent) [35], thus the remaining moisture needs to be removed by the application of thermal drying to reach the required moisture content.

The energy consumption in mechanical de-watering of biomass is much lesser than what is involved in thermal drying. Thus it would be beneficial to dry the biomass to the maximum extent possible before the application of thermal drying[35]. Mechanical de-watering can be achieved by using the following equipment's: screw press, belt filter press, drum press and roller press[36].

Thermal drying involves the usage of the following modes of heating: flashing, conduction, convection, microwave or radiation to remove the moisture content that is remaining after mechanical dewatering. The types of dryers available vary with the flows, sizes and configurations required for the purpose of drying and have been described extensively in literature[26]. The considerations that need to be made in thermal drying of biomass are shown in Figure 4 below:

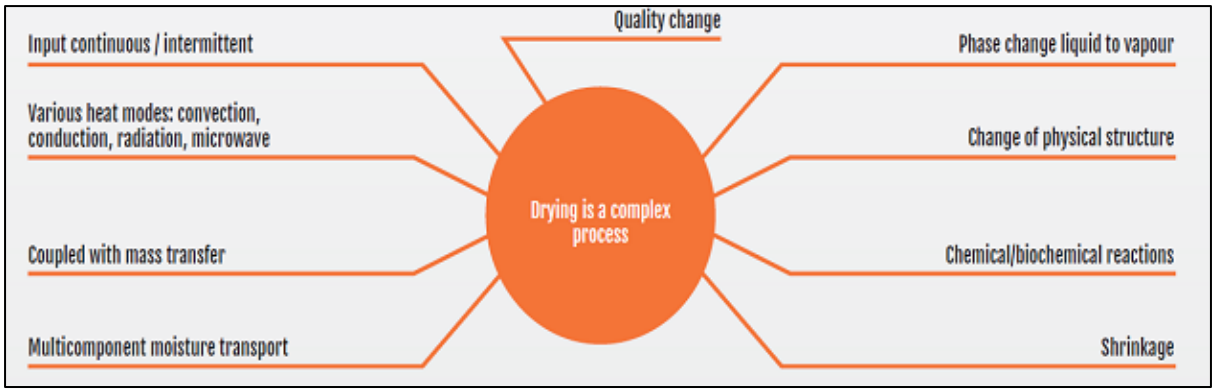

Figure 4: Thermal Drying[36,37]

The research carried out in this work deals with the thermal drying pre-treatment[8] of second generation biomass fuels and the sections that follow in this chapter deal with an introduction to drying fundamentals, deep bed dryer modelling theories and mathematical modelling.

2.2. Drying Fundamentals

The separation operation of drying converts a solid, semi-solid or liquid feedstock into a solid product by evaporation of the liquid into a vapour phase through the application of heat[18]. The latent heat of vaporisation of water is about 2260 kJ/kg (at 25℃), which underlines the fact that the drying process is energy intensive. The latent heat to vaporise the moisture is provided by the medium used for drying[38] (e.g. drying air). The primary objective of a dryer is to provide the product with enough heat to sufficiently raise the vapour pressure to enhance the evaporation of moisture contained within it[39].

The processes that occur simultaneously when a solid is subjected to thermal drying are:

- The transfer of energy (mainly in the form of heat) from the surrounding environment to evaporate the surface moisture (i.e. removal of water as vapour from the material surface and this depends on the external conditions such as inlet air temperature, air humidity and flow velocities, area of material surface exposed to air flow and the pressure)
- And, the transport of internal moisture to the surface of the material being dried and its subsequent evaporation due to the first process[18] (deals with the movement of moisture internally within the solid and is a function of the physical nature, temperature and moisture content of the solid).

The transport of energy as heat from the surrounding environment to the wet solid can occur as a result of conduction (from a hot, solid surface in contact with the material), convection (from a hot gas in contact with the material being dried) or radiation (from a hot gas or surface in contact with the material) and in some cases as a result of the combination of all the three[18,40].

The physical mechanisms which occur during the transfer of moisture can be identified[18,41] as:

- Capillary flow (liquid movement due to surface tension)
- Diffusion (concentration differences)
- Surface diffusion (diffusion of moisture through the surface)
- Vapour diffusion (vapour diffusion due to moisture concentration differences)
- Thermal diffusion (due to temperature differences) and
- Hydrodynamic flow (pressure differences which result in vapour and moisture movement)

A thorough understanding and design of a drying process would involve the measurement and/or calculation of[40]:

- Heat and mass balances in either phase,
- Thermodynamics,
- Mass and heat transport rates and
- Product quality considerations.

A fundamental knowledge of heat, mass and momentum transfer along with a knowledge of the material properties is essential when the design and analysis of a dryer has to be performed[18].

The process of removal of unbound moisture in solids can be carried out by the following two methods[18]:

- Evaporation which occurs when the vapour pressure on the solid surface is equal to the atmospheric pressure.
- Vaporisation which takes place by the mode of convection heat transfer. In this process the warm air passing through the solid material, is cooled by it and moisture transfer takes place from the solid to the air.

2.2.1. Mechanism of Drying and Drying Periods

The drying behaviour of solid materials can be characterised by the measurement of the change in moisture content as a function of time[40]. If the curve is differentiated with respect to time and multiplied by the ratio of mass of dry solid to the interfacial area between the mass of wet solid and gas, a plot of the drying flux can be made:

$$w_D = -\frac{m_S}{A}.\frac{dX}{dt} \qquad [2.1]$$

Where,

w_D is the drying rate flux,
m_S is the mass of bone dry solid,
A is the interfacial area between the solid and the drying medium,
X is the moisture content of the solid and
t is the time for drying.

A typical drying rate curve of a solid product is shown in Figure 5.

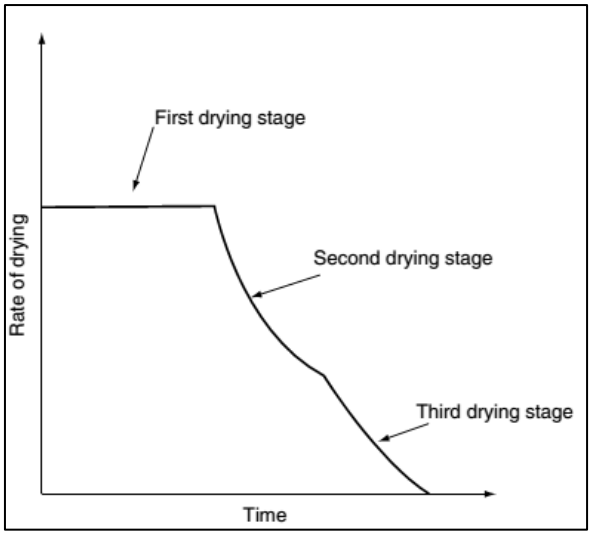

Figure 5: Typical Drying Rate Curve of solid[18]

As can be seen from the figure, in the first drying stage the rate of drying is constant. In this stage, the surface consists of free moisture and vaporisation takes place on the surface. The rate of drying is controlled by the external heat and mass transfer between the exposed surface of the wet solid and the bulk gas[40]. In the constant rate period, the rate of mass transfer is determined by the gas-phase boundary layer or film resistance on the surface of the solid[40]. Also the solid is assumed to be at a constant temperature therefore, the only resistance offered to the convection heat transfer can be considered to be from the gas phase. The drying rate flux for the constant drying period (in terms of convection heat transfer) can be given by[40]:

$$R_c = \frac{h(T_g - T_w)}{\Delta h_v} \qquad [2.2]$$

Where,

h is the convective heat transfer coefficient$\left(\frac{kW}{m^2-K}\right)$,
T_g is the gas temperature(℃),
T_w is the wet-bulb temperature (℃) and
Δh_v is the latent heat of vaporisation of water$\left(\frac{kJ}{kg}\right)$.

The drying rate calculations are performed based on heat transfer correlations when air is the drying medium and water is the moisture being taken out, this is because of the wide availability of psychometric data for this system(air-water)[40]. Towards the end of the constant drying period, the movement of water from within the solid to the surface takes place by means of capillary forces and the drying rate can still be constant. When the moisture content of the solid reaches the critical moisture content then dry spots start to appear on the surface of the solid[18].

A transition from the constant drying period to the falling-rate drying period occurs when the drying rate in the constant drying period is high and/or when the distance that the moisture

has to travel to reach the surface is large. This results in the moisture not being able to reach the surface fast enough to maintain a constant drying period[40]. The heat transfer in this falling-rate drying period is attributed to the transfer of heat to the surface and the heat of conduction within the product[18].

2.3. Fixed (Deep) Bed Drying

A deep bed dryer (also known as a fixed bed dryer which is more than 20cm deep) consists of a stationary solid phase which remains in the bed for a certain amount of time while the gas (drying medium) flows through the system continuously[26]. It is a bed in which the process of drying occurs (mainly) by means of convection and in which gradients of moisture content and temperature can exist[22]. The drying in a deep bed is faster at the inlet than at the exhaust end[23] (due to a decrease in the exhaust air humidity with time as it moves through the bed).

2.3.1. Deep Bed (Grain) Drying Model Theories

In literature several mathematical models have been developed for the case of deep-bed grain drying and they have been classified as described below[22,24,38]:

a) Logarithmic Models

These models were developed & initially proposed by Hukill in 1954 and they are based on the relationship between the rate of drying of a layer of grain in a bed and the air temperature gradient across that layer[22,38]. In terms of computational power, these models were known for their simplicity, low accuracy[22] and were used mainly because of their ease of computation[38]. These models are mainly used to model low temperature drying in stationary beds[22].

The relationship between the rate of drying in a layer of grain and the air temperature gradient has been shown in the work of Sharp[42] who presented the mass and energy balance equations for the drying of grain in a deep bed. The balance equations have been presented below:

$$G_a \frac{\delta h}{\delta x} = -\rho \frac{\delta M}{\delta \theta} - \varepsilon \rho_a . \frac{\delta h}{\delta \theta} \quad [2.3]$$

$$G_a (c_a + c_v . H) \frac{\delta t_g}{\delta x} = \rho . c_v . (t_a - t) - h . (t_a - t) - \rho_a . \varepsilon . (c_a + c_v . H) \frac{\delta t_a}{\delta \theta} \quad [2.4]$$

$$\rho . (c + c_w . M) \frac{\delta t}{\delta \theta} = h . (t_a - t) + h_v . \rho . \frac{\delta M}{\delta \theta} \quad [2.5]$$

$$\frac{\delta M}{\delta \theta} = -K(M - M_e) \quad [2.6]$$

Where,

c_a is the specific heat of dry air$\left(\frac{kJ}{kg-K}\right)$,

c_w is the specific heat of water$\left(\frac{kJ}{kg-K}\right)$,
G_a is the air mass flow rate per unit area$\left(\frac{kg}{m^2-s}\right)$,
c_v is the specific heat of water vapour$\left(\frac{kJ}{kg-K}\right)$,
h is the convection heat transfer coefficient$\left(\frac{J}{m^2-K-s}\right)$,
H is the humidity ratio of air$\left(\frac{kg_{H2O}}{kg_{dryair}}\right)$,
M is the moisture content of grain $\left(\frac{kg}{kg}\right)$ dry basis,
θ is the drying time(s),
ρ is the density of grain$\left(\frac{kg}{m^3}\right)$,
ρ_a is the density of drying air$\left(\frac{kg_{dryair}}{m^3}\right)$,
ε is the porosity,
x is the thickness of a bed of grain(m),
M_e is the moisture content at equilibrium $\left(\frac{kg}{kg}\right)$ dry basis,
K is the drying coefficient$\left(\frac{J}{s}\right)$,
t is the temperature of the grain (℃) and
t_a is the temperature of air(℃).

Combining equations [2.4] and [2.5] to cancel out common terms and eliminating $\frac{\delta t_a}{\delta \theta}$ yields:

$$G_a(c_a + c_v.H)\frac{\delta t_a}{\delta x} = -\rho(c + c_w.M)\frac{\delta t}{\delta \theta} + \rho(h_v + c_v.(t_a - t))\frac{\delta M}{\delta \theta} \quad [2.7]$$

The above equation has been further simplified under the following assumptions:

- The sensible heat to raise the temperature of the grain and of the moisture removed from the grain are negligible in comparison to the latent heat of water vapour removed,
- The increase in the sensible heat of the air due to the increase in the relative humidity of the air is negligible and
- The grain density is constant.

Applying the assumptions yields:

$$G_a.c_a.\frac{\delta t_a}{\delta x} = \rho.h_v.\frac{\delta M}{\delta \theta} \quad [2.8]$$

The generated equation [2.8] is then further simplified by the introduction of the concept of travel rate of drying zone[22]:

$$Q = \frac{(t_{eq} - t_{wb})}{(M_o - M_{eq})}.\frac{c_a.G_a}{h_v} \quad [2.9]$$

The travel rate of the drying zone may be related to the air flow rate:

$$G_a.c_a.\frac{\delta t_a}{\delta x} = -Q.h_v.\frac{\delta M}{\delta x} \quad [2.10]$$

Solving equations [2.8] and [2.10], analytically with a thin layer grain drying equation, for e.g.:

$$\frac{\delta M}{\delta \theta} = -K.(M - M_{eq}) \quad [2.11]$$

From this, the logarithmic model is obtained:

$$\frac{M - M_e}{M_o - M_e} = \frac{e^D}{e^D + e^Y - 1} \quad [2.12]$$

$$D = \frac{k.h_v.\rho.(M_o - M_e)_x}{Q.c_a.(t_{ao} - t_{wb})} \quad [2.13]$$

$$Y = K.\theta \quad [2.14]$$

b) Equilibrium models

These models are used in low temperature and low airflow conditions under which the drying can be considered to occur at near equilibrium conditions in a stationary bed[22].

The assumptions made in the developments of these models are:

- no resistance to heat and mass transfer within the bed (under this assumption the heat transfer coefficient and thermal conductivity are infinite)[22],
- equilibrium of air and grain temperatures and the solid moisture content being in equilibrium always[38].

Also assumed in the development of mass and heat balances in these models are that the solid temperature being equal to the drying air temperature[22]. The assumptions made to these model mean that they are applicable only for very slow drying processes[22]. Depending on the temperature of the drying operation the equilibrium models can be further classified into:

- high temperature (up to 60℃) and
- low temperature models where, the drying air is up to 5℃ above ambient conditions[29].

An equilibrium model has been shown by Cenkowski[22] using the drying model proposed by Laws and Parry. The net of drying in this case is defined as follows:

$$\dot{m} = \rho.K.(M - M_e) \quad [2.15]$$

Using the assumptions of the equilibrium model (air temperature is equal to the grain temperature and the grain moisture content is the equilibrium moisture):

$$t_a(x,\theta) = t(x,\theta) \quad [2.16]$$

$$M(x,\theta) = M_o(x,\theta) \quad [2.17]$$

The net rate of drying under equilibrium conditions is given by:

$$\dot{m} = -\rho \frac{dM}{d\theta} \quad [2.18]$$

The equilibrium moisture content is a function of the air humidity and the temperature:

$$M_e = M_e(H, t_g) \quad [2.19]$$

Equation [2.18] can be re-written as follows:

$$\dot{m} = -\rho\left(\frac{\delta M_e}{\delta H}.\frac{\delta H}{\delta \theta} + \frac{\delta M_e}{\delta t_a}.\frac{\delta t_a}{\delta \theta}\right) \quad [2.20]$$

Substituting equations [2.16], [2.19] and [2.20] into [2.15] yields

$$[A]\frac{\delta(u)}{\delta\theta} + [B]\frac{\delta(u)}{\delta x} = 0$$

$$\{u\} = u[H, t_a]^T, \gamma = c_a + c_v H \; and \; c_g = c + c_w M$$

$$A = \begin{bmatrix} \varepsilon\rho_a + \rho\dfrac{\delta M_e}{\delta H} & \rho\dfrac{\delta M_e}{\delta t_a} \\ \rho\dfrac{\gamma\delta M_e}{\delta H} & \varepsilon\rho_a c_{al} + \rho\left(c_g + \dfrac{\gamma\delta M_e}{\delta t_g}\right) \end{bmatrix} \quad [2.21]$$

$$B = \begin{bmatrix} \varepsilon\rho_a v_a & 0 \\ 0 & \varepsilon\rho_a v_a c_{al} \end{bmatrix}$$

According to the review article by Cenkowski[22] this model has so far not been validated.

The logarithmic and equilibrium models are in principle the simplifications of the non-equilibrium model as they can be derived from the non-equilibrium models by making simple asusmptions[38].

c) Non-Equilibrium models (Partial Differential Equation Models)

The non-equilibrium models assume that there is no heat and mass equilibrium between the drying medium and the grain throughout the deep bed[22,29]. These models are also referred to as partial differential equation models which have been developed under the standard laws of heat and mass balance in a controlled volume[38]. Their application in general is for high temperature drying but they could be used to explain the broad spectrum of drying and cooling. The models developed using this theory could be improved by considering the validity of the assumptions made during their development, though this process adds to the complexity of the model and increases computational time.

These models are built under the assumptions that the bed consists of a series of thin-layers and that the drying takes place in each of these layers in series[23].

This work uses the non-equilibrium theory of drying to design and develop the heat and mass balance equations in both the phases (gaseous and solid) within the bed.

2.3.2. Constitutive Equations

In the thesis report of Haket[1], a method to describe the mass transport and heat transport coefficients by means of the effective surface area of the material being dried has been shown. The present work uses the same approach to derive the effective heat and mass transport correlations.

The effective surface area of the material being dried (grass in this case) can be computed by using the surface area of the grass particle, volume of the grass within the bed and by assuming that the density of grass within the dryer as constant with the formula shown below:

$$A_{eff} = \frac{S_{grass}}{V_{grass} \cdot \rho_{grass}} \qquad [2.22]$$

Where,

A_{eff} is the effective surface area$\left(\frac{m^2}{kg_{drygrass}}\right)$,
S_{grass} is the cross sectional area of the grass(m^2),
V_{grass} is the volume of the grass in the bed (m^3) and
ρ_{grass} is the density of the wet grass$\left(\frac{kg}{m^3}\right)$.

Since the calculation of characteristic interfacial area is difficult in the case of packed beds, in this work, the approach as suggested by Haket has been used, by defining it as the product of the density of the grass and the void fraction of the dryer[1].

a) Drying Rate

The interfacial non-convective mass flux can be computed using equation [2.23]; this formula is useful when the drying is controlled by the gas-side resistance. The driving force in this case is the difference between the absolute humidity at equilibrium with the solid surface and that of the bulk gas[26,43].

$$w_D(Y,T,X) = k_Y.(Y^* - Y) \qquad [2.23]$$

Where,

w_D is the drying rate$\left(\frac{kg_{water}}{kg_{drygrass}-s}\right)$,
$k_Y = h_M.A_{eff}$ is the effective mass transfer coefficient$\left(\frac{kg_{water}}{m^2-S}.\frac{m^2}{kg_{drygrass}}\right)$,
Y is the absolute humidity in dry basis $\left(\frac{kg_{water}}{kg_{dryair}}\right)$ and
Y^* is the absolute humidity on the solid surface at equilibrium in dry basis$\left(\frac{kg_{water}}{kg_{dryair}}\right)$.

b) Absolute humidity on the solid surface at equilibrium

$$Y^*(T) = \frac{M_A}{M_B}.\frac{p^S}{p_o - p^S} \quad [2.24]$$

Where,

Y^* is the absolute humidity on the solid surface at equilibrium in dry basis$\left(\frac{kg_{water}}{kg_{dryair}}\right)$,
M_A is the molar mass of water in$\left(\frac{kg}{kmol}\right)$,
M_B is the molar mass of air in $\left(\frac{kg}{kmol}\right)$,
p^S is the saturation vapour pressure in (kPa) and
p_o is the system pressure in (kPa).

The saturation vapour pressure can be calculated by using the Antoine equation and which is valid in the temperature range [0-200(℃)][26,44]:

$$p^S = \exp\left(A - \frac{B}{C + t}\right) \quad [2.25]$$

c) Heat Flux

The constitutive heat flux is calculated using equation [2.26] presented below:

$$q(t_g, t_m) = \alpha.(t_g - t_m) \quad [2.26]$$

Where,

q is heat flux$\left(\frac{W}{kg}\right)$,
$\alpha = h_H.A_{eff}$ is the effective heat transfer coefficient in this study, $\left(\frac{kW}{m^2-K}.\frac{m^2}{kg_{drygrass}}\right)$,
t_g is the humid gas temperature (℃) and
t_m is the temperature of the solid at the interface(℃).

Equations [2.23] & [2.26] can be used when the drying is externally controlled and when the Biot number for heat and mass transfer are less than 0.1[43].

2.3.3. Correlations for heat and mass transfer coefficients

Since both heat and mass transfer coefficients are influenced by thermal and flow properties of the air and of course by the geometry of the system. The following section presents the correlations obtained from literature for the calculation of the heat and mass transport coefficients for packed beds[43].

The correlations developed and presented in literature for the calculation of the heat and mass transfer coefficients for a packed bed have been considered because their geometry is similar to the bed in this work and are presented below:

a) Heat transfer coefficient

$$j_H = 1.06.(Re)^{-0.41} \quad [2.27]$$

Applicable when Re is in the range: 350<Re<4000

$$j_H = St.(Pr)^{\frac{2}{3}} \quad [2.28]$$

Where,

j_H is the heat transfer factor,
Re is the Reynolds number$\left(\frac{u_B.\rho_B.d_p}{\mu_B}\right)$,
c_B is the specific heat capacity of dry air$\left(\frac{kJ}{kg-K}\right)$,
u_B is the superficial air velocity$\left(\frac{m}{s}\right)$,
ρ_B is the density of dry air$\left(\frac{kg_{dryair}}{m^3_{bed}}\right)$,
d_p is the particle diameter(m),
μ_B is the dynamic viscosity of the air$\left(\frac{kg}{m-s}\right)$,
St is the Stanton number$\left(\frac{h_H}{u_B.\rho_B.c_B}\right)$,
h_H is the heat transfer coefficient $\left(\frac{kW}{m^2-K}\right)$
k_B is the thermal conductivity of the air $\left(\frac{kW}{m-K}\right)$ and
Pr is the Prandtl number$\left(\frac{c_B.\mu_B}{k_B}\right)$.

Using the correlations for the Stanton number, Prandtl number and the Reynolds number the equation for the heat transfer coefficient can be re-written:

$$1.06.(Re)^{-0.41} = St.(Pr)^{\frac{2}{3}} \quad [2.29]$$

$$1.06.\left(\left(\frac{u_B.\rho_B.d_p}{\mu_B}\right)\right)^{-0.41} = \left(\frac{h_H}{u_B.\rho_B.c_B}\right).\left(\left(\frac{c_B.\mu_B}{k_B}\right)\right)^{\frac{2}{3}} \quad [2.30]$$

$$h_H = \frac{1.06 * u_B.\rho_B.c_B.\left(\left(\frac{u_B.\rho_B.d_p}{\mu_B}\right)\right)^{-0.41}}{\left(\left(\frac{c_B.\mu_B}{k_B}\right)\right)^{\frac{2}{3}}} \quad [2.31]$$

b) Mass transfer coefficient

$$j_M = 1.82.(Re)^{-0.51} \quad [2.32]$$

Applicable when Re is in the range: 40<Re<350

$$j_M = \left(\frac{h_M}{u_B.\rho_B}\right).(Sc)^{\frac{2}{3}} \quad [2.33]$$

Where,

j_M is the mass transfer factor,
Re is the Reynolds number$\left(\frac{u_B.\rho_B.d_p}{\mu_B}\right)$,
c_B is the specific heat capacity of dry air$\left(\frac{kJ}{kg-K}\right)$,
u_B is the superficial air velocity$\left(\frac{m}{s}\right)$,
ρ_B is the density of dry air$\left(\frac{kg_{dryair}}{m^3_{bed}}\right)$,
d_p is the particle diameter(m),
μ_B is the dynamic viscosity of the air$\left(\frac{kg}{m-s}\right)$,
h_M is the mass transfer coefficient $\left(\frac{kg}{m^2-s}\right)$
Sc is the Schmidt number $\left(\frac{\mu_B}{\rho_B.D_{12}}\right)$ and
D_{12} is the water diffusivity in air$\left(\frac{m^2}{s}\right)$.

Using the correlations the equations for the mass transfer coefficient can be re-written:

$$a.(Re)^n = \left(\frac{h_M}{u_B.\rho_B}\right).(Sc)^{\frac{2}{3}} \quad [2.34]$$

$$a.\left(\left(\frac{u_B.\rho_B.d_p}{\mu_B}\right)\right)^n = \left(\frac{h_M}{u_B.\rho_B}\right).\left(\left(\frac{\mu_B}{\rho_B.D_{12}}\right)\right)^{\frac{2}{3}} \quad [2.35]$$

$$h_M = \frac{a.u_B.\rho_B.\left(\left(\frac{u_B.\rho_B.d_p}{\mu_B}\right)\right)^n}{\left(\left(\frac{\mu_B}{\rho_B.D_{12}}\right)\right)^{\frac{2}{3}}} \quad [2.36]$$

The calculation checks to deduce if the used correlations for the calculation of heat and mass transfer coefficients are valid have been presented in the Appendix 3.

2.3.4. Deep Bed Drying Mathematical Model

In a fixed bed, the drying medium (air) is considered to move from bottom to the top of the dryer (in this work). The temperatures of the material being dried and the air, humidity of the air and the moisture content of the material being dried at any instant depend on the position in the bed[29]. As the gas phase flows in only one direction it can be considered to be in pseudo-steady state.

Since the case of fixed-bed drying requires the simulation of four process variables namely the gas phase humidity, gas temperature, solid phase moisture and solid temperature, the mathematical model would require four independent equations to be setup for their calculation. A system of coupled differential equations has been used to set up the heat and mass balance of the solid and gas phase within the dryer bed in literature[26,29–31]. A schematic of the drying process in a deep layer has been shown in Figure 6.

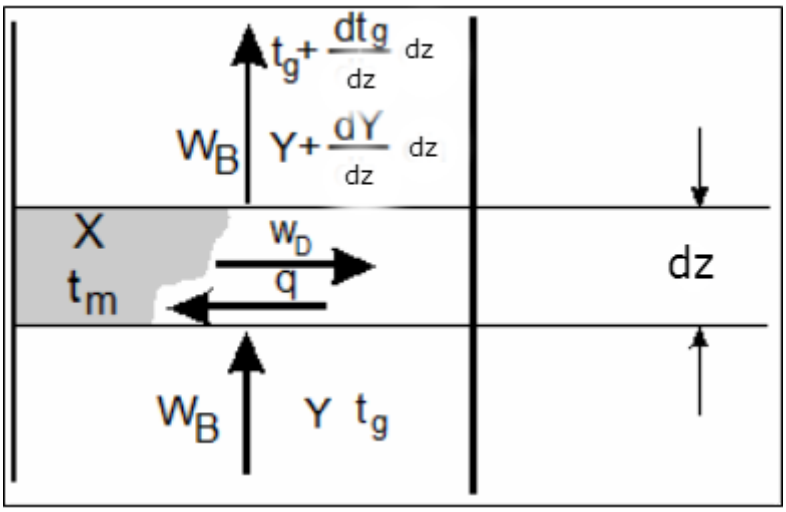

Figure 6: Deep Bed-Drying Schematic[26]

a) Model Assumptions

The model assumes the following while performing the calculations in the direction of flow for a thin layer for a fixed-time step and then uses the data to perform calculations for the next thin layer:

- There is one dimensional transport of mass and energy within the system.
- The air which flows through the column is assumed to be completely dry.
- The distribution of air velocity within the dryer is uniform[1,31].
- The system is well insulated (adiabatic)[31] there is no losses from the system, i.e. no heat and mass losses from the system.
- The drying medium immediately surrounding the grass particle is assumed to be saturated at the temperature of the solid and not at the bulk temperature.
- The effects of shrinkage are not considered in the development of the model.
- The density of the grass, dynamic viscosity, thermal conductivity and diffusivity of water in air has been maintained constant in the drying time interval considered in this study.

- The specific heat capacity (at constant pressure) of grass has been maintained constant under the assumption that it does not vary during the time interval considered.

The balance equations in this work were obtained from the "*Handbook of Industrial Drying*"[26] and have been presented below:

i. Mass Balance for water in the gas phase

The steady state (i.e. by ignoring the mass holdup and start up periods) gas phase input-output balance equation for a differential space element in the direction of flow of gas can be written as following:

$$Flow\ in - Flow\ out = Rate\ of\ Accumulation$$

$$W_B.Y - W_B.\left(Y + \frac{dY}{dz}.dz\right) - w_D.dA = 0 \quad [2.37]$$

$$dA = a_v.S.dz$$

$$W_B.Y - W_B.\left(Y + \frac{dY}{dz}.dz\right) - w_D.a_v.S.dz = 0 \quad [2.38]$$

$$W_B.Y - W_B.Y - W_B.\frac{dY}{dz}.dz - w_D.a_v.S.dz = 0 \quad [2.39]$$

Cancelling out common terms and re-arranging the terms of equation [2.39], the gas phase balance equation is shown below:

$$\frac{dY}{dz} = \frac{w_D(Y,T,X).a_V.S}{W_B} \quad [2.40]$$

Where,

Y is the absolute humidity in dry basis$\left(\frac{kg_{water}}{kg_{dryair}}\right)$,
z is the height of the dryer(m),
w_D is the drying rate$\left(\frac{kg_{water}}{kg_{drygrass}-s}\right)$,
a_V is the characteristic interfacial area per unit volume of the dryer$\left(\frac{kg_{drygrass}}{m^3_{bed}}\right)$,
S is the cross sectional area normal to the direction of flow (m^2) and
W_B is the gas flow velocity$\left(\frac{kg_{dryair}}{S}\right)$.

ii. Energy Balance in the gas phase

The steady-state input-output energy balance in the gas phase is given by:

$$Heat\ flow\ in - Heat\ flow\ out = Rate\ of\ Accumulation$$

$$W_B.h_g - W_B\left(h_g + \frac{dh_g}{dz}.dz\right) - (q - w_D.h_{av}).dA = 0 \qquad [2.41]$$

The enthalpy of steam emanating from the solid is given by:

$$h_{av} = c_A.t_m + \Delta h_v^o$$

$$W_B.h_g - W_B.h_g - W_B.\frac{dh_g}{dz}.dz - (q - w_D.h_{av}).dA = 0 \qquad [2.42]$$

$$dA = a_v.S.dz$$

Cancelling out common terms and re-arranging the terms of equation [2.42], the gas phase energy balance equation is shown below:

$$\frac{dh_g}{dz} = \frac{(q - w_D.h_{av}).a_v.S}{W_B} \qquad [2.43]$$

The energy balance equations written in terms of enthalpy are rewritten as a function of the temperature to enable easier comparison of the modelling and experimentally determined values[1,26]. The differential enthalpy of the humid gas (per unit mass of dry gas) given in literature[26] is given by:

$$\frac{dh_g}{dh} = (c_B + c_A.Y)\frac{dt_g}{dz} + \left(c_A.t_g + \Delta h_v^o\right)\frac{dY}{dz} \qquad [2.44]$$

Substituting the mass balance & energy balance terms into the humid gas enthalpy equation, the equation can be expressed as:

$$\frac{\left(q - w_D.(c_A.t_m + \Delta h_v^o)\right).a_v.S}{W_B} = (c_B + c_A.Y)\frac{dt_g}{dz} + \left(c_A.t_g + \Delta h_v^o\right)\frac{w_D(Y,T,X).a_V.S}{W_B} \qquad [2.45]$$

Rearranging the terms of the equation and expressing in terms of temperature, the gas phase energy balance is given by:

$$\frac{dt_g}{dz} = -\frac{S.a_V}{W_B}\frac{1}{(c_B + c_A.Y)}\left[q\left(t_g, t_m\right) + c_A\left(t_g - t_m\right).w_D(Y,T,X)\right] \qquad [2.46]$$

Where,

t_g is the humid gas temperature(℃),

c_A is the specific heat capacity of moisture in the vapour phase$\left(\frac{J}{kg-K}\right)$,

c_{Al} is the specific heat capacity of moisture in the liquid phase$\left(\frac{J}{kg-K}\right)$,

c_B is the specific heat capacity of the dry gas $\left(\frac{J}{kg-K}\right)$ and

q is the heat flux$\left(\frac{W}{kg-K}\right)$.

iii. Mass Balance in the Solid phase

The mass balance in the solid phase for a differential space element is given by the equation:

$$Flow\ in - Flow\ out = Rate\ of\ Accumulation$$

$$W_S.X - W_S.\left(X + \frac{\delta X}{\delta z}.dz\right) - w_D.dA = dm_s.\frac{\delta X}{\delta \tau}$$

$$dA = a_v.S.dz \qquad [2.47]$$

$$dm_s = \rho_S.(1-\varepsilon).S.dz$$

$$W_S.X - W_S.\left(X + \frac{\delta X}{\delta z}.dz\right) - w_D.a_v.S.dz = \rho_S.(1-\varepsilon).S.dz.\frac{\delta X}{\delta \tau} \qquad [2.48]$$

$$W_S.X - W_S.X - W_S.\frac{\delta X}{\delta z}.dz - w_D.a_v.S.dz = \rho_S.(1-\varepsilon).S.dz.\frac{\delta X}{\delta \tau} \qquad [2.49]$$

Cancelling out common terms and re-arranging the terms of the equation (accounting for the fact that there is no mass change in the solid along the height of the bed), the above expression [2.49] can be expressed by:

$$\frac{dX}{d\tau} = -\frac{w_D(Y,T,X).a_V}{\rho_S.(1-\varepsilon)} \qquad [2.50]$$

Where,

X is the moisture content in dry basis$\left(\frac{kg_{water}}{kg_{drygrass}}\right)$,

τ is the time step(s),

w_D is the drying rate$\left(\frac{kg_{water}}{kg_{drygrass}-s}\right)$,

a_V is the characteristic interfacial area per unit volume of the dryer$\left(\frac{kg_{drygrass}}{m^3_{bed}}\right)$,

S is the cross sectional area normal to the direction of flow (m^2) and

ρ_S is the density of the solid in$\left(\frac{kg_{drygrass}}{m^3_{bed}}\right)$.

iv. Energy Balance in the Solid phase

The energy balance in the solid phase is given by:

$$Heat\ flow\ in - Heat\ flow\ out = Rate\ of\ Accumulation$$

$$W_S.h_m - W_S.\left(h_m + \frac{dh_m}{dz}.dz\right) + (q - w_D.h_{av}).dA = 0$$

$$dA = a_v.S.dz$$

[2.51]

The enthalpy of steam emanating from the solid is given by:

$$h_{av} = c_A.t_m + \Delta h_v^o$$

$$W_S.h_m - W_S.h_m - W_S.\frac{dh_m}{dz}.dz + (q - w_D.h_{av}).a_v.S.dz = 0 \quad [2.52]$$

The cancellation of common terms from the above equation and the re-arrangement of terms results in the following equation:

$$\frac{dh_m}{dz} = \frac{(q - w_D.h_{av}).a_v.S}{W_S} \quad [2.53]$$

The energy balance equation can also be expressed as shown below:

$$\frac{dh_m}{dt} = (c_S + c_{Al}.X)\frac{dt_m}{dt} + c_{Al}.t_m\frac{dX}{dt} \quad [2.54]$$

Substituting the mass balance & energy balance terms into the enthalpy balance equation, the equation can be written as:

$$\left(\frac{\left(q - w_D.(c_A.t_m + \Delta h_v^o)\right).a_v.S}{W_S}\right) = (c_S + c_{Al}.X)\frac{dt_m}{dt} + c_{Al}.t_m\left(-\frac{w_D(Y,T,X).a_V}{\rho_S.(1-\varepsilon)}\right) \quad [2.55]$$

Rearranging the terms of the equation and expressing in terms of temperature, the solid phase energy balance is given by:

$$\frac{dt_m}{d\tau} = \frac{a_V}{\rho_S.(1-\varepsilon)}\frac{1}{(c_S + c_{Al}.X)}\left[q(t_g,t_m) - \left((c_A - c_{Al})t_m + \Delta h_v^o\right)w_D(Y,T,X)\right] \quad [2.56]$$

Where,

t_m is the solid temperature (℃)

c_A is the specific heat capacity of moisture in the vapour phase$\left(\frac{J}{kg-K}\right)$,

c_{Al} is the specific heat capacity of moisture in the liquid phase$\left(\frac{J}{kg-K}\right)$,

Δh_v is the latent heat of vaporization $\left(\frac{kJ}{kg}\right)$

c_B is the specific heat capacity of the dry gas $\left(\frac{J}{kg-K}\right)$ and

q is the heat flux$\left(\frac{W}{kg-K}\right)$.

This system of equations are solved by using a Runge-Kutta method (using an ODE solver in MATLAB®) and by a finite difference discretization to represent the results for case of drying in a thick bed[26,31]. The methodology followed to develop the mathematical equations for finite difference discretization and the flow structure of the algorithm developed is shown in the next chapter.

3.Discretization and Simulation Strategy

This chapter describes the structure of the algorithm used to model the deep bed. It also outlines the finite difference scheme used in the mass and heat balances for the determination of moisture and solid temperatures.

3.1. Discretization and Finite Difference Scheme

The equations for the energy and mass balance in the solid phase have been expressed in terms of finite difference variations in the humidity and gas temperature along the height of the dryer with an assumed time step.

The basic principle behind the use of the finite difference method is to replace the derivatives of governing equations with algebraic difference quotients. This would result in generation of algebraic equations which are solvable for dependent variables at discrete grid points[45].

3.1.1. Mass balance for water in the solid phase

Since the first step involved in the development of a mathematical would involve the derivation of a set of balance equations to describe the mass and energy balance in a thin layer during a small time step. The balance equations for the gas phase have been presented in the previous chapter and they are solved using a Runge-Kutta approach using MATLAB®. The balance equations for the solid phase are solved by the use of a finite difference approach. The finite difference approach is considered because there is no accumulation of mass within the dryer and there is a transfer of mass from the solid to the air and not vice-versa.

As the change in moisture in the solid phase must equal the change in humidity of the gas phase. Therefore, the mass balance for water in the solid phase was derived by expressing it in terms of finite differences of the humidity along the height of the dryer with an assumed time step.

The balance equation for a property continuously varying along the flow direction can be written only for a differential space element. Since the solid phase in deep bed dryer remains within the bed for a period of time, while the gas phase flows continuously through the bed. The balance in the solid can be expressed as follows:

$$-w_D . dA = dm_s \frac{dX}{dt} \qquad [3.1]$$

After substituting $dA = a_V . S . dz$and $dm_S = \rho_s . (1 - \varepsilon) . S . dz$ equation [3.1] can be re-written as:

$$-w_D . a_V . S . dz = \rho_s . (1 - \varepsilon) . S . dz \frac{dX}{dt} \qquad [3.2]$$

Cancelling out common terms from both sides of the equation [3.2] yields:

$$\frac{-w_D.a_V}{\rho_s.(1-\varepsilon)} = \frac{dX}{dt} \quad [3.3]$$

The difference in humidity between two points across the height of the dryer is given by:

$$\frac{(Y_2 - Y_1)}{(z_2 - z_1)} = \frac{w_D.a_V.S}{W_B} \quad [3.4]$$

Equating common terms in equations [3.3] & [3.4] and re-arranging the terms of the equation, the difference in moisture content between two points for a time step is given by:

$$X_2 = X_1 - (\Delta t).\left(\left[\frac{Y_2 - Y_1}{z_2 - z_1}\right].\frac{W_B}{S}.\frac{1}{\rho_S.(1-\varepsilon)}\right) \quad [3.5]$$

3.1.2. Energy balance in the solid phase

The energy balance in the solid phase was derived after performing an enthalpy balance in the gas phase and the equation when expressed in terms of finite differences as a function of temperature would be derived as follows:

The enthalpy of humid gas (per unit mass of the dry grass)[26] is expressed as a function of the gas phase humidity and gas temperature:

$$h_g = (c_A.Y + c_B).t + \Delta h_v^o.Y \quad [3.6]$$

Where,

c_A is the specific heat capacity of moisture in the vapour phase$\left(\frac{J}{kg-K}\right)$,
c_B is the specific heat capacity of the dry gas$\left(\frac{J}{kg-K}\right)$,
Δh_v is the latent heat of vaporization $\left(\frac{kJ}{kg}\right)$ and
h_g is the enthalpy of humid gas$\left(\frac{kJ}{kg-K}\right)$.

The difference in enthalpy between two points across the height of the dryer, from equation [2.24]:

$$(h_{g2} - h_{g1}) = (c_A.Y + c_B).(T_{g2} - T_{g1}) + (c_A.T_g + \Delta h_v^o).(Y_2 - Y_1) \quad [3.7]$$

The energy balance in the solid phase between two points written in terms of solid temperature can be expressed as:

$$\Delta h_m = [(c_S + c_{Al}.X).\Delta T_m + c_{Al}.T_m.\Delta X] \quad [3.8]$$

Where,

c_S is the specific heat capacity of the solid$\left(\frac{J}{kg-K}\right)$,

c_{Al} is the specific heat capacity of moisture in the liquid phase $\left(\frac{J}{kg-K}\right)$ and

h_m is the enthalpy of the solid$\left(\frac{kJ}{kg-K}\right)$.

The solid phase enthalpy can be related to the finite differences in gas enthalpy over the height of the dryer for a fixed time step (this equation is valid only in the case of a completely insulated system) as shown:

$$\Delta h_m = -\Delta t.\frac{dh_g}{dz}\left[\frac{W_B}{S}.\frac{1}{z.\rho_s(1-\varepsilon)}\right] \quad [3.9]$$

Rearranging the terms of the expression [3.9], the energy balance can expressed in terms of temperature by the following equation (steps in deriving the expression shown in chapter 2):

$$\frac{dt_m}{d\tau} = \frac{a_V}{\rho_S.(1-\varepsilon)}\frac{1}{(c_S + c_{Al}.X)}\left[q(t_g,t_m) - \left((c_A - c_{Al})t_m + \Delta h_v^o\right)w_D(Y,T)\right] \quad [3.10]$$

3.2. Numerical Scheme

In Figure 7, the image on the left illustrates a sample grid where Δx andΔy, represent the spacing in the x and y direction. The size of the spacing does not need to be uniform. The grid points are by indices 'i' and 'j' in the x and y direction[45].

The complete dryer bed is modelled as thin layers which resembles a rectangular grid with 'i' grid points in space (which are spaced equally) and 'j' grid points in time (which are equally spaced time steps) for the purpose of modelling the process variables in the drying direction at various points in time. A sample representation of the grid points in a thin layer in the direction of flow for a finite step (in space & time) has been shown on the right side in Figure 7. The height of the dryer is considered to be the abscissa co-ordinate (i) of the grid point and the movement in time is therefore the ordinate coordinate (j).

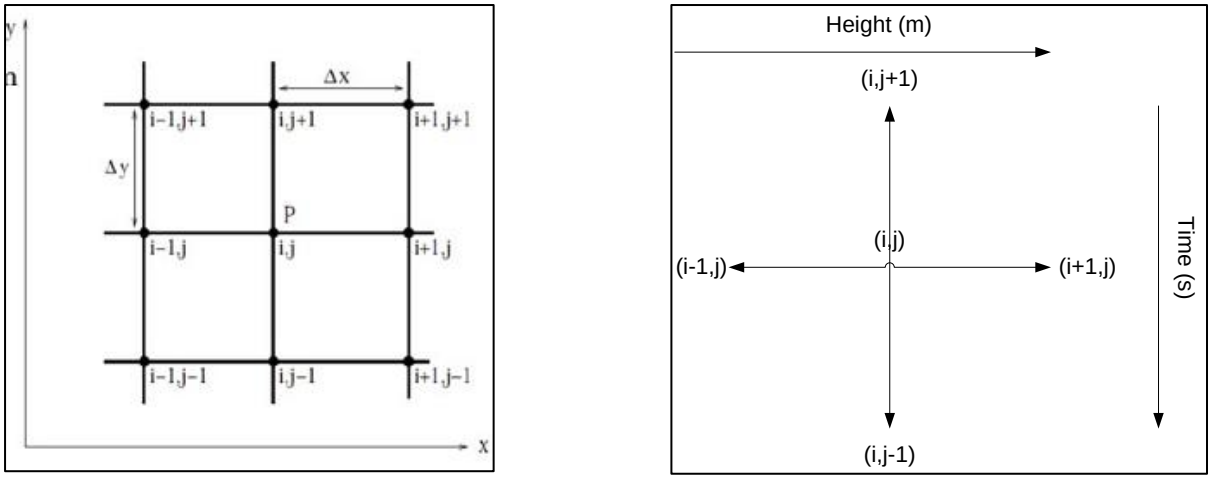

Figure 7: Sample Representation of Grid points in the Finite Difference Grid[45]

Expressing equation [3.5] by accounting for the variation of the quantities for a finite time step and with the humidity variation in space the equation can be rewritten as follows:

$$X_i^j = X_i^{j-1} - (\Delta t).\left(\left[\frac{Y_{i+1}^j - Y_i^j}{z_{i+1} - z_i}\right].\frac{W_B}{S}.\frac{1}{\rho_S.(1-\varepsilon)}\right) \quad [3.11]$$

Where,

X is the moisture content in dry basis$\left(\frac{kg_{water}}{kg_{drygrass}}\right)$,
Δt is the assumed time step(s),
Δz is the difference in space(m),
i refers to the spatial co-ordinate,
j refers to the time co-ordinate and
ρ_s is the density of the solid$\left(\frac{kg_{drygrass}}{m_{bed}^3}\right)$.

Similarly expressing [3.9] in terms of temperature from [3.8] and accounting for the variation of the quantities for a finite time step, the equation can be rewritten as follows:

$$Tm_i^j = Tm_i^{j-1} - \Delta t.\left[\frac{-\left\{\left[(C_B + C_A Y)\left(\frac{dt_g}{dz}\right) + (C_A.T_g + h_v)\left(\frac{dY}{dz}\right)\right]\left[\frac{W_B}{S}.\frac{1}{h.\rho_s(1-\varepsilon)}\right] - C_{Al}.T_m.\Delta X\right\}}{C_s + C_{Al}.X}\right] \quad [3.12]$$

Where,

T_m is the temperature in the solid phase(℃),
c_S is the specific heat capacity of the solid $\left(\frac{J}{kg-K}\right)$ and
Δh_v is the latent heat of vaporisation$\left(\frac{J}{kg}\right)$.

3.3. Algorithm Flow Description

The program requires a number of input parameters to be specified which include: initial moisture content, inlet air temperature and humidity, solid temperature, inlet air flow rate and the time interval[27,31].

The ordinary differential equations for the mass [2.21] and energy balance [2.27] in the gas phase are solved by using the in-built ODE solver (a simple explanation regarding the method of solution used by the ODE solver and the methodology for implementation has been provided in the Appendix 1 & 2) in MATLAB®. The solver uses the Runge-Kutta method for the solution of the equations and generates air humidity and temperature profiles in the fixed-bed drying direction. The mass [3.11] and energy balances [3.12] in the solid phase are then solved for generating moisture and solid temperature profiles for a finite time step. When this step is complete; the algorithm would have generated values for all the process variables (humidity, gas temperature, solid moisture content and solid temperature) in the drying direction for a fixed-time step. The variables generated from the balance equations for the solid are then used to solve for the air humidity and temperature profiles for the next time step and the process is repeated for the desired drying time. The code is run until the moisture

content is reduced completely to almost zero moisture content (this is done using the assumption that the air passing through the column is completely dry).

4. Experimental Setup

The experiments were performed by Master of Science student (Miao Wang, SPET) on a lab-scale fixed bed setup housed in the laboratory of the Process & Energy Department of the Delft University of Technology (schematic shown in Figure 8) which served the purpose of drying and the torrefaction of the biomass feedstock.

Completely dry N_2 passes through the column and serves as the primary heat transport media. Other than the valve which controls (Aalborg, model GFC-54, 0-186$\frac{stdL}{min}$) the flow of N_2 through the column, there exists a separate valve for regulating the flow of a mixture of air and CO_2 (flow measured using Aalborg, model 37, 0-30$\frac{stdL}{min}$) into the column. The biomass feedstock to the column was separated into three equal parts and filled within the column to ensure that the density throughout the column is similar. The dryer/reactor column employs direct convective heating through heated media; a similar mechanism is used in large-scale industrial setups. The total height of the column is 360mm and the diameter of the column is 56mm.

The gases passing through the column are heated using an electric heater (Power rating of 2.5 kW, Heating Group, TPE FLANGE IMMERSION HEATER), the temperature of the gases are recorded using thermocouple 'TC1'. The maximum temperature of the heater was set at 700℃ to prevent thermal meltdown of the heating element. The temperatures of the solid within the column are recorded using three thermocouples 'TC3', 'TC4' & 'TC5'. Thermocouples 'TC3', 'TC4', 'TC5' are located at depths of 60mm, 180 mm and 300 mm within the column. Two thermocouples 'TC2' & 'TC6' have been placed to record the temperature of the inlet and outlet gas streams from the column. The setup also houses a relative humidity detector (RH, Michell instruments, model WR283) upstream and a pressure sensor (dP, Endress & Hauser, model PMD70) to record the pressure drop across the dryer column.

All pipelines leaving the electric heater are thermally insulated and the inlet gas line electrically trace heated to minimize heat loss within the column. The mass flows within the system are controlled electronically using the LabVIEW® (2012 edition) program.

The feedstock used for performing the experiments in this work is fresh 'verge grass' and the experiments were performed by varying inlet gas flow rates and temperatures. The freshly collected samples contain approximately 70-80% average moisture contents. Experimental data was first collected using the Data Acquisition (DAQ) system from NATIONAL INSTRUMENTS, and then recorded also by LabVIEW®.

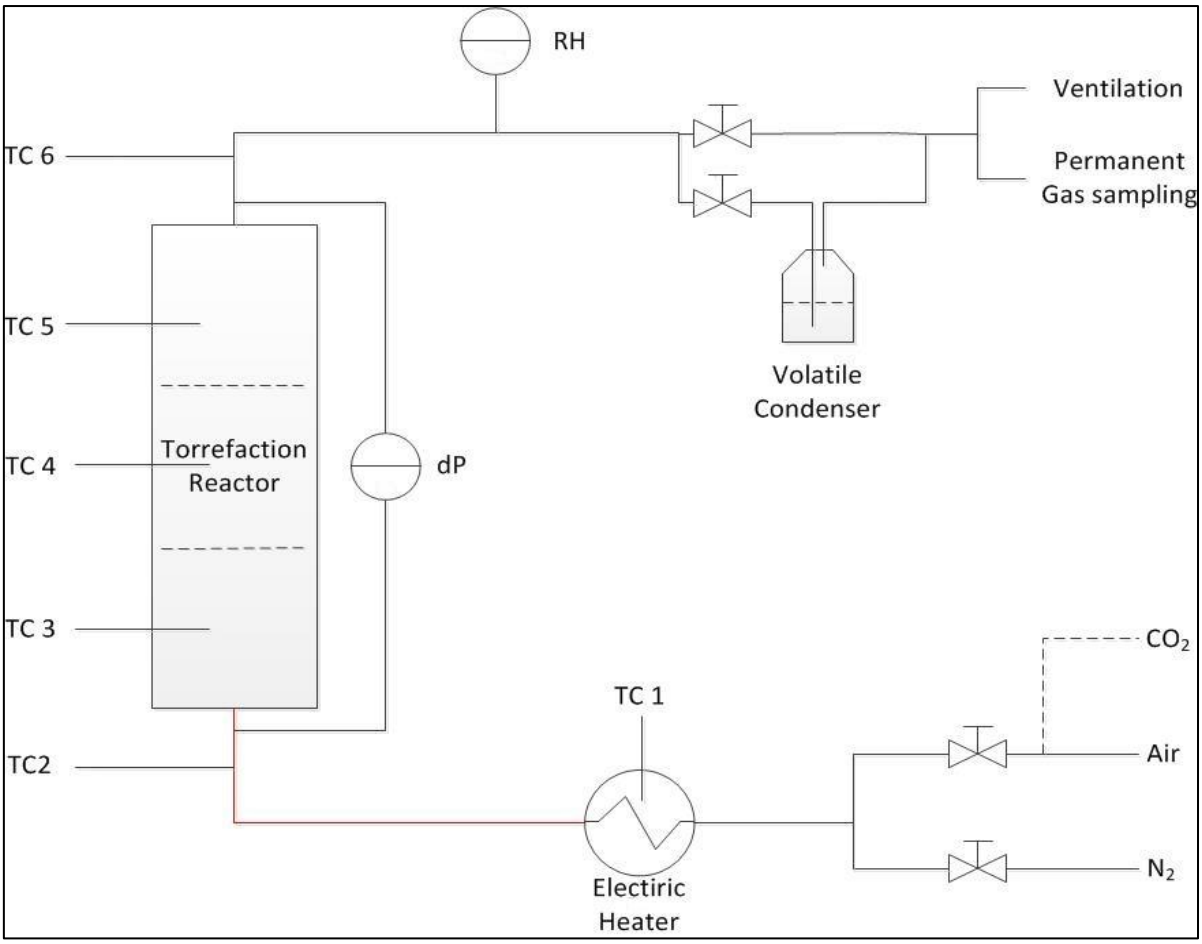

Figure 8: Lab-Scale Drying and Torrefaction Setup

5. Results and Discussion

This chapter presents the results of simulation of the mathematical model developed in section 2.3.4 of ***Chapter 2*** and ***Chapter 3*** and proceeds to further test some sample cases to understand the influence of the variation of certain input parameters on the process. The influence of the variation of the flow rate of the drying medium, inlet gas temperatures, number of grid spacing's used the iteration and choice of ODE solver used in MATLAB® have been analysed. The simulated model is then tested/evaluated using experimental data to test the validity of the simulated model when compared against actual experimental results.

5.1. Model Constants and Bed Properties

For the purpose of modelling certain input parameters were held constant during the simulations performed. The constants that were defined in the model are shown below in Table 5-1:

Table 5-1: Process Constants

Symbol	*Description*	*Value*	*Unit*
W_B	*Air Mass flow rate*	$\frac{Vol.flow\ rate * \rho_{air}}{60 * 1000}$	$\left(\frac{kg_{dryair}}{S}\right)$
X_{inlet}	*Inlet Moisture Content (dry basis)*	1	$\left(\frac{kg_{water}}{kg_{drygrass}}\right)$
Y_{inlet}	*Inlet Air Humidity (dry basis)*	0	$\left(\frac{kg_{water}}{kg_{dryair}}\right)$
T_m	*Solid Temperature*	25	(℃)
T_g	*Inlet Gas Temperature*		(℃)
Δh_v	*Latent Heat of vaporisation*	$2.35 * 10^6$	$\left(\frac{J}{kg}\right)$
μ_B	*Dynamic Viscosity of Air*	$2.0750 * 10^{-5}$	$\left(\frac{kg}{m-s}\right)$
k_B	*Thermal Conductivity of Air*	0.0299	$\left(\frac{W}{m-K}\right)$
D_{12}	*Water Diffusivity in Air*	$24 * 10^{-6}$	$\left(\frac{m^2}{s}\right)$
c_{Ps}	*Specific Heat Capacity of Grass*	$1.3 * 10^3$	$\left(\frac{J}{kg-K}\right)$

The values of the thermal conductivity and dynamic viscosity of air were average from the values between 300 and 400K obtained from the Chemical Engineer's Handbook[46].

The bed properties obtained from the work of Haket[1] and used in the model are provided below in:

Table 5-2: Bed Properties

Symbol	*Description*	*Value*	*Unit*
ε	*Porosity*	0.5	
ρ_{bulk}	*Bulk Density of grass*	100	$\left(\frac{kg_{drygrass}}{m^3_{bed}}\right)$
a_V	*Specific area/Characteristic Interfacial Area per unit volume of bed*	$\rho_S.(1-\varepsilon)$	$\left(\frac{kg_{drygrass}}{m^3_{bed}}\right)$
z	*Height of the dryer*	0.5	(m)
S	*Cross-sectional area normal to flow direction* $\frac{\pi d^2}{4}$	0.0020	(m^2)

The parameters that are dependent on temperature have been defined by using correlations available in literature and the correlations have been defined in Appendix 3.

5.2. Parameter Analysis

To analyse the response of the model when input process parameters are varied and total drying time defined in the model, a few cases have been tested. Extensive simulations have been performed to understand the influence of variation of selected process parameters. The cases that have been tested in the sections that follow are:

- Variation of the inlet gas flow rate,
- Variation of the inlet gas temperature,
- Variation of the total drying time defined (thus increasing or decreasing the number of grid points defined in time),
- Variation of the number of grid points defined in space and,
- Finally the influence of using another ODE solver in MATLAB®.

It was noticed as the number of data points chosen in time or space for iteration increased, the amount of redundant data generated also increased. Thus for practical purposes and for reducing the redundancy in order to improve the accuracy of the model in providing values that converge to the same solution a sensitivity analysis needs to be carried out.

Further, an attempt is made to evaluate the developed model against experimental results obtained from a lab-scale fixed-bed dryer and torrefaction setup.

5.2.1. Inlet Gas Temperature

The model is first simulated at an inlet gas temperature of 50℃ and the parameters that are varied in the subsequent sections are the inlet gas flow rate and the total drying time. The model has been simulated for the following conditions:

- flow rate of $30\frac{Nl}{min}$ at drying times of 60 minutes and,
- flow rate of $90\frac{Nl}{min}$ at drying times of 60 minutes.

The results for the variation of the process variables 'humidity' (Figure 9), 'inlet gas temperature' (Figure 10), 'grass moisture content' (Figure 11) and 'grass temperature' (Figure 12) with time and with bed height are presented.

The analyses has initially been performed on the results obtained from the simulations after a drying time of 60 minutes, the results obtained in both conditions (variation of flow rates) by increasing or decreasing the drying time (or number of grid points in space) have been presented in the Appendix 4.

a) Case 1

The input parameters used in simulation for this case have been presented in Table 5-3 below:

Table 5-3: Simulation parameters Case 1

dt	1 s
Total drying time	60 min
Inlet gas temperature, T_g	50 (℃)
Drying Medium Flow rate, W_B	90 $\left(\frac{Nl}{min}\right)$
Number of grid points in space, N_s	1000

The model has been simulated for 1000 grid points in the space direction, because when much lower points in space (around 300 grid points in space, plots shown in Appendix 4) were considered the model results weren't consistent (the moisture content values tended to drop into the negative).

In Figure 9, Figure 10, Figure 11 & Figure 12 the results from the computer simulations for the variation in the humidity, gas temperature, solid temperature and moisture distribution within the material with time at different bed heights have been illustrated.

The fluctuation the humidity and also in temperature after reaching equilibrium conditions are due to the numerical schemes that were used in the solution of the model. These deviations however were removed when a higher number of grid points in the space or time

direction were considered. The conditions in which the fluctuations arose have been presented in the additional plots section in Appendix 4.

Figure 9 illustrates the humidity profiles as a function of time at different bed heights. It can be seen from the figure that for a particular bed height (h = 0.0746m and similarly at heights deeper in the bed as well) as time increases, the rate of evaporation of moisture from the material being dried decreases (decrease of the drying rate) and hence the humidity decreases. The humidity or partial pressure driving force for mass transfer tends to approach zero as the equilibrium moisture content is approached. As the gas moves through the bed, at h = 0.2298m (and similarly as the gas is moving deeper within the bed), more heat needs to be supplied (because from the behaviour of the simulated model it can be understood that heat is being quenched from the inlet air and the extent of this quenching with time increases as the gas moves through the bed) to remove the moisture, hence the variation in humidity is much more gradual than at h = 0.0746m (close to the inlet) and takes much longer to approach equilibrium conditions. It can be seen that the humidity (at h = 0.0746m and also noticeable at higher bed depths) as it approached equilibrium falls below the assumed input value in programming (for a small time duration); this arises due to the inconsistencies that were generated by the numerical schemes being used.

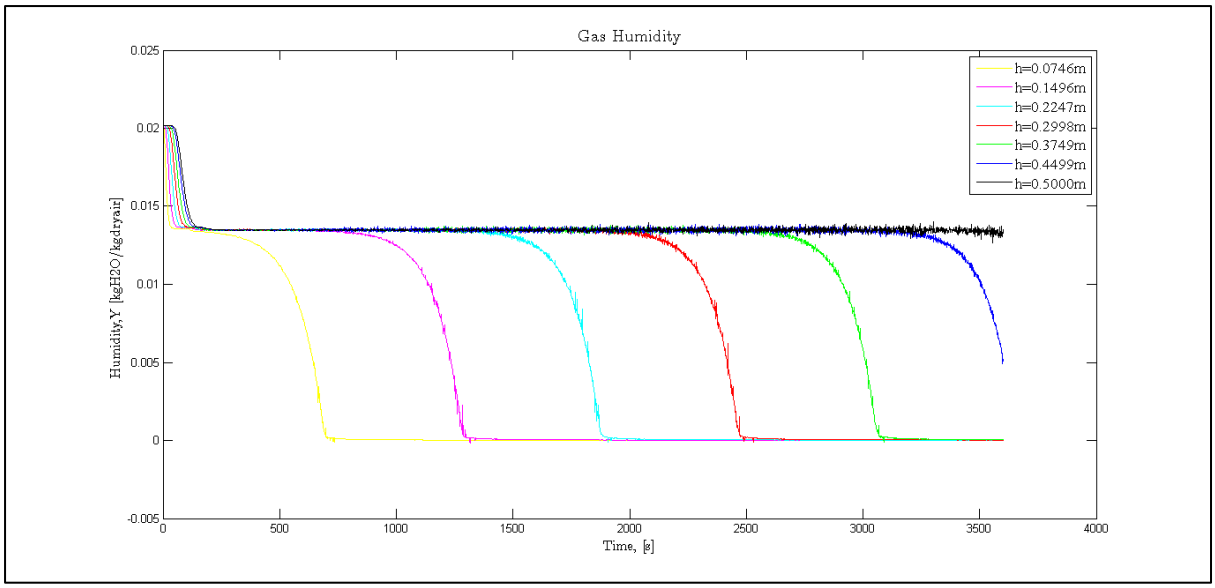

Figure 9: Humidity Profile versus time

Figure 10 shows the variation of the air temperature as a function of time at different bed heights. The gas temperature increases with increase in time for a particular height in the bed as moisture removal decreased. The temperature of the drying medium is lower as it moves through the bed than at the inlet, this is because more heat is required to facilitate the transfer of moisture deeper in the bed due to a decrease in the rate of evaporation (drying decreases as equilibrium moisture conditions are approached) from the material. It can also be understood from the behaviour of the simulated model that heat is being quenched from the inlet air and the extent of this quenching with time increases as the gas moves through the bed, as a result of which temperature rises much more gradually deeper within the bed.

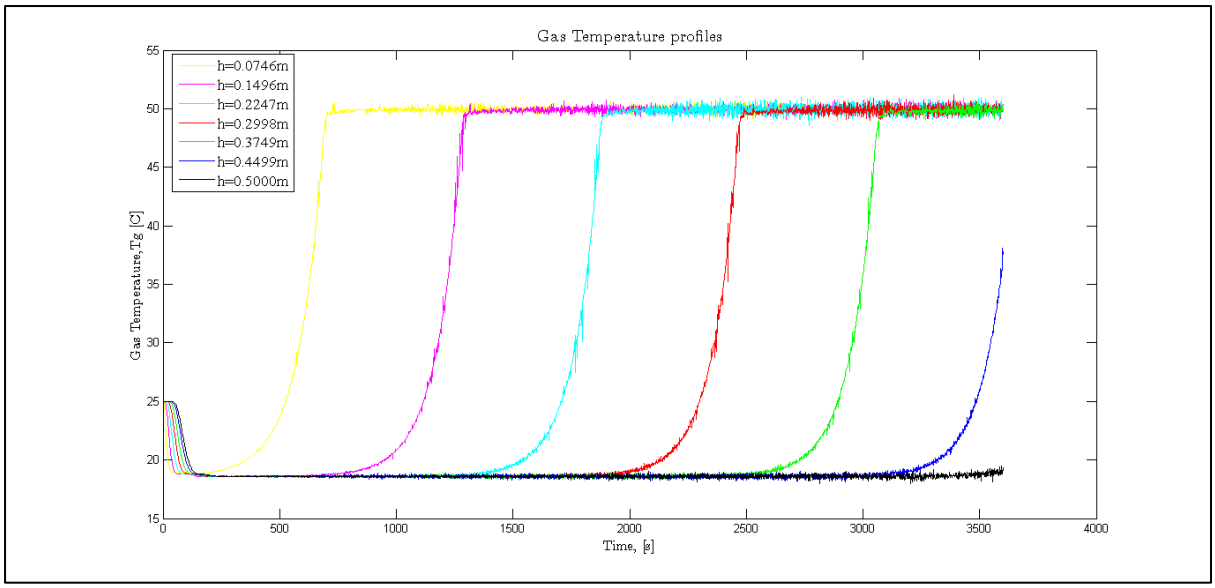

Figure 10: Air Temperature versus time

Figure 11 shows the grass moisture content distribution profiles as a function of time for various bed heights. At a particular bed depth, as the moisture content of the material approaches the critical moisture content (at the end of the constant drying period) the drying rate decreases. This results in the onset of the falling-rate drying period and moisture content falls. It can be seen that the surface of grass which is directly exposed to the drying medium approaches equilibrium moisture conditions faster than deeper in the bed. The moisture removal is small towards the end of the drying period (approaching equilibrium moisture conditions) because of the dependence of moisture diffusivity on temperature and grass moisture content.

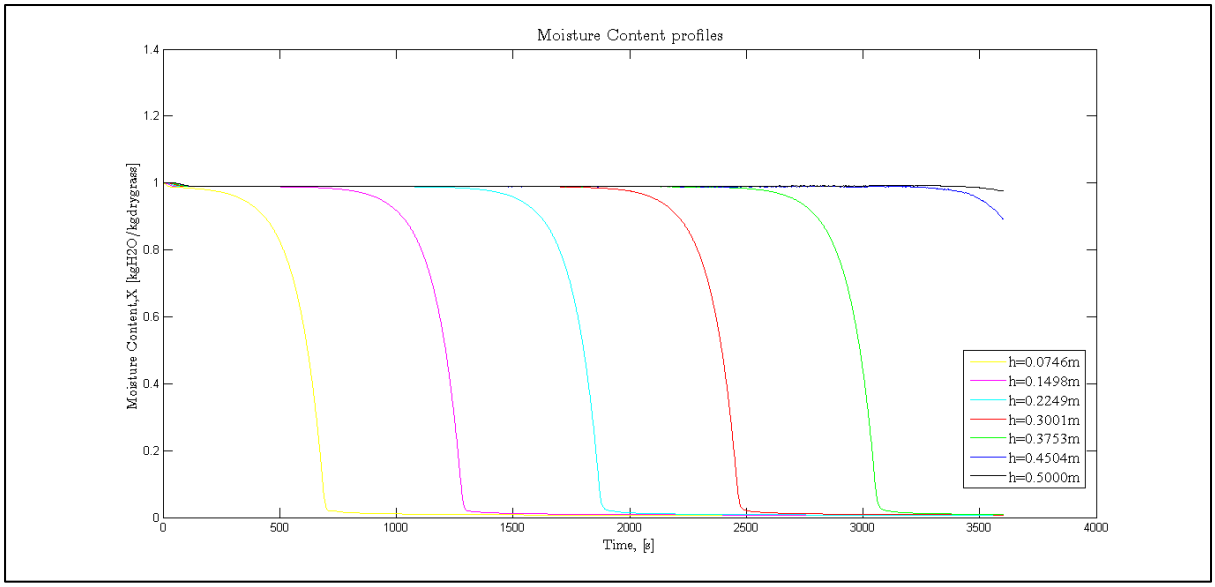

Figure 11: Grass Moisture Content versus time

Figure 12 shows the variation of the grass temperature as a function of time at different bed heights. At a particular height in the bed, with an increase in time there is an increase in the temperature of the grass. The initial decrease in the grass temperature with time is due to moisture condensation on the surface of the grass and the subsequent evaporation of

unbounded moisture from the surface. Once the temperature on the grass surface rises above the wet-bulb temperature of the grass, surface-transfer takes place and continues till the surface temperature approaches the dry-bulb temperature of the air. This leads to the reduction of the temperature driving force for heat transfer.

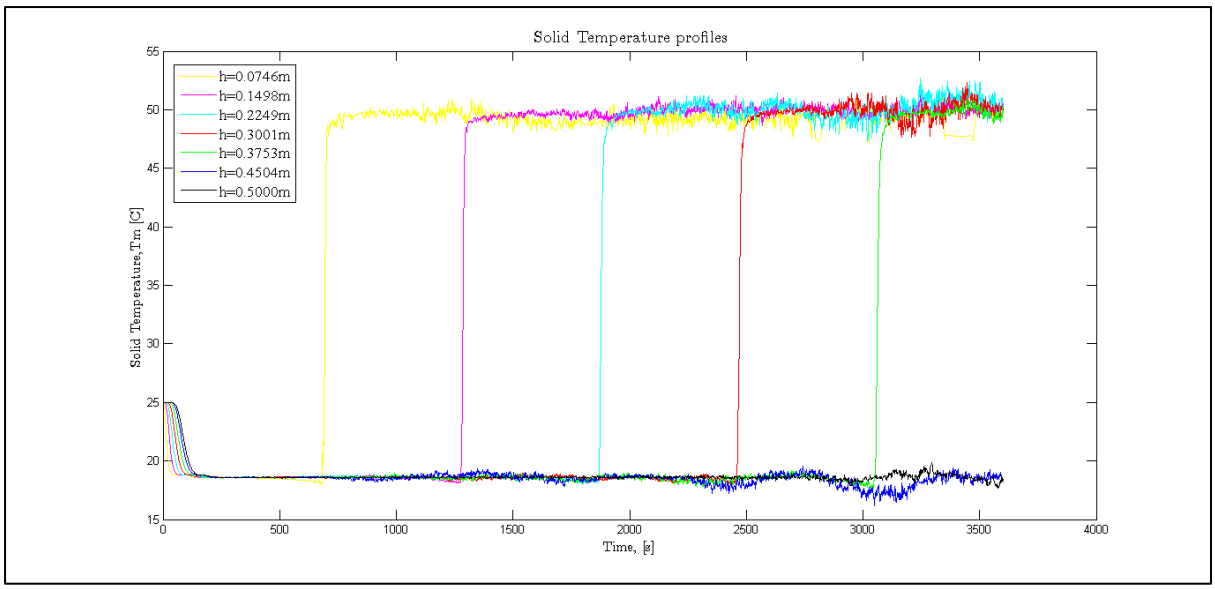

Figure 12: Grass Temperature versus time

5.2.2. Varying flow rates

The following section aims to understand the influence of varying the inlet air flow rates on the drying process. In this case inlet flow rate of the drying medium has been varied and its influence analysed without varying the rest of the process parameters described in Table 5-3.

The parameters used for the simulation after varying the air flow rate have been presented in Table 5-4.

Table 5-4: Simulation Parameters when flow rate=30 $Nlmin^{-1}$

dt	1 s
Total drying time	60 min
Inlet gas temperature, T_g	50 (°C)
Drying Medium Flow rate, W_B	30 $\left(\frac{Nl}{min}\right)$
Number of grid points in space, N_s	1000

In Figure 13, Figure 14, Figure 15 & Figure 16; the variation in the humidity, gas temperature, solid temperature and moisture content distribution with height at various time intervals have been presented for the parameters mentioned in Table 5-4 above.

The heat and mass flux are influenced by the increase in the air flow rate which in turn has a direct influence on the convective transport coefficients.

From Figure 13, it can be seen that for a particular height in the fixed bed, a decrease in the air flow rate increases the humidity. This happens because at a decreased flow rate, the rate of evaporation from the surface of the solid decreases (drying rate falls much more slowly) and hence increasing the drying time at each individual depth. Since the air leaving the bed is expected to be saturated; with an increase in the air flow (Figure 9), the air is assumed to be capable of taking more water vapour out of the dryer bed.

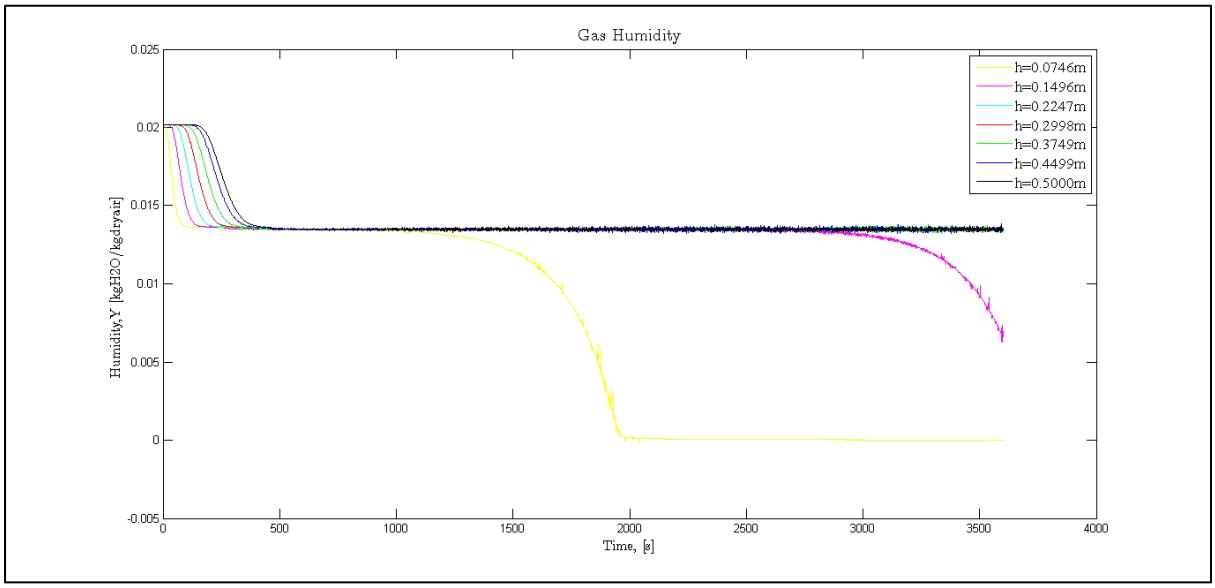

Figure 13: Humidity versus bed time

Figure 14 shows the variation in the inlet gas temperature with bed height at various points in time for the inlet gas flow rates of $30\frac{Nl}{min}$. By comparison with Figure 10 it can be seen that for decreased flow rates at a fixed bed depth, with a decrease in the air flow rate with time, the amount of heat transferred to the grass from the air is decreased (indicating quenching of the exhaust air) and also that layer dries up faster at higher flow rates.

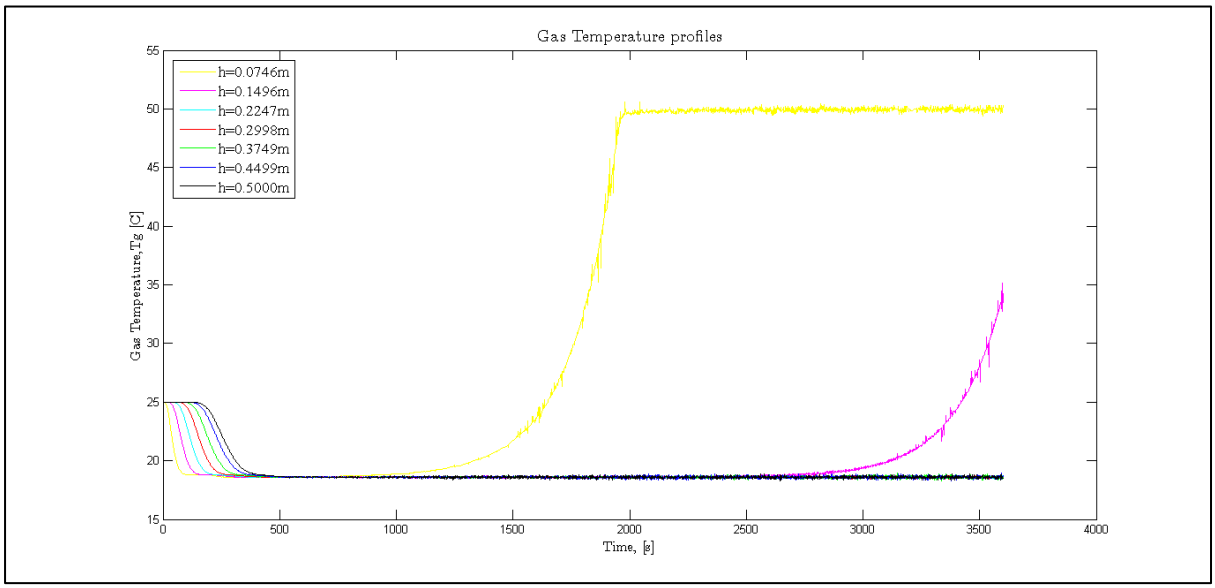

Figure 14: Gas Temperature versus time

Figure 15 shows the variation in the grass moisture content with height for various points in time for the inlet gas velocities of $30\frac{Nl}{min}$. By comparison with Figure 11, it can be seen that for increased flow rates, the moisture content is lower for a fixed depth of the bed due to the fact that with increased air flow rates there is an increase in the rate of evaporation from the surface (drying rate falls much faster) of the solid which results reduction in the total drying time.

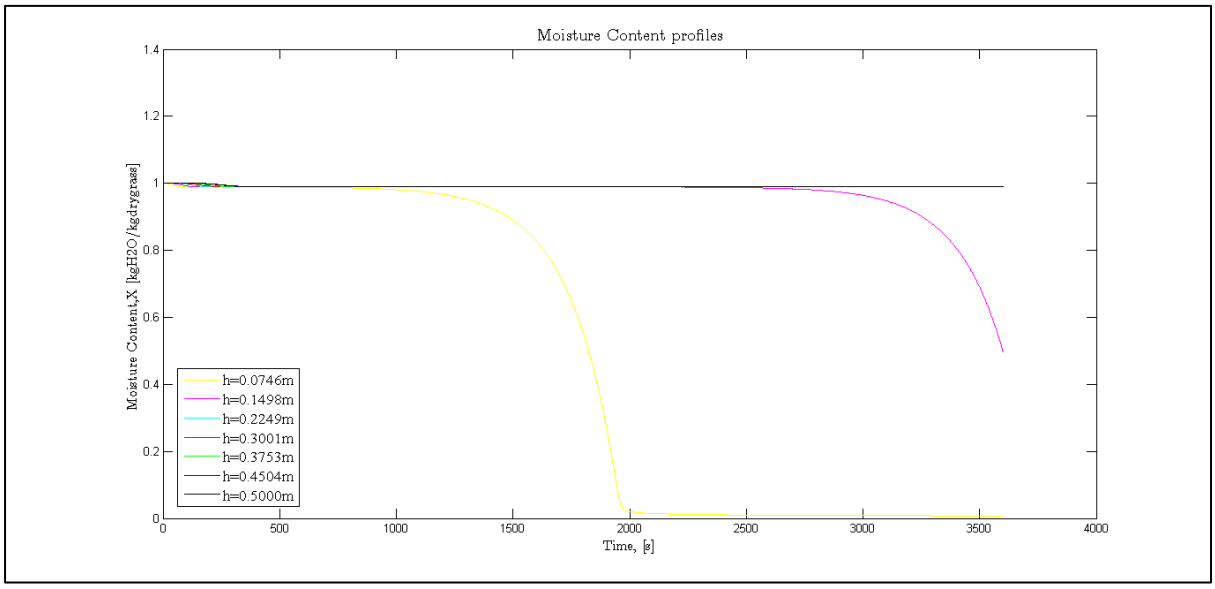

Figure 15: Grass Moisture Content versus time

Figure 16 shows the variation in the grass temperature with height for various points in time for the inlet gas velocities of $30\frac{Nl}{min}$. By increasing the air flow rate (in comparison with Figure 12) there is an increase in heat transferred and as a result the temperature at that depth approaches the dry-bulb temperature of gas and thus equilibrium conditions faster. For a fixed bed depth, the variation in solid temperature with time is insignificant.

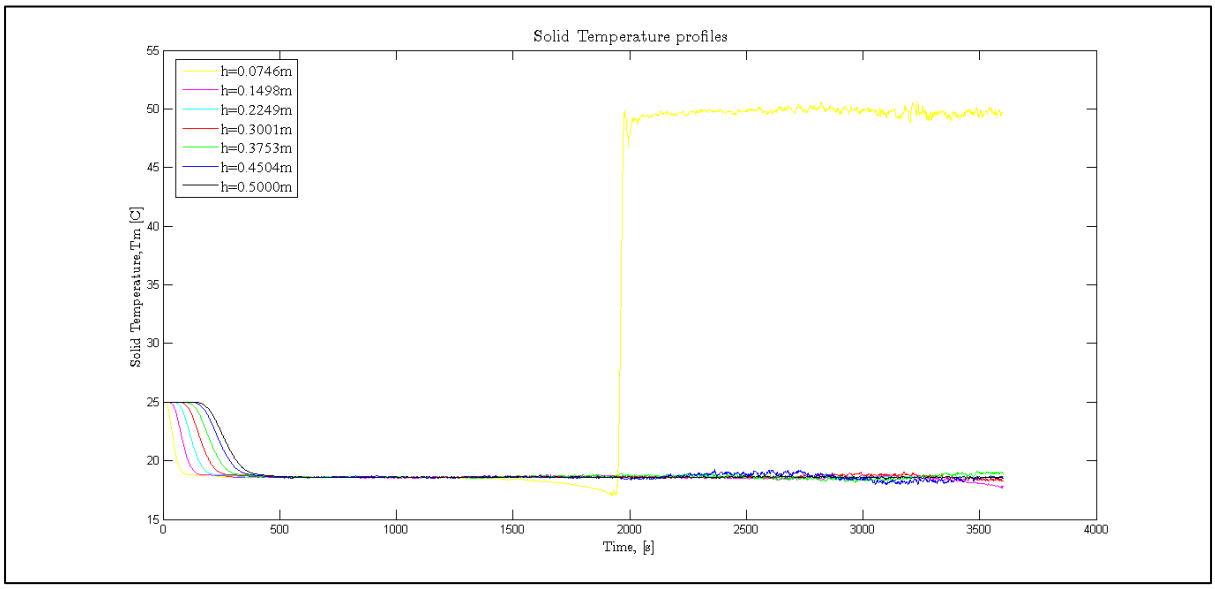

Figure 16: Grass Temperature versus time

It can be inferred that by increasing the inlet air flow rate, the time for drying decreases because there is an increase in the rate of evaporation from the surface of grass. This indicates that with increase in the air flow there is an effect on the convective heat and mass flux which in turn increases the rate of evaporation of water from the surface.

5.2.3. Comparison of simulated and experimental results

One of objectives of this work is to validate the computer model developed by using data from experiments performed for drying verge grass. The model's prediction of moisture distribution in the grass, air temperature and the absolute humidity of the air are investigated under different drying conditions.

This section compares the results generated by computer simulations executed with inlet gas temperature at 50℃ and a flow rate of $30\frac{Nl}{min}$ to the results obtained at similar conditions from experiments.

Three thermocouples are placed within the column ('TC3', 'TC4' & 'TC5') which measured the temperature of the air passing through at different depths (60mm, 180mm and 300mm) of the bed. The inlet and outlet gas temperatures were tracked by the thermocouples placed before ('TC2') and after ('TC6') the column. Computer simulations play an important role in understanding the variation in solid temperature and the results at different bed depths could be compared with the experimental observations to validate the simulated model.

By comparing experimental results with the gas temperatures from the simulated model at individual bed depths (Figure 17, Figure 18 and Figure 19), it can be clearly seen that the simulations result in significant differences in comparison to the experiments. The temperature curves resulting from the simulations (Figure 17) show that the temperature of the air is relatively stable till about 1000s (probably indicating that this occurs due to heat from the air being quenched as the air moves through the column) after which it shows an increasing trend due to the reduction in the absolute humidity of the air with time. Also noticeable, is the sharp gradient in the gas temperature before it approached the dry-bulb temperature of the inlet gas and thus equilibrium moisture conditions. On the other hand, the temperature profile obtained from experiments show an increasing trend till about 1000s and then gradually becomes stable as it approached equilibrium moisture conditions. The profiles generated by both the simulations and the experiments are in agreement as they approach equilibrium conditions.

The behaviour of the simulation against experimental observation at the middle and top of the column is shown in Figure 18 and Figure 19. The temperature profiles from the simulations at the middle and the top of the column also show that drying takes longer in the simulations in comparison to the experiments performed. It was noticed that the transport coefficients generated by the model correlations were high. This could be due to the use of packed bed correlations for the heat and mass transport coefficients in the model and not using separate transport coefficients for the gas and solid phase. These correlations for heat and mass transfer need to be investigated and incorporated into the model before it is applied to further validation in this particular case.

It should also be mentioned that probably some of the assumptions made during modelling development need further investigation along with the numerical schemes to understand why the agreement with experimental data fails.

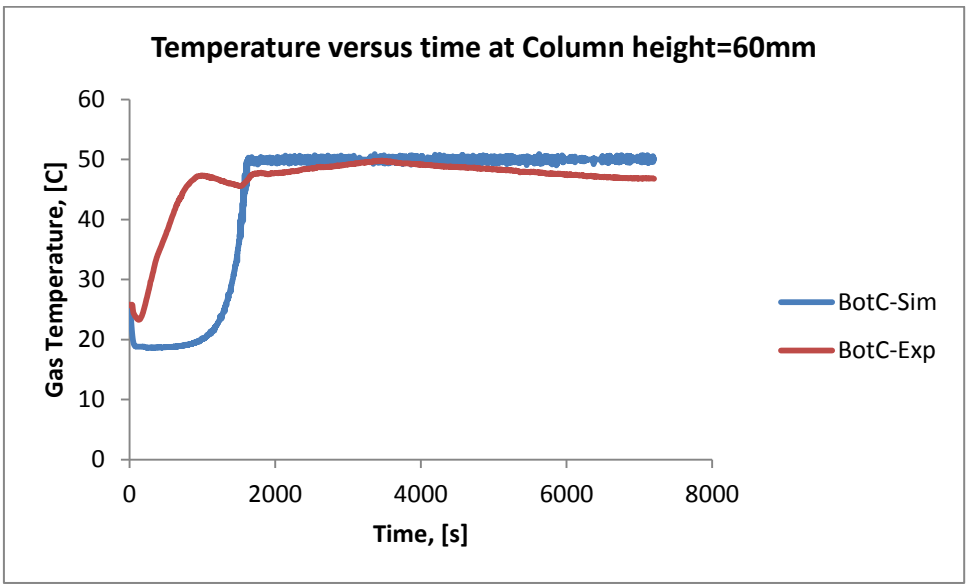

Figure 17: Predicted and Experimental Temperature measured at the bottom of the column with time

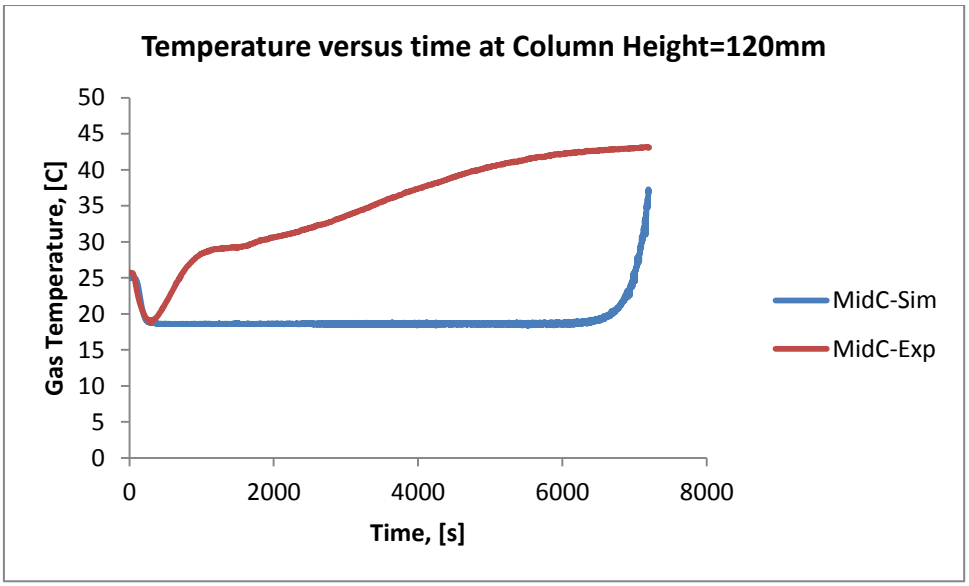

Figure 18: Predicted and Experimental Temperature measured at the middle of the column with time

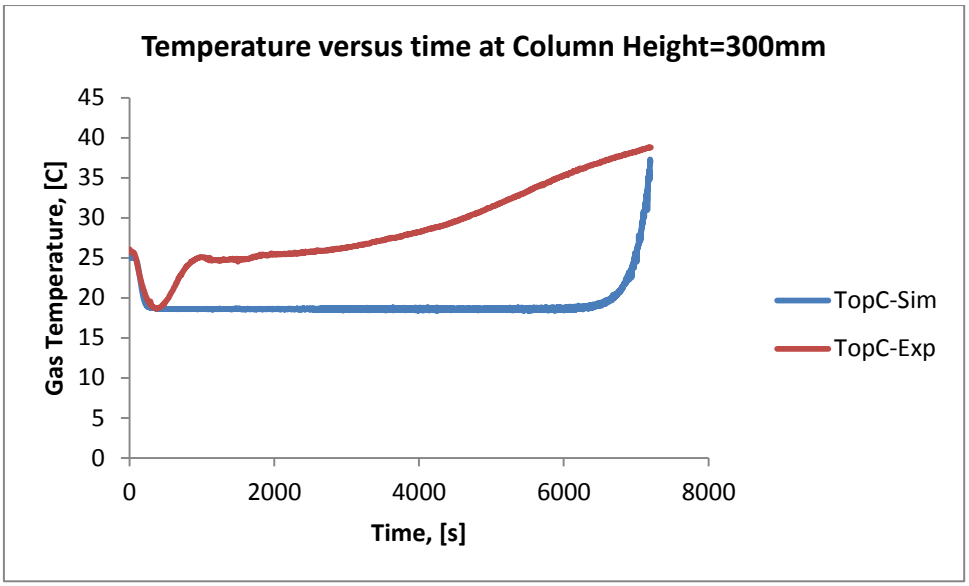

Figure 19: Predicted and Experimental Temperature measured at the top of the column with time

5.2.4. Varying Inlet Gas Temperature

In the section that follows, the inlet gas temperature is increased from the value set in the previous section and is held constant at 70℃. To understand the influence of the increase in inlet gas temperature on the driving force for drying, the profiles obtained for the gas humidity and the moisture content of the solid with time have been illustrated. Further, an attempt has been made to compare with the profiles obtained at an inlet gas temperature of 50℃. The profiles generated at a higher temperature of 90℃ are included in Appendix 4.

The parameters in the simulation used are presented in the Table 5-5 below:

Table 5-5: Simulation Parameters

dt	1 second
Total drying time	60 minutes
Inlet gas temperature, T_g	70 (℃)
Drying Medium Flow rate, W_B	90 $\left(\frac{Nl}{min}\right)$
Number of grid points in space, N_s	2000

Figure 20 illustrates the variation in the moisture content with time by increasing the inlet gas temperature. With increase in the inlet gas temperature, the moisture content at a fixed bed depth with time is relatively lower when compared against moisture content distribution at a lower inlet gas temperature. This is due to the fact that with an increase in the temperature there is an increase in the amount of water evaporating from the surface of grass (increase in the drying potential which in turn increases the convective fluxes from the grass).

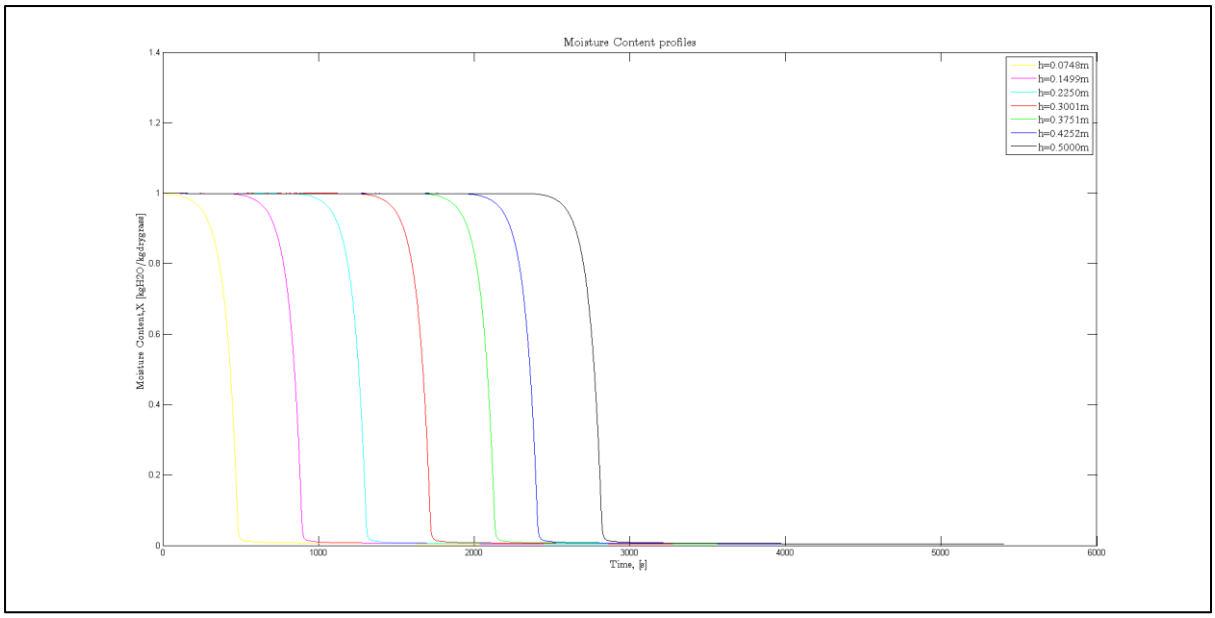

Figure 20: Grass Moisture Content versus time

It can be inferred from these figures that with an increase in the inlet gas temperature, there is a direct effect on the drying process (drying potential increases and driving force for drying reduces) with the rate of evaporation of water increasing as the total time for drying reduces.

This behaviour with regard to sensitivity with flow rate and increase in inlet gas temperature is in line with results described in literature for tests carried out for drying other materials such as grains[29], tropical fruits[47] and bananas[48].

5.2.5. Sensitivity to grid points in space and time

Figure 21 & Figure 22, it can be clearly seen that the model is largely stable/insensitive to the number of grid points when the flow rate is 90 $\left(\frac{Nl}{min}\right)$ and inlet gas temperature is 70℃ (only moisture content variation shown here) in space and time at a constant inlet gas temperatures and flow rate. In this section the number of grid points has been varied only by a factor of 2 whereas the number of grid points in time has been varied by increasing drying time from 45 to 60 minutes. Variation of the number of grid points by increasing or decreasing them in space or time at different inlet conditions have been presented in Appendix 4.

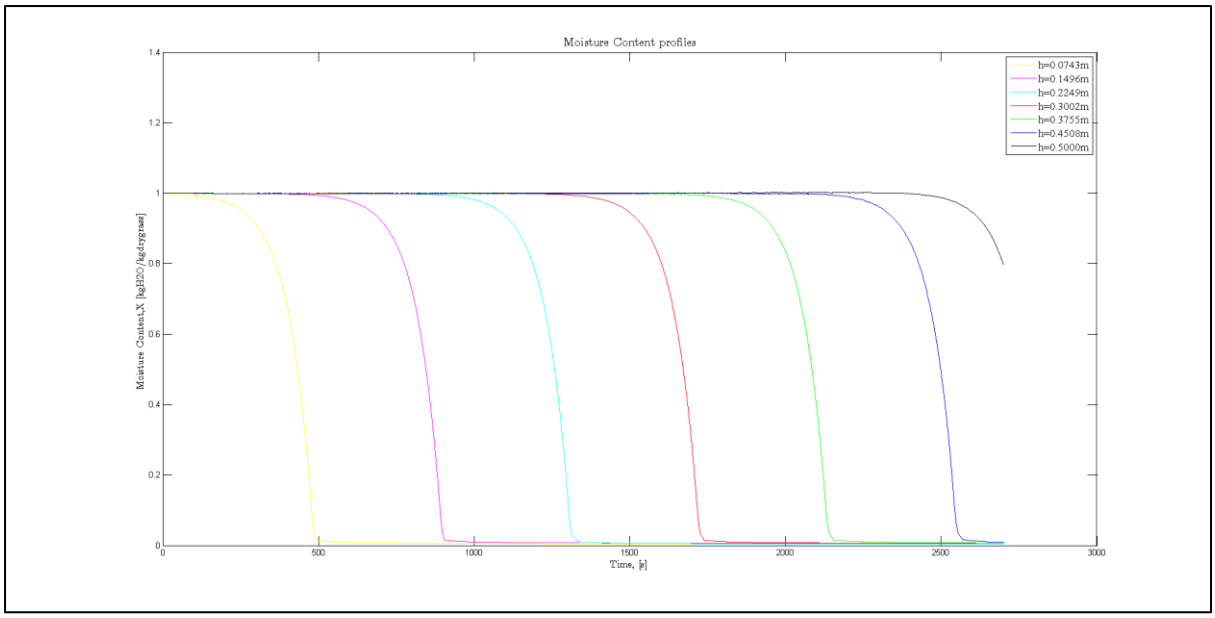

Figure 21: Grass Moisture Content versus time (Ns=500, Nt = 2700)

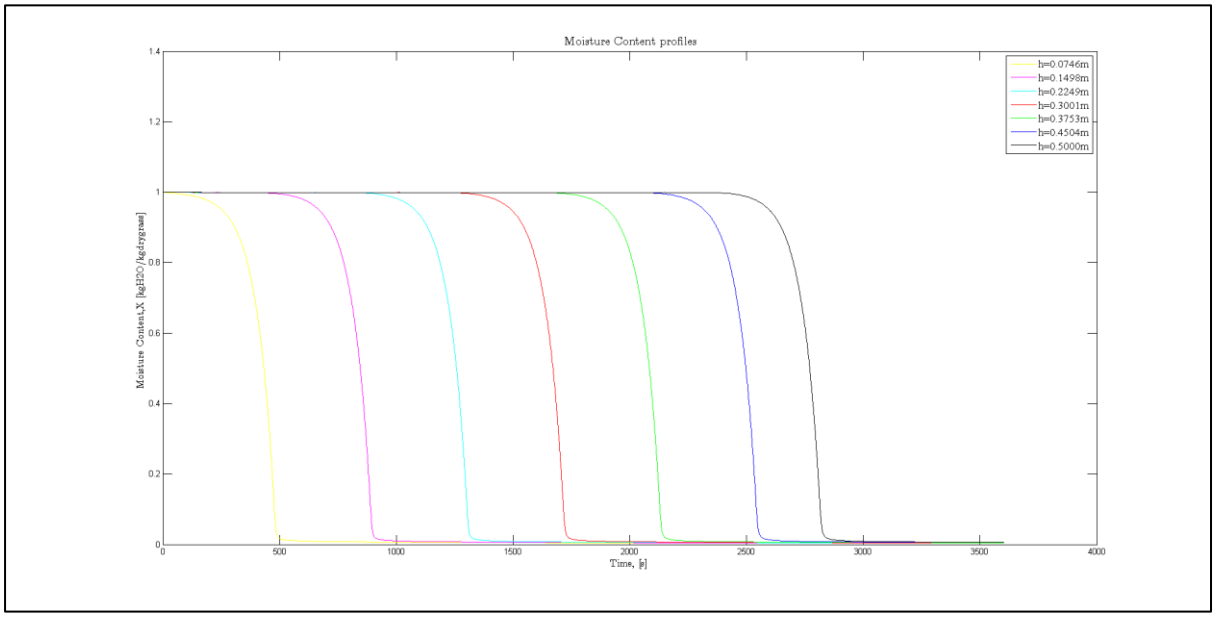

Figure 22: Grass Moisture Content versus time (Ns = 1000, Nt = 3600)

It must be stated here that when much smaller number of grid points were chosen in space. There are inconsistencies generated in the moisture content values as mentioned previously (where unchecked it drops to negative values). Therefore, the number of grid points in space must be chosen reasonably.

6. Conclusion & Recommendations

6.1. Conclusions

Studies available in literature describe the development of mathematical models and the investigation of the influence of varying process parameters in deep bed drying[27,29,31,48]. This work though was primarily aimed at understanding the theory behind the model development available in the work of Mujumdar[26] and also to perform a parameter analysis (to understand the influence of varying inlet air flow rates, inlet air temperatures, sensitivity to variation of grid points in space or time) for the case of verge grass drying in deep beds.

This section of the report serves to provide an overview of the various sections and results obtained in this study:

- A model for the drying of verge grass in deep beds has been investigated and presented in this work.
- The influence of varying process parameters such as the inlet air flow rate and inlet gas temperature have been investigated and analysed. It was found that the drying time reduced because of the increase in the rate of evaporation when either the flow rate or gas temperature was increased. However the increase in the air flow rate would probably imply higher consumption of electrical energy, but the drying process would on the other hand be more productive.
- It is also found that when the model when simulated for a reasonable number of grid points in space and time (mainly chosen by using the trial and error approach) was largely insensitive with regard to the spacing. However when the choice of grid points was done for a smaller number of grid points in space, it fails and hence the alteration with regard to increment scheme needs to be investigated possibly by changing the numerical scheme used.
- The validation process of the model largely fails, probably due to the usage of transport correlations for a packed bed (the Reynolds number generated was within the range for the mass transport coefficient (shown in Appendix 3) and not within the range for the heat transport coefficient).
- The assumptions made to reduce the complexity during model development, probably reduce the range of application for these models by neglecting phenomena which may occur in experiments performed in deep beds. The same holds for the transport correlations used in the process of modelling which need to further investigated to test their validity.

6.2. Recommendations

- The model fails in accurately resulting in an agreement between the experimental results and computer simulations. This could be attributed to the correlations used for heat and mass transport coefficient which in some cases generated values which were significantly high (probably higher than in actual experiments, some values shown for a certain position in the bed in Appendix 3) in comparison with experimental obtained values. These need to be corrected by using proper correlations for the transfer

coefficients for grass obtained from experiments and by not one using which has been developed for packed beds.

- In order to find use over large increments in space and time the numerical scheme needs to be further investigated and modified/altered before it is applied in further studies.
- There exists work in literature which has been performed for malt and hazelnut which describe the thin layer drying rate being defined in terms of the equilibrium moisture content values; this could be investigated for the case of grass. This could be investigated for improving the model to generate results which are in agreement with experimentally obtained values.
- Further, higher order discretization methods can be investigated to check if they generate results (cases where numerical schemes investigated in this model fail) which are in agreement with the experiments and have advantages over the first order discretization used in this work.

References

1. Haket C. On - site drying of verge grass for large scale co - combustion (MSc. Thesis). 2012;(July).

2. Brundtland GH. *Report of the World Commission on environment and development:" our common future."*; 1987.

3. Naik SN, Goud V V., Rout PK, Dalai AK. Production of first and second generation biofuels: A comprehensive review. *Renew Sustain Energy Rev*. 2010;14:578–597. doi:10.1016/j.rser.2009.10.003.

4. Dragone G, Fernandes B, Vicente A, Teixeira J. Third generation biofuels from microalgae. *Curr Res Technol Educ Top Appl Microbiol Microb Biotechnol*. 2010:1355–1366.

5. Demirbas A, Fatih Demirbas M. Importance of algae oil as a source of biodiesel. *Energy Convers Manag*. 2011;52(1):163–170. doi:10.1016/j.enconman.2010.06.055.

6. Delft TU. *Biomass composition, properties and characterization, Lecture Notes ('Energy from Biomass')*.; 2014.

7. Sheldon RA. Utilisation of biomass for sustainable fuels and chemicals: Molecules, methods and metrics. *Catal Today*. 2011;167(1):3–13. doi:10.1016/j.cattod.2010.10.100.

8. Chew JJ, Doshi V. Recent advances in biomass pretreatment – Torrefaction fundamentals and technology. *Renew Sustain Energy Rev*. 2011;15(8):4212–4222. doi:10.1016/j.rser.2011.09.017.

9. Edenhofer O, Pichs-Madruga R, Sokona Y. *Renewable energy sources and climate change mitigation: Special report of the intergovernmental panel on climate change*. Cambridge University Press; 2011.

10. Demirbas MF, Balat M, Balat H. Potential contribution of biomass to the sustainable energy development. *Energy Convers Manag*. 2009;50:1746–1760. doi:10.1016/j.enconman.2009.03.013.

11. Dell R., Rand DA. Energy storage -□" a key technology for global energy sustainability. *J Power Sources*. 2001;100(1-2):2–17. doi:10.1016/S0378-7753(01)00894-1.

12. IEA. Database of Biomass Cofiring initiatives. Available at: http://www.ieabcc.nl/database/cofiring.html. Accessed January 31, 2015.

13. Pedroli B, Elbersen B, Frederiksen P, et al. Is energy cropping in Europe compatible with biodiversity? – Opportunities and threats to biodiversity from land-based production of biomass for bioenergy purposes. *Biomass and Bioenergy*. 2013;55:73–86. doi:10.1016/j.biombioe.2012.09.054.

14. ECN. Verge Grass (#1301). *Phyllis Database*. Available at: https://www.ecn.nl/phyllis2/Browse/Standard/ECN-Phyllis#verge grass. Accessed January 31, 2015.

15. Ståhl M, Granström K, Berghel J, Renström R. Industrial processes for biomass drying and their effects on the quality properties of wood pellets. *Biomass and Bioenergy*. 2004;27(6):621–628. doi:10.1016/j.biombioe.2003.08.019.

16. Agriculture, Food and Rural Affairs M of. Biomass Burn Characteristics. Available at: http://www.omafra.gov.on.ca/english/engineer/facts/11-033.htm. Accessed January 31, 2015.

17. ECN. Wood, willow (#345). *Phyllis Database*. Available at: https://www.ecn.nl/phyllis2/Browse/Standard/ECN-Phyllis#willow. Accessed January 31, 2015.

18. Mujumdar AS. Principles, Classification, and Selection of Dryers. In: *Handbook of Industrial Drying, Third Edition*. CRC Press; 2006. doi:10.1201/9781420017618.pt1.

19. Bates RB, Ghoniem AF. Modeling kinetics-transport interactions during biomass torrefaction: The effects of temperature, particle size, and moisture content. *Fuel*. 2014;137:216–229. doi:10.1016/j.fuel.2014.07.047.

20. Joshi Y, de Vries H, Woudstra T, de Jong W. Torrefaction: Unit operation modelling and process simulation. *Appl Therm Eng*. 2015;74:83–88. doi:10.1016/j.applthermaleng.2013.12.059.

21. Menshutina N, Kudra T. COMPUTER AIDED DRYING TECHNOLOGIES. *Dry Technol*. 2001;19(8):1825–1849. doi:10.1081/DRT-100107275.

22. Cenkowski S, Jayas DS, Pabis S. Deep-Bed Grain Drying - A Review of Particular Theories. *Dry Technol*. 1993;11(7):1553–1582. doi:10.1080/07373939308916919.

23. López A, Piqué MT, Romero A. SIMULATION OF DEEP BED DRYING OF HAZELNUTS. *Dry Technol*. 1998;16(3-5):651–665. doi:10.1080/07373939808917428.

24. Zare D, Chen G. Evaluation of a simulation model in predicting the drying parameters for deep-bed paddy drying. *Comput Electron Agric*. 2009;68(1):78–87. doi:10.1016/j.compag.2009.04.007.

25. MATLAB. 2012.

26. Pakowski Z, Mujumdar A. Basic Process Calculations and Simulations in Drying. In: *Handbook of Industrial Drying, Third Edition*. CRC Press; 2006. doi:10.1201/9781420017618.ch3.

27. López A, Virseda P, Martinez G, Llorca M. DEEP LAYER MALT DRYING MODELLING. *Dry Technol*. 1997;15(5):1499–1526. doi:10.1080/07373939708917305.

28. López A, Piqué MT, Boatella J, Ferrán A, Garcia J, Romero A. Drying Characteristics of the Hazelnut. *Dry Technol*. 1998;16(3-5):627–649. doi:10.1080/07373939808917427.

29. Srivastava VK, John J. Deep bed grain drying modeling. *Energy Convers Manag*. 2002;43(13):1689–1708. doi:10.1016/S0196-8904(01)00095-4.

30. Nellist M. The drying of ryegrass seeds in deep layers (PhD Thesis). 1974;1&2.

31. Herman E, Rodríguez GC, García MA. MATHEMATICAL MODELING FOR FIXED-BED DRYING CONSIDERING HEAT AND MASS TRANSFER AND INTERFACIAL PHENOMENA*. *Dry Technol*. 2001;19(9):2343–2362. doi:10.1081/DRT-100107503.

32. Karunanithy C, Muthukumarappan K, Donepudi a. Moisture sorption characteristics of switchgrass and prairie cord grass. *Fuel*. 2013;103:171–178. doi:10.1016/j.fuel.2012.05.004.

33. Colin F, Gazbar S. Distribution of water in sludges in relation to their mechanical dewatering. *Water Res*. 1995;29(8):2000–2005. doi:10.1016/0043-1354(94)00274-B.

34. Tsang KR, Vesilind PA. Moisture distribution in sludges. *Water Sci Technol*. 1990;22(12):135–142.

35. Yoshida T, Sasaki H, Takano T, Sawabe O. Dewatering of high-moisture wood chips by roller compression method. *Biomass and Bioenergy*. 2010;34(7):1053–1058. doi:10.1016/j.biombioe.2010.02.013.

36. Delft TU. *Biomass Pretreatment Lecture Notes ('Energy from Biomass')*.; 2014.

37. Delft TU. Dryer. Available at: http://www.io.tudelft.nl/onderzoek/onderzoeksprogrammas/technology-transformation/design-for-sustainability-emerging-markets/sub-theme-3-emerging-markets/reinvent-the-toilet/team-process-energy-3me/dryer/.

38. Sun D-W, Woods JL. SIMULATION OF THE HEAT AND MOISTURE TRANSFER PROCESS DURING DRYING IN DEEP GRAIN BEDS. *Dry Technol*. 1997;15(10):2479–2492. doi:10.1080/07373939708917371.

39. Dincer I. On energetic, exergetic and environmental aspects of drying systems. *Int J Energy Res*. 2002;26(8):717–727. doi:10.1002/er.792.

40. Henley E, Seader J. *Separation process principles*. 2nd ed.; 2006.

41. Sitompul JP, Widiasa IN. MODELING AND SIMULATION OF DEEP-BED GRAIN DRYERS. *Dry Technol*. 2001;19(2):269–280. doi:10.1081/DRT-100102903.

42. Sharp JR. A review of low temperature drying simulation models. *J Agric Eng Res*. 1982;27(3):169–190. doi:10.1016/0021-8634(82)90060-9.

43. Marinos-Kouris D, Maroulis ZB. Transport Properties in the Drying of Solids. In: *Handbook of Industrial Drying, Third Edition*. CRC Press; 2006. doi:10.1201/9781420017618.ch4.

44. Smith JM, Van Ness HC, Abbott MM. *Introduction to Chemical Engineering Thermodynamics*. 6th ed. McGraw Hill; 2001.

45. Agarwal S. Fundamentals of Finite Difference Methods. 2014. Available at: http://www.leb.eei.uni-erlangen.de/winterakademie/2010/report/content/course02/pdf/0203.pdf. Accessed May 10, 2014.

46. Maloney JO. Conversion Factors and Mathematical Symbols. In: Green DW, Perry RH, eds. *Perry's Chemical Engineer's Handbook*. McGraw Hill.

47. Karim MA, Hawlader MNA. Mathematical modelling and experimental investigation of tropical fruits drying. *Int J Heat Mass Transf*. 2005;48(23-24):4914–4925. doi:10.1016/j.ijheatmasstransfer.2005.04.035.

48. Karim MA, Hawlader MNA. Drying characteristics of banana: theoretical modelling and experimental validation. *J Food Eng*. 2005;70(1):35–45. doi:10.1016/j.jfoodeng.2004.09.010.

49. ode45. *Inc, The Mathworks*. 2014. Available at: http://nl.mathworks.com/help/matlab/ref/ode45.html. Accessed December 15, 2014.

50. Shampine LF, Reichelt MW. The MATLAB ODE Suite. *SIAM J Sci Comput*. 1997;18(1):1–22. doi:10.1137/S1064827594276424.

51. ode23. *Inc, The Mathworks*. 2014. Available at: http://nl.mathworks.com/help/matlab/math/ordinary-differential-equations.html. Accessed January 15, 2015.

APPENDIX

APPENDIX 1: (ODE45 Solver)

The ode-45 solver is used when non-stiff differential equations are solved. The order of accuracy of the solution is of medium order[49]. It is based on an explicit Runge-Kutta (4, 5) formula, the Dormand prince pair. It is a one-step solver in computing $y(t_n)$ it only needs the solution at the preceeding point $y(t_{n-1})$ [49,50]. This type of solver is in general, the best function to apply as a first try for most problems.

The basic syntax for calling the ODE solver is of the type[49]:

$$[T, Y] = solver(odefun, tspan, y0, options)$$

The detailed description of the solver and the function arguments to be specified can be found on the Mathworks website[49].

APPENDIX 2: (ODE23 Solver)

This is based on an explicit Runge-Kutta (2, 3) pair of Bogacki and Shampine. It is more efficient in comparison to ode45 at crude tolerances and in the presence of mild stiffness and is one step solver[51]. The syntax for calling the ode23 solver is similar to the one for calling the ode45 solver and the detailed description is provided on the Mathworks website[51].

APPENDIX 3: Calculation Checks and Temperature Dependent Correlations

1) Reynolds Number

This section attempts to check if the calculated Reynolds number calculated at the particle level can be implemented at the different flow rate considerations under which the model has been simulated.

a) Flow rate = 90 $Nlmin^{-1}$

$$Re = \left(\frac{u_B.\rho_B.d_p}{\mu_B}\right) = \frac{90 * 10^{-3} * 1.21 * 3 * 10^{-3}}{60 * 2.0750 * 10^{-5}} = 133.6441$$

Where,

u_B is the superficial air velocity $\left(\frac{m}{s}\right)$,
ρ_B is the density of dry air $\left(\frac{kg_{dryair}}{m^3_{bed}}\right)$,
d_p is the particle diameter (m) and
μ_B is the dynamic viscosity of the air $\left(\frac{kg}{m-s}\right)$.

Clearly, this is applicable only for the mass transfer correlation and the correlation is not valid for the heat transfer regime and this needs to be further investigated.

b) Flow rate = 30 $Nlmin^{-1}$

$$Re = \left(\frac{u_B.\rho_B.d_p}{\mu_B}\right) = \frac{30 * 10^{-3} * 1.21 * 3 * 10^{-3}}{60 * 2.0750 * 10^{-5}} = 44.5480$$

Where,

u_B is the superficial air velocity $\left(\frac{m}{s}\right)$,
ρ_B is the density of dry air $\left(\frac{kg_{dryair}}{m^3_{bed}}\right)$,
d_p is the particle diameter (m) and
μ_B is the dynamic viscosity of the air $\left(\frac{kg}{m-s}\right)$.

Clearly, this is applicable only for the mass transfer correlation and the correlation is not valid for the heat transfer regime and this needs to be further investigated.

2) Void Fraction Calculation

$$\varepsilon = 1 - \frac{\rho_{bulk}}{\rho_{overall}} = 1 - \frac{100}{200} = 0.5$$

Where,

ρ_{bulk} is the bulk density $\frac{kg_{dry-grass}}{m^3}$ and

$\rho_{overall}$ is the solid density $\frac{kg_{wet-grass}}{m^3}$

3) Heat and Mass transport coefficients

	Heat transfer Coefficient	*Mass transfer coefficient*
Flow= 90$\left(\frac{Nl}{min}\right)$ *Tg=50* (℃) *Drying Time = 60 min Ns=1000*	Calculated between points (located at 60 mm and 180 mm) in the bed: ~ 667 $\left(\frac{W}{kg-K}\right)$	Calculated between points (located at 60 mm and 180 mm) in the bed: 0.6935 $\left(\frac{kg_{H2O}}{kg_{drygrass}-s}\right)$
Flow= 30$\left(\frac{Nl}{min}\right)$ *Tg=50* (℃) *Drying Time = 60 min Ns=1000*	~ 350 $\left(\frac{W}{kg-K}\right)$	0.4048 $\left(\frac{kg_{H2O}}{kg_{drygrass}-s}\right)$
Flow= 90$\left(\frac{Nl}{min}\right)$ *Tg=70* (℃) *Drying Time = 90 min Ns=2000*	~ 668 $\left(\frac{W}{kg-K}\right)$	0.6935 $\left(\frac{kg_{H2O}}{kg_{drygrass}-s}\right)$

4) Biot Number Check for Wood Sample

Considering the following:

- Characteristic Length 'L_c'= 10 μm
- Thermal Conductivity of Wood = 0.17 $\left(\frac{W}{m-K}\right)$ obtained from the engineering toolbox website for oak wood.
- Heat transfer Coefficient of around = 50 $\left(\frac{W}{m^2-K}\right)$

$$Bi = \frac{hL_c}{k_b} = \frac{50 * 10 * 10^{-6}}{0.17} = 0.00294$$

5) Specific Heat Capacity coefficients and correlation obtained from Introduction to Chemical Engineering Thermodynamics[44] by Smith and Van Ness.

$$C_p(T) = A + BT + CT^2 + DT^{-2}, \frac{kJ}{kg}$$

	A	*B*	*C*	*D*
Water, vapour	3.470	$1.450 * 10^{-3}$	0	$0.121 * 10^5$
Water,liquid	8.712	$1.25 * 10^{-3}$	$-0.18 * 10^{-6}$	0
Air	3.355	$0.575 * 10^{-3}$	0	$-0.016 * 10^{-5}$

6) Coefficient for Antoine Equation Correlation for calculation of saturated vapour pressure obtained from Chapter 3 of the Handbook of Industrial Drying[26].

$$p^S = \exp\left(A - \frac{B}{C + t}\right), kPa$$

	A	B	C
Water	16.376953	3878.8223	229.861

APPENDIX 4: Additional Plots generated

Additional plots (process variables versus height and time) generated from the test simulations at different conditions have been presented in this section

1) Flow rate = 30$\frac{\boldsymbol{Nl}}{\boldsymbol{min}}$, Tg = 50℃, Ns=300 and drying time = 30 minutes

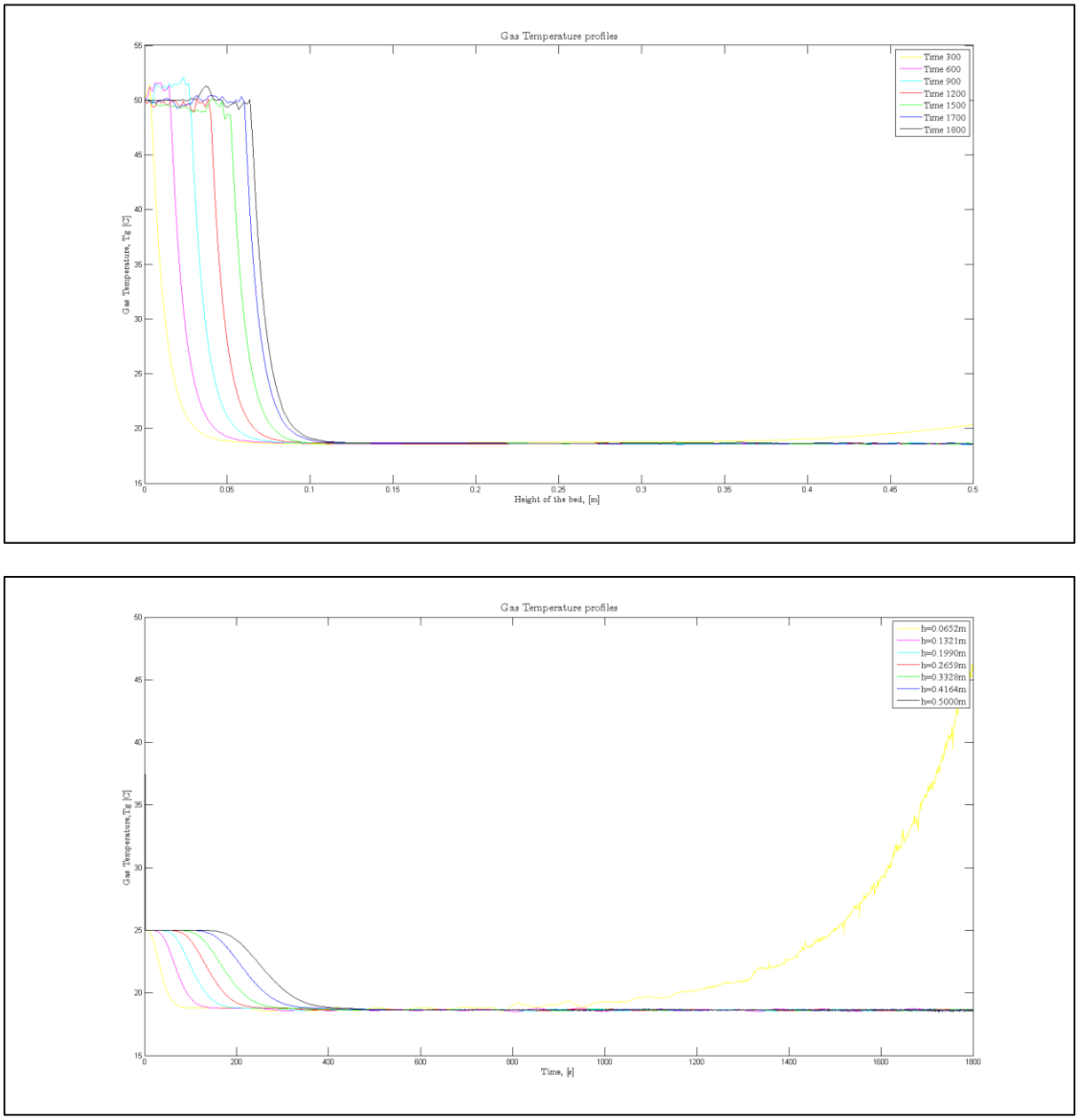

Figure 23: Gas Temperature Profiles versus height and time

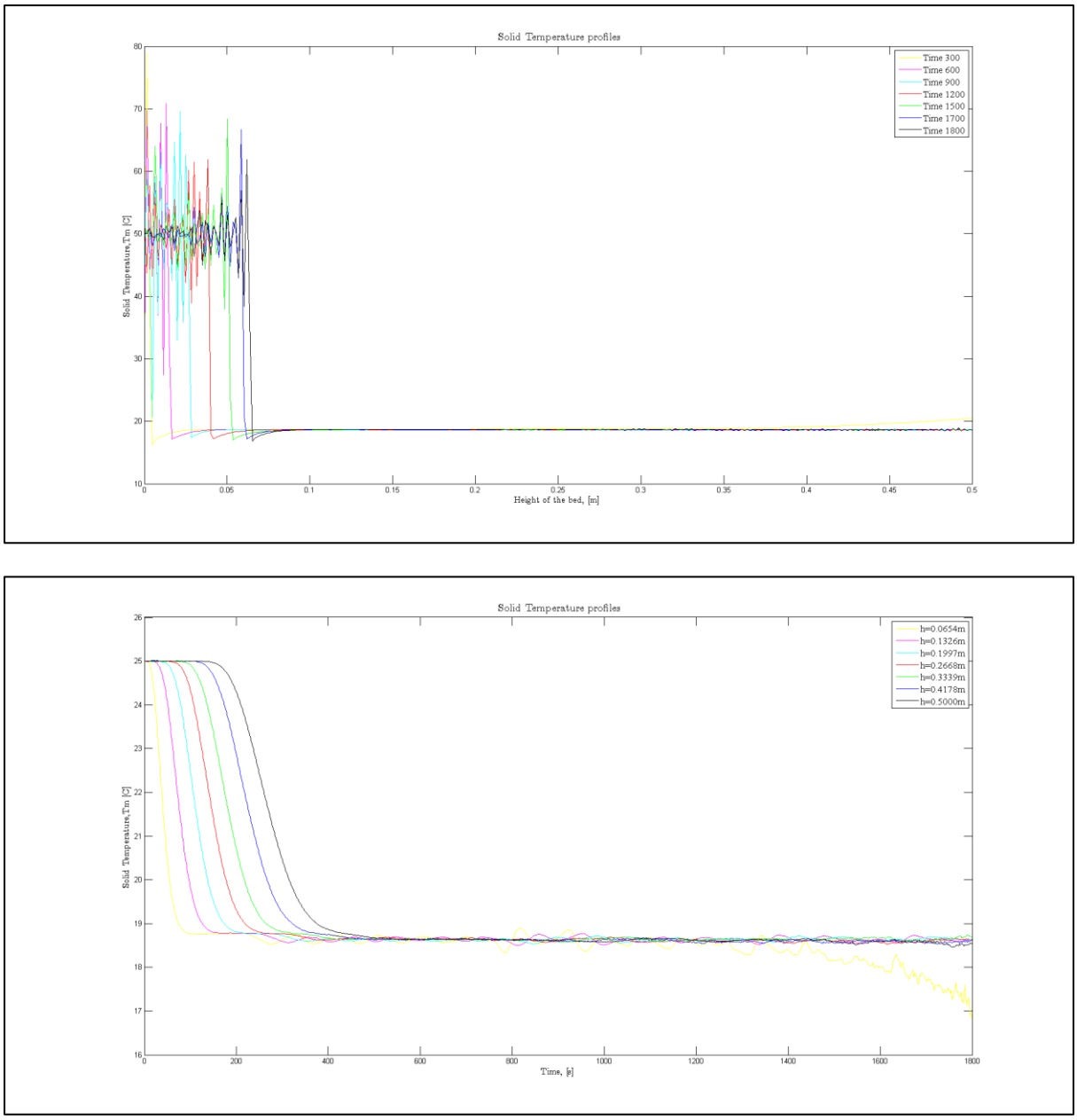

Figure 24: Solid Temperature profiles versus height and time

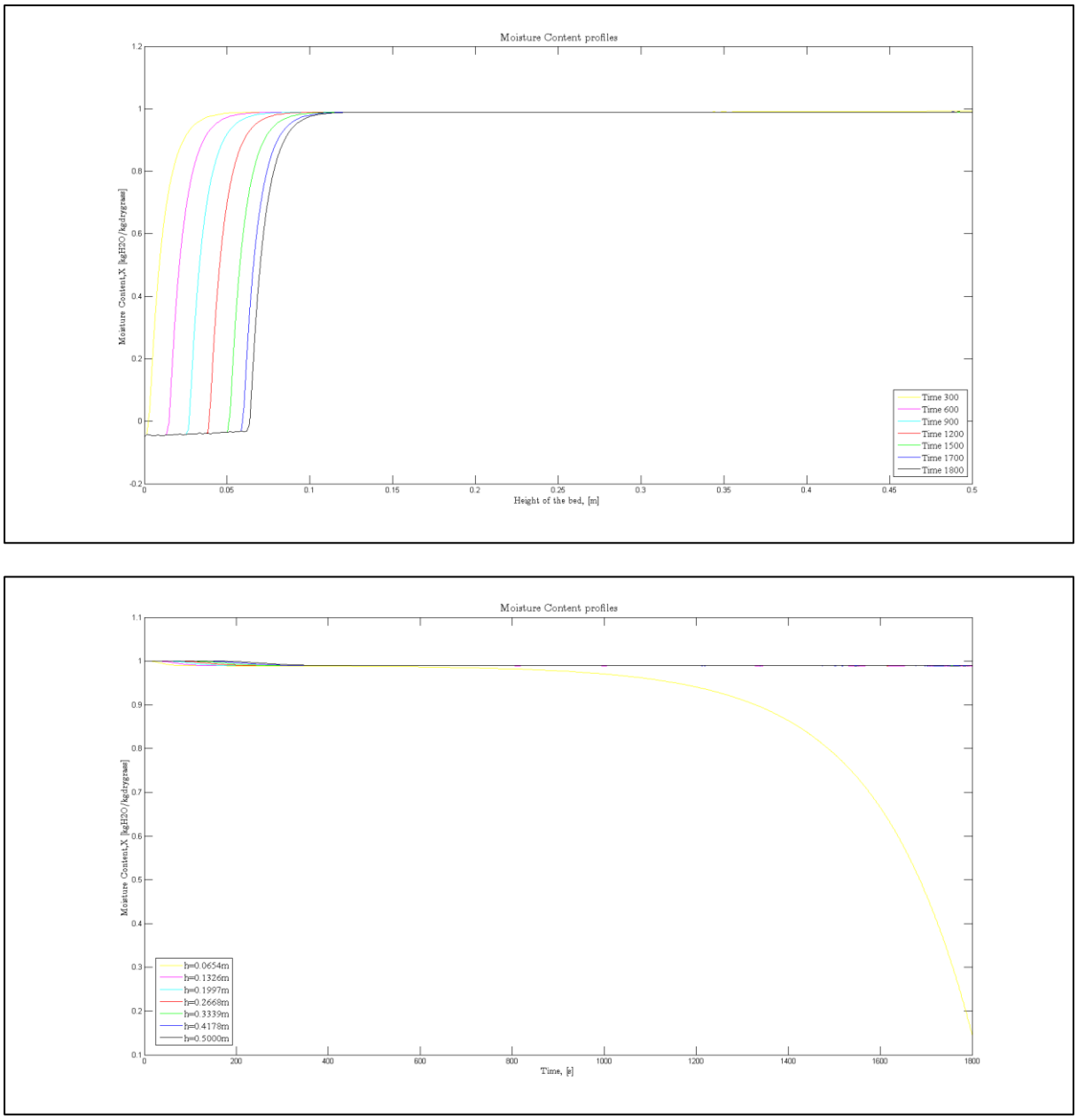

Figure 25: Moisture Content profiles versus height and time

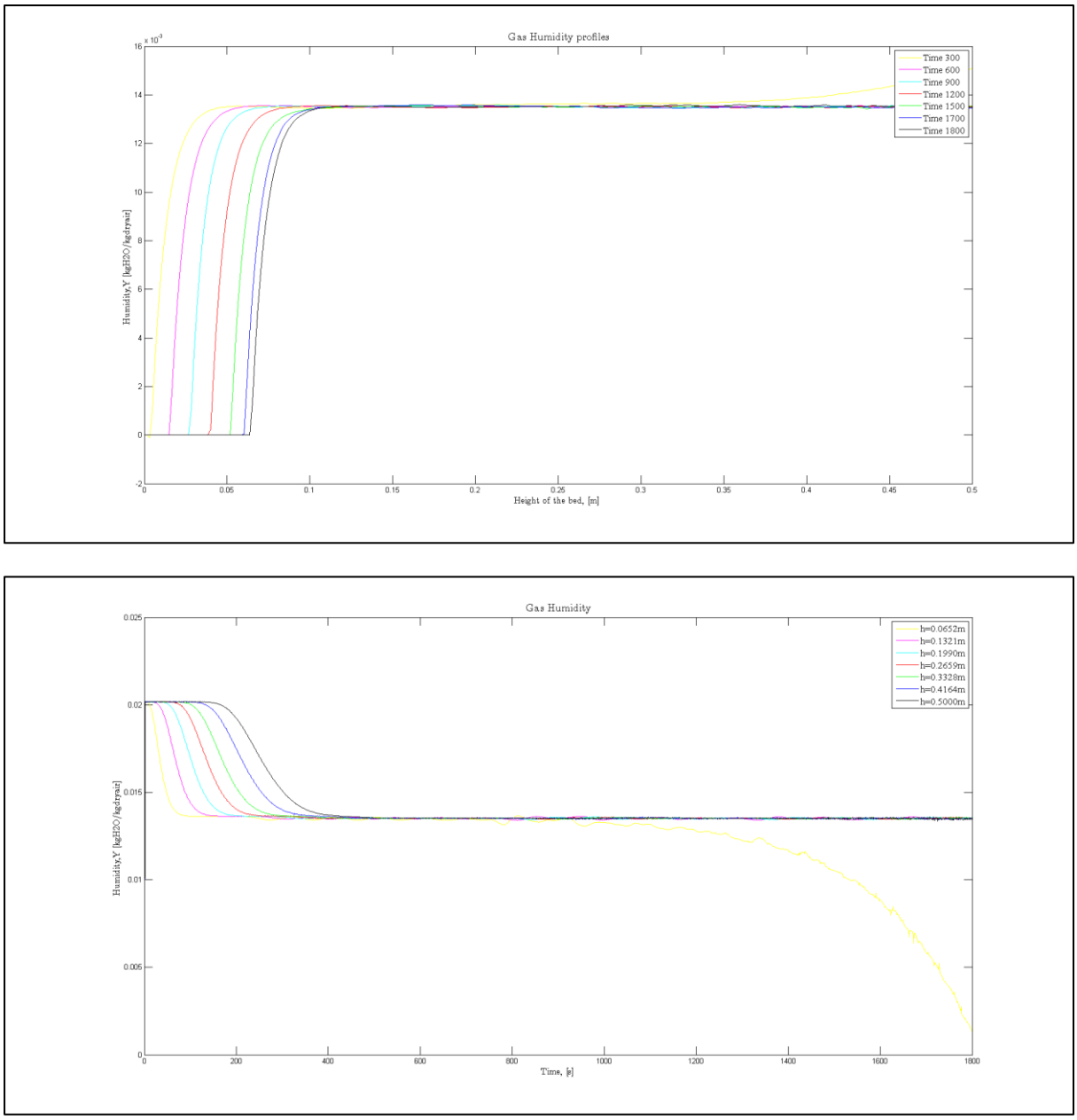

Figure 26: Gas Humidity profiles versus height and time

2) Flow rate = 30$\frac{Nl}{min}$, Tg = 50°C, Ns=500 and drying time = 45 minutes

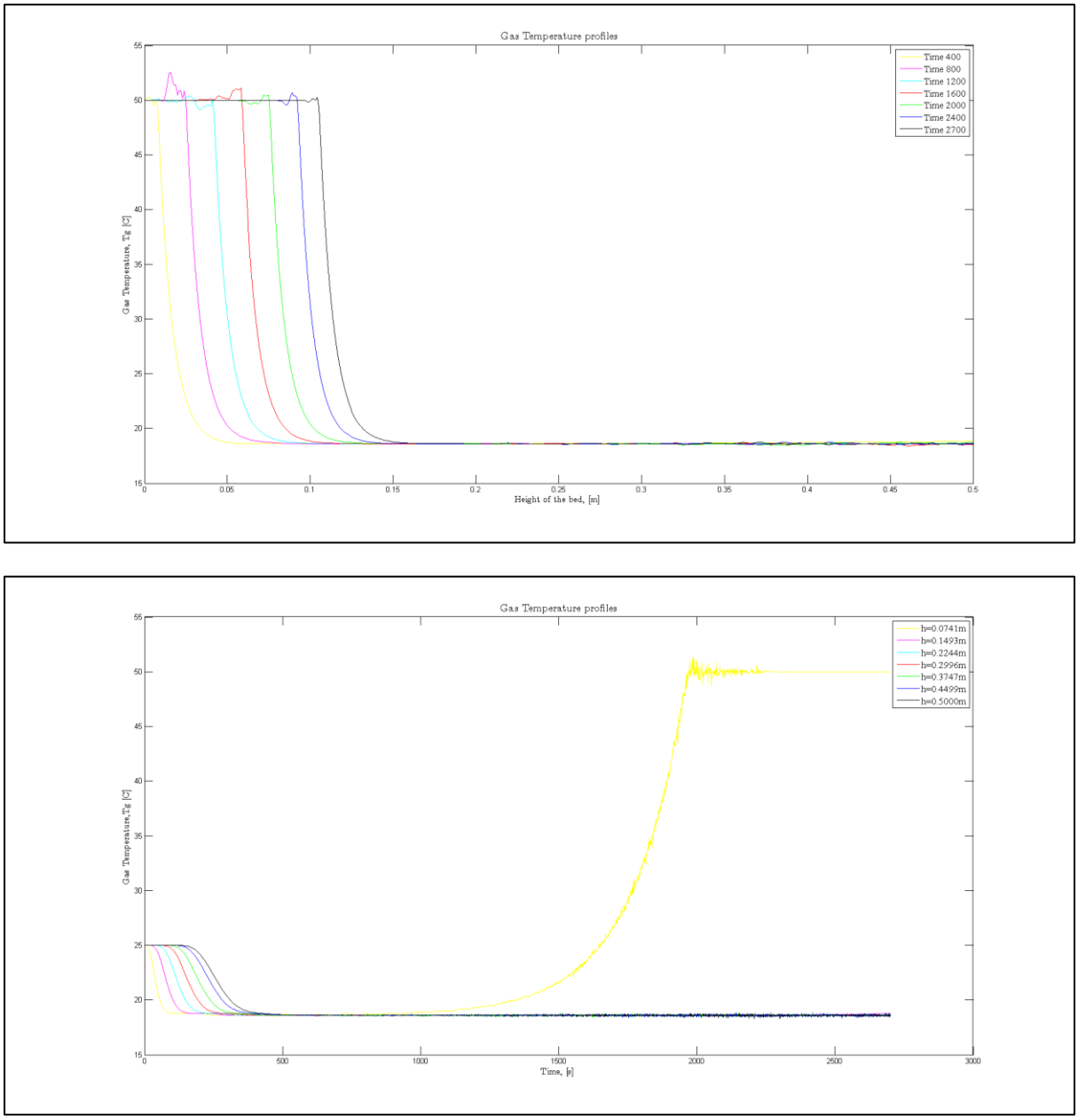

Figure 27: Gas Temperature Profiles versus height and time

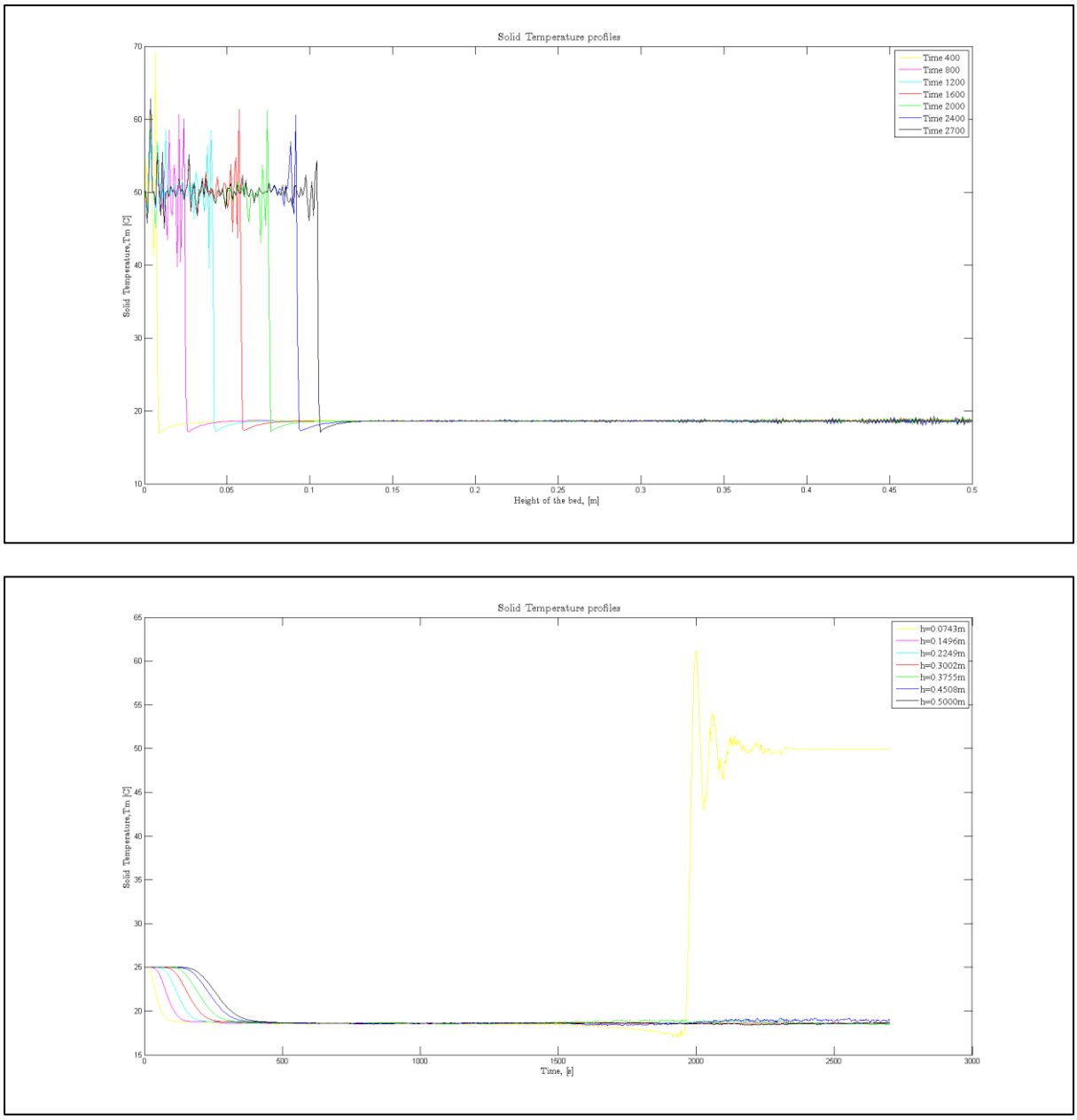

Figure 28: Solid Temperature Profiles versus height and time

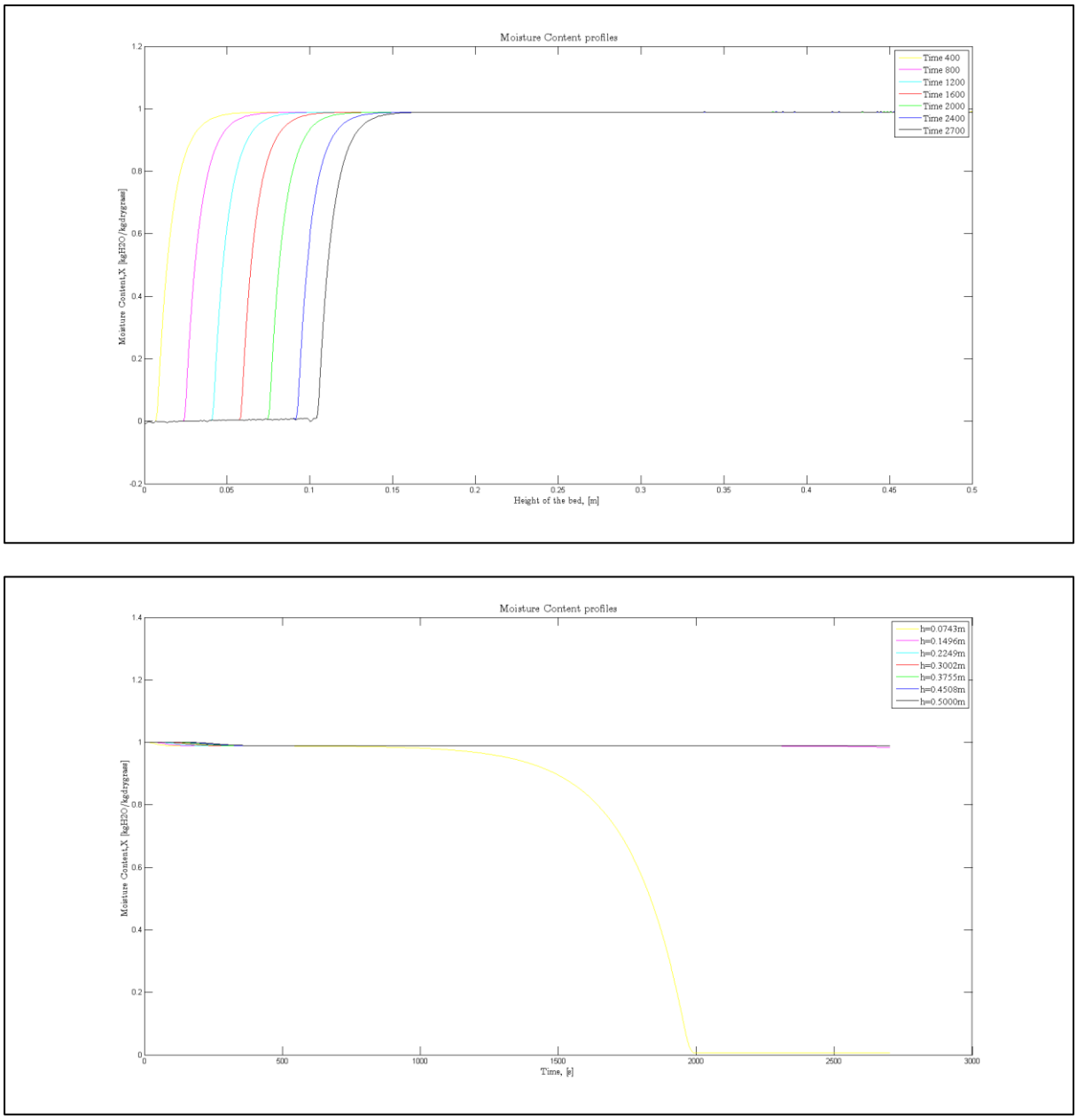

Figure 29: Moisture Content Profiles versus height and time

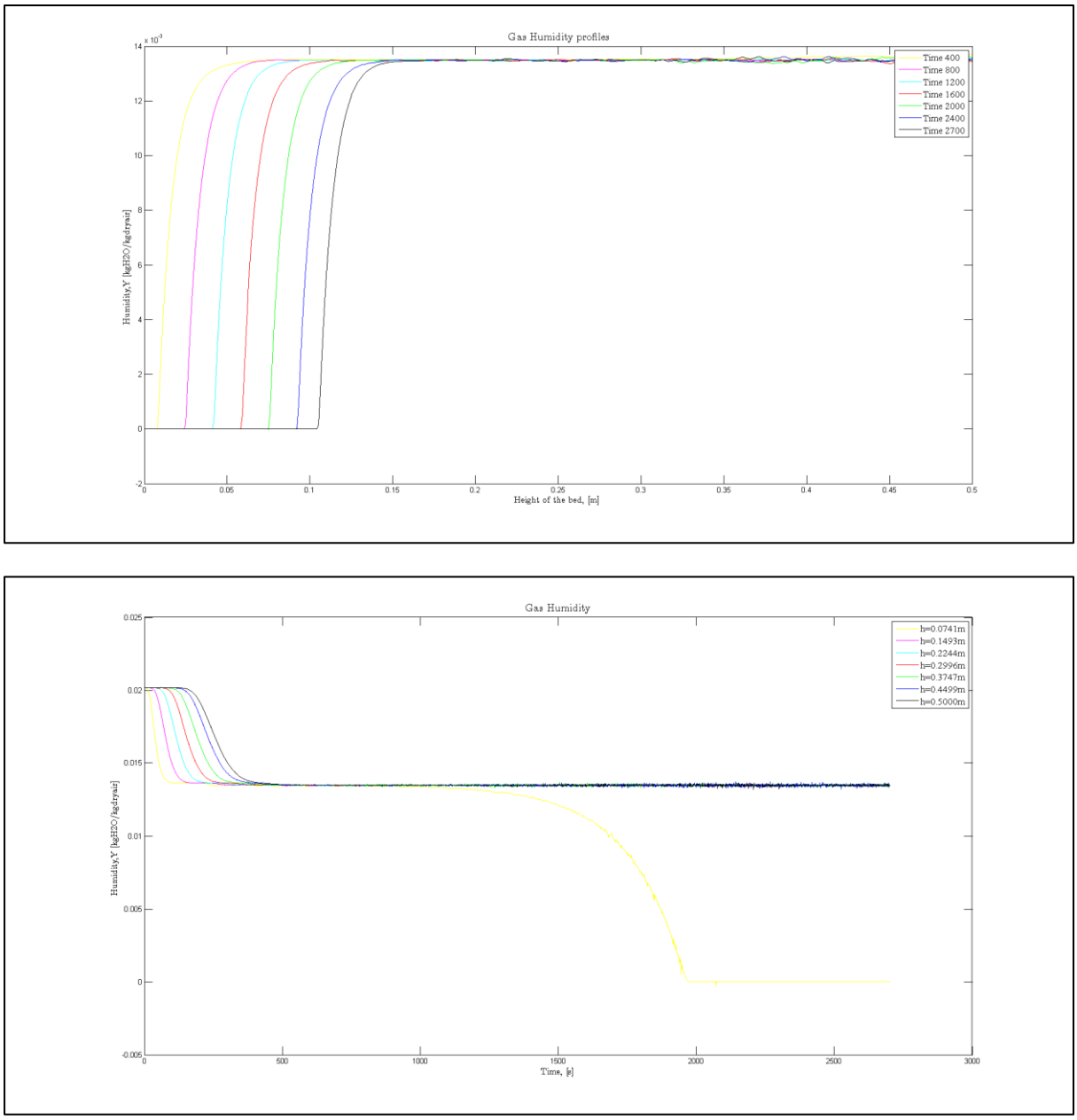

Figure 30: Gas Humidity Profiles versus height and time

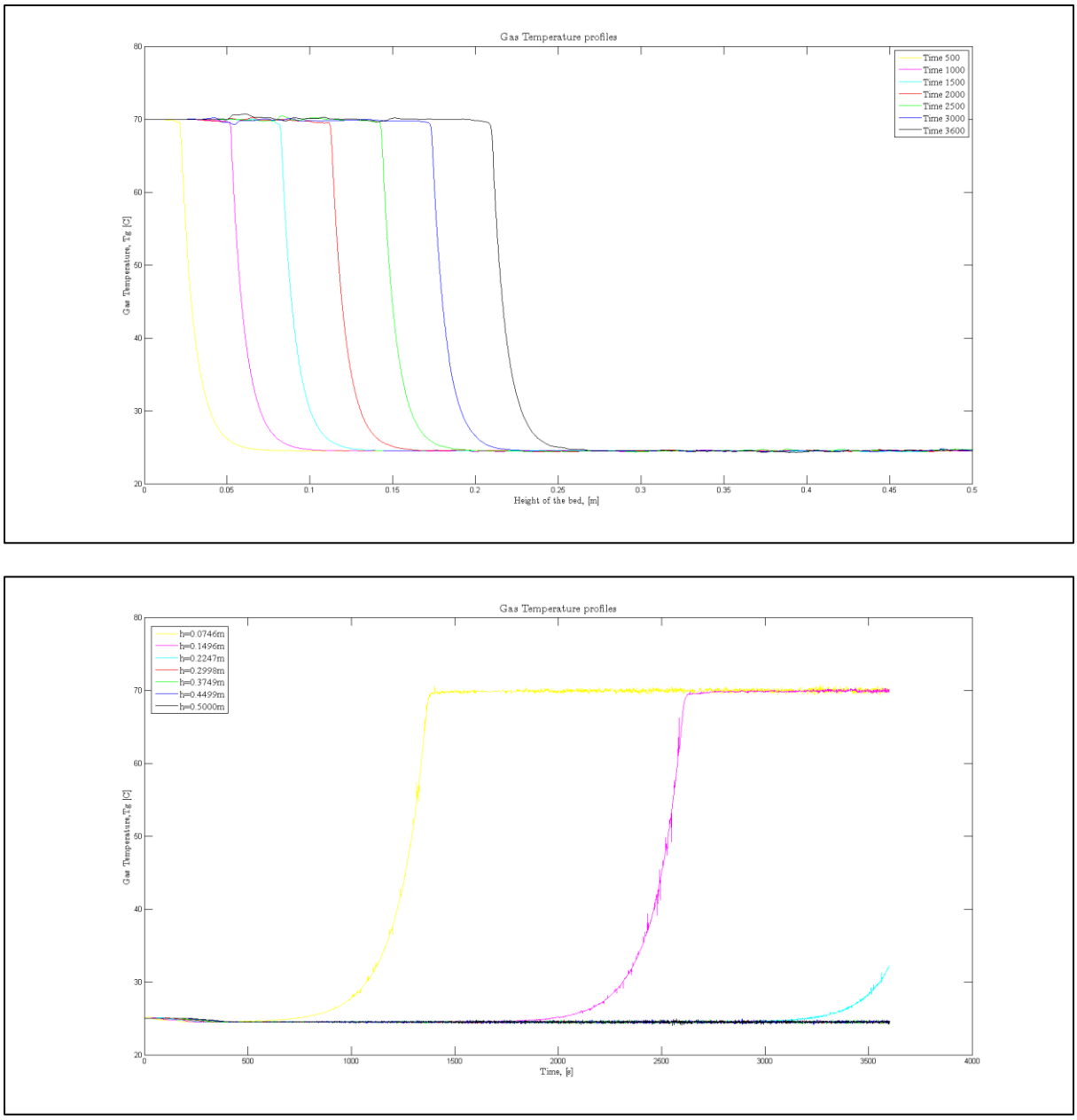

Figure 31: Gas Temperature Profiles versus height and time

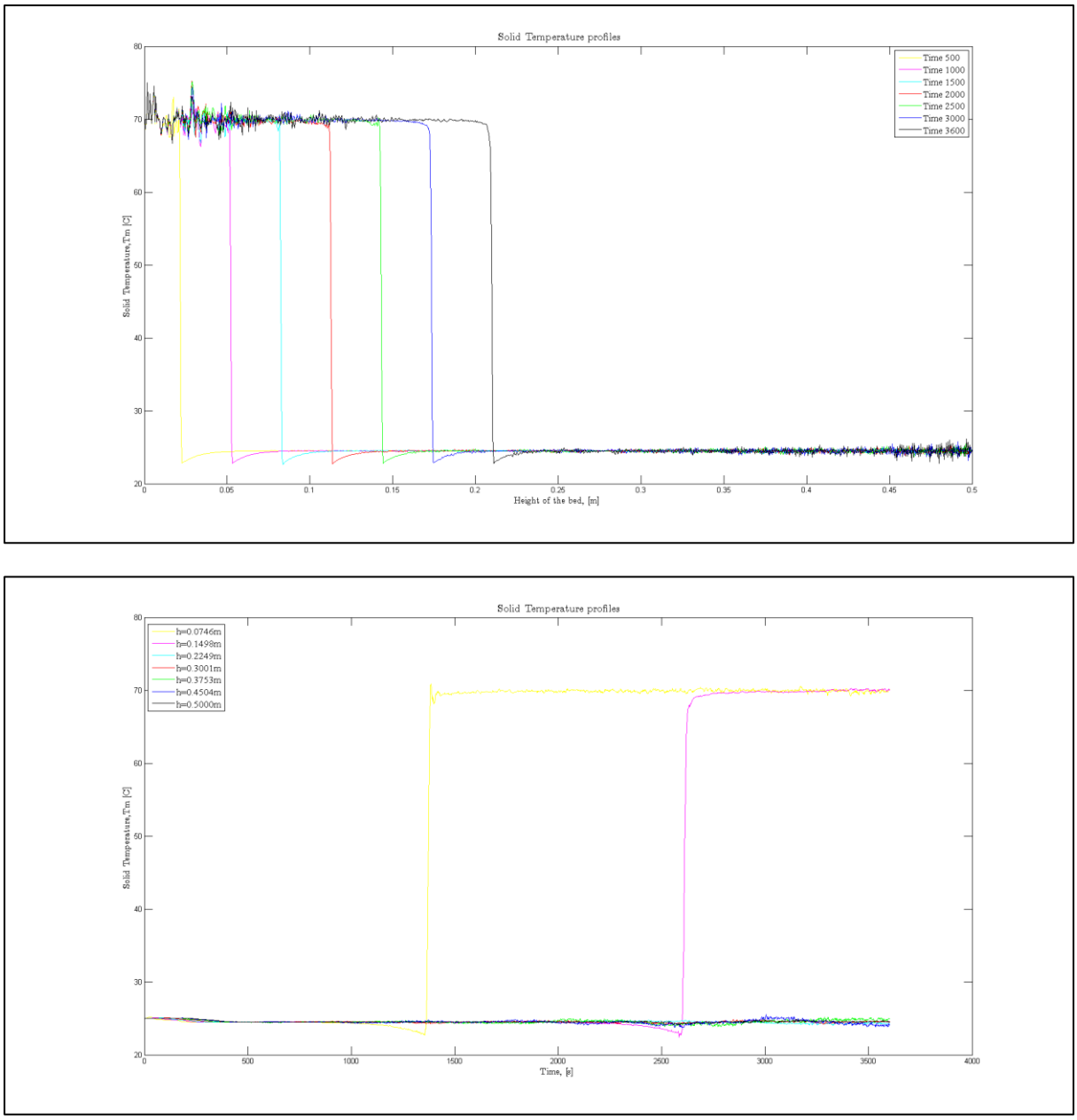

Figure 32: Solid Temperature Profiles versus height and time

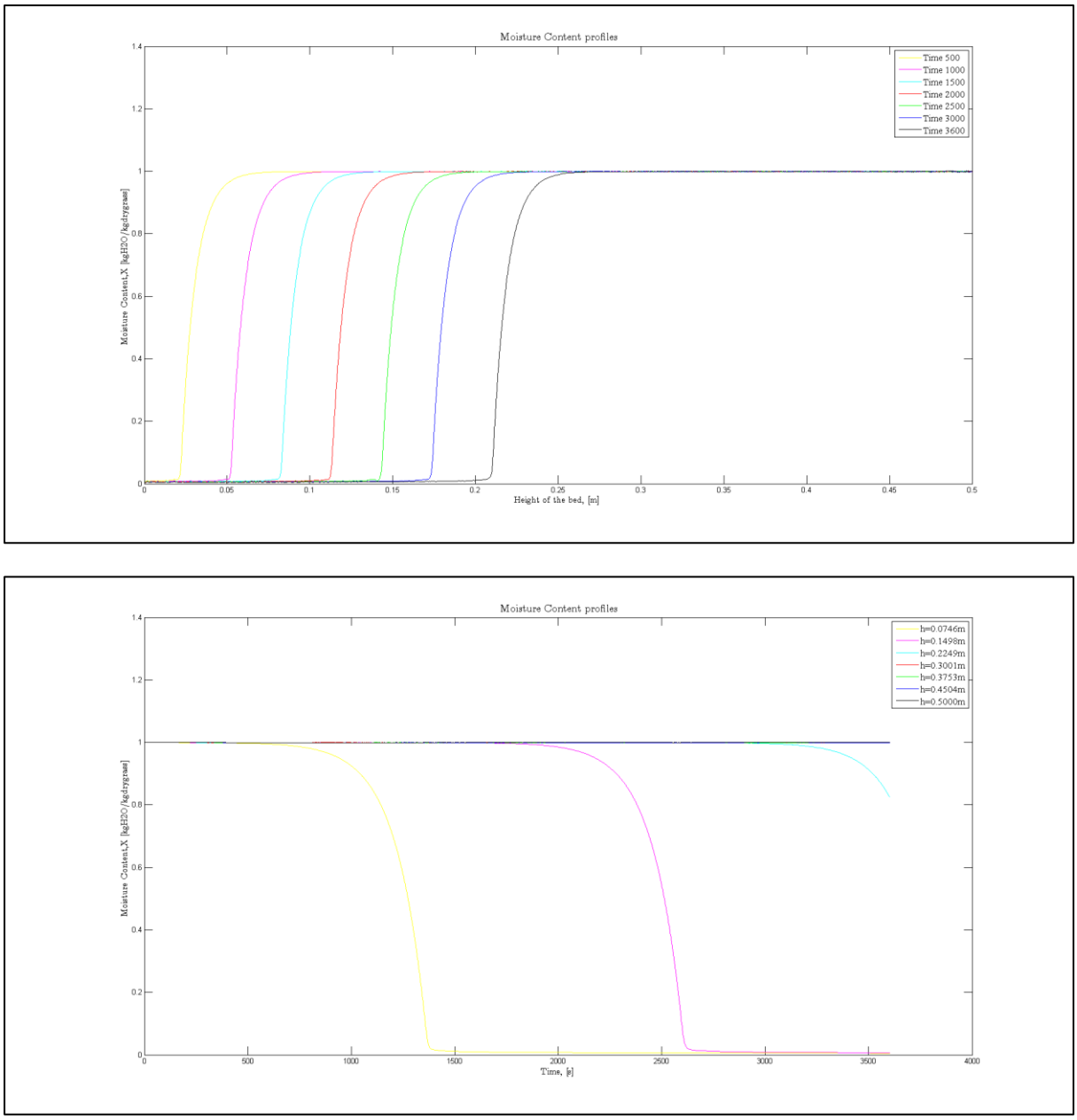

Figure 33: Moisture Content profiles versus height and time

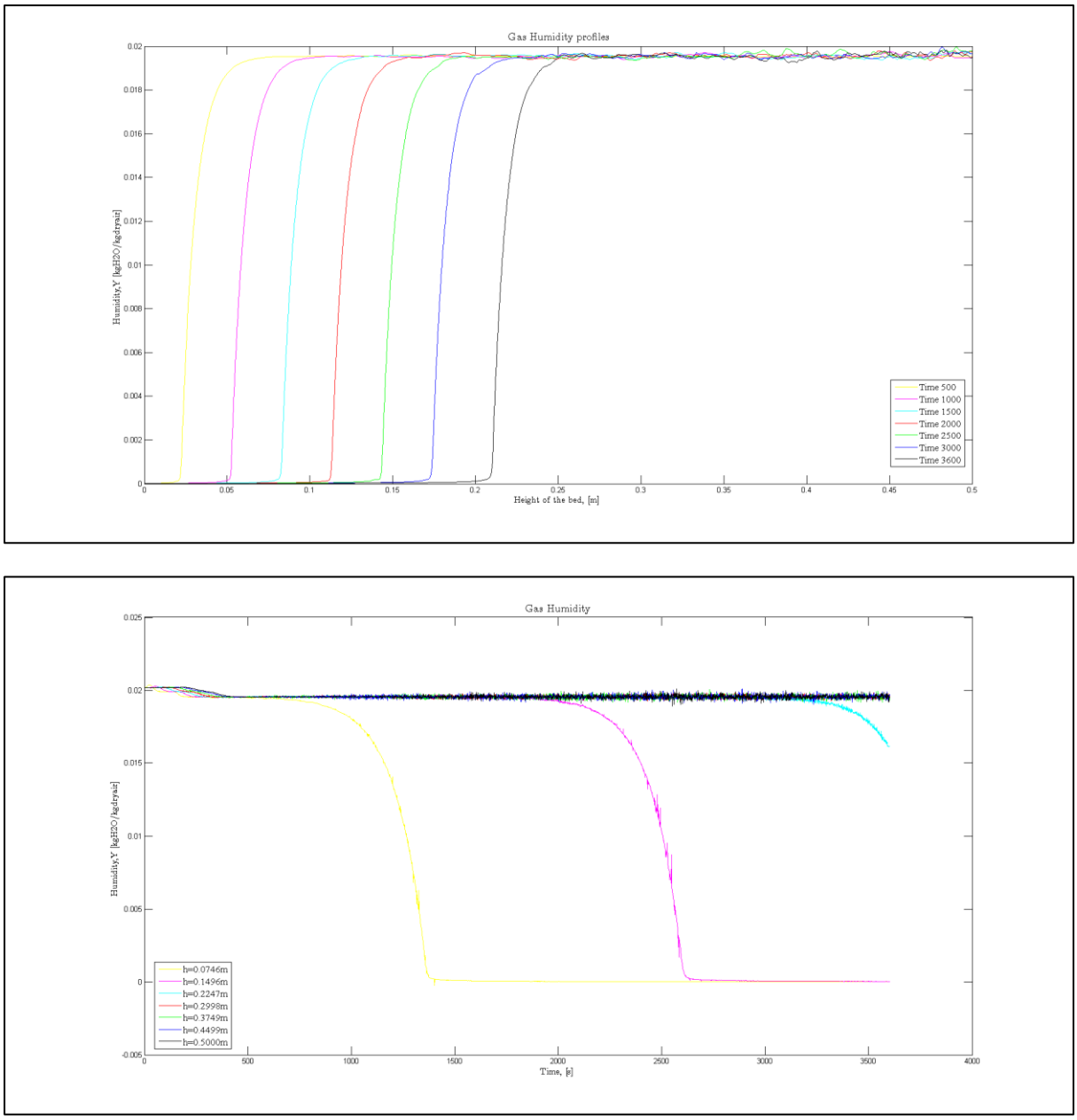

Figure 34: Gas Humidity Profiles versus height and time

3) Flow rate = 30$\frac{\boldsymbol{Nl}}{\boldsymbol{min}}$, Tg = 70℃, Ns=1000, ode23 and drying time = 60 minutes

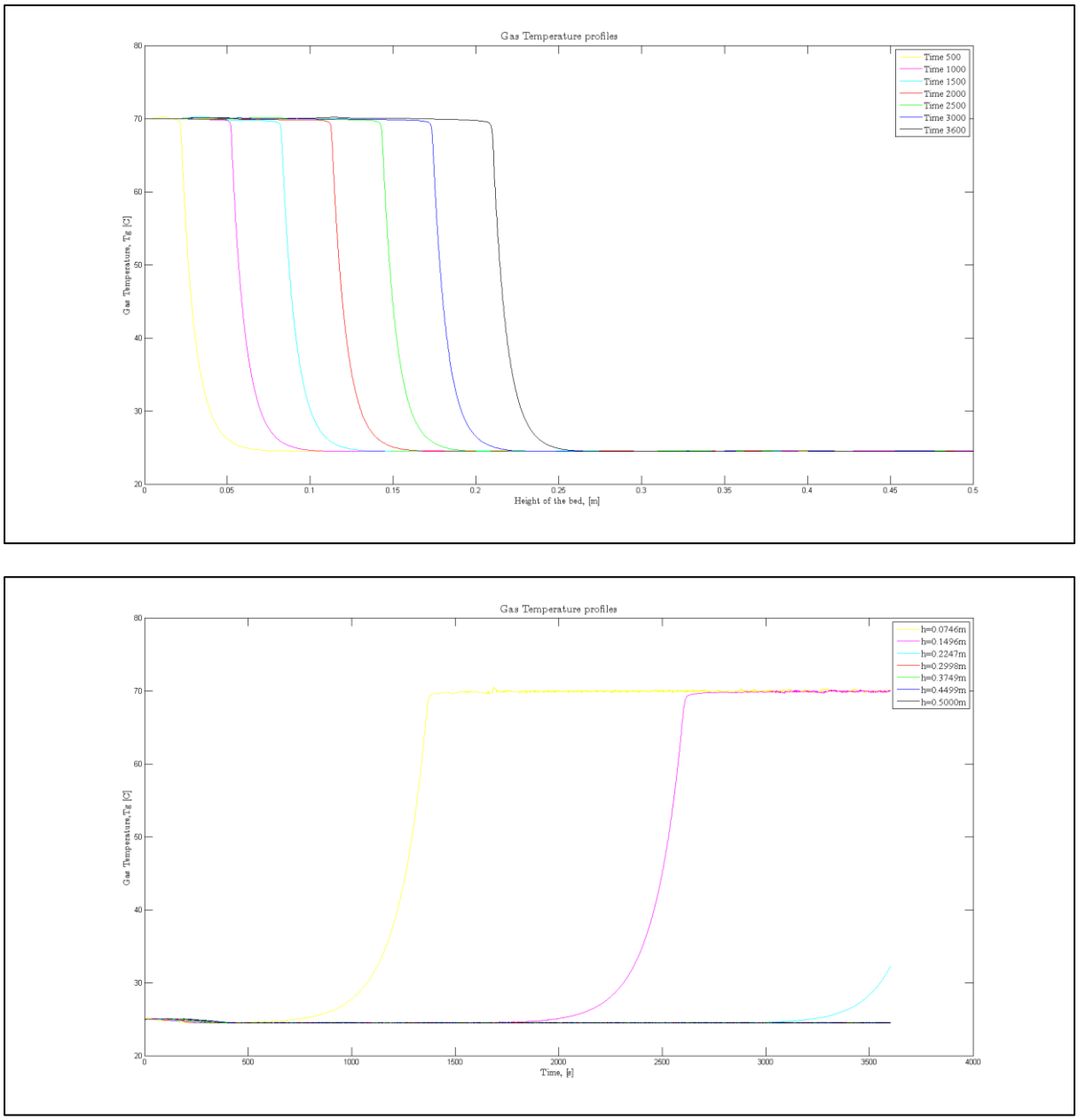

Figure 35: Gas Temperature Profiles versus height and time

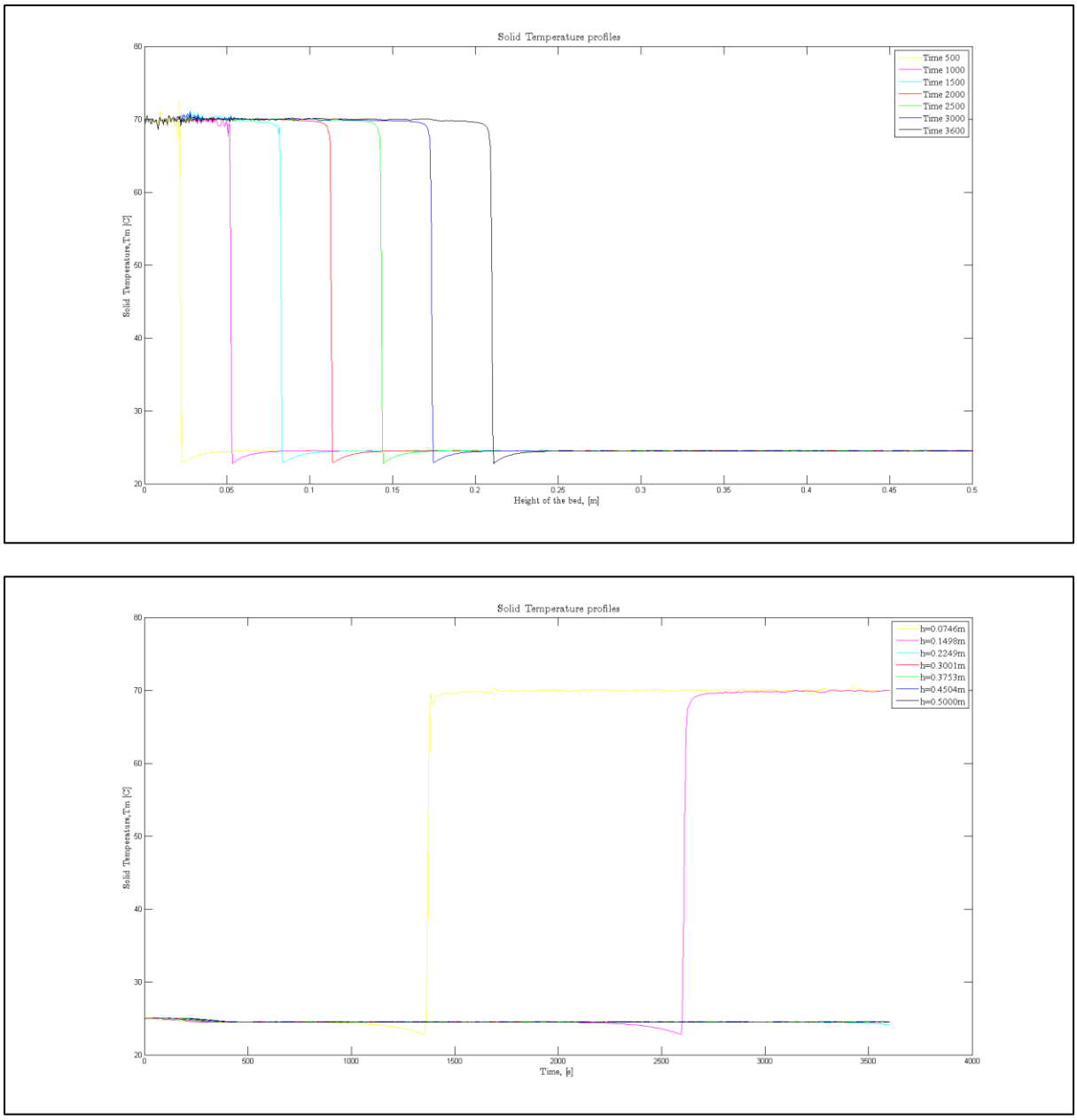

Figure 36: Solid Temperature Profiles versus height and time

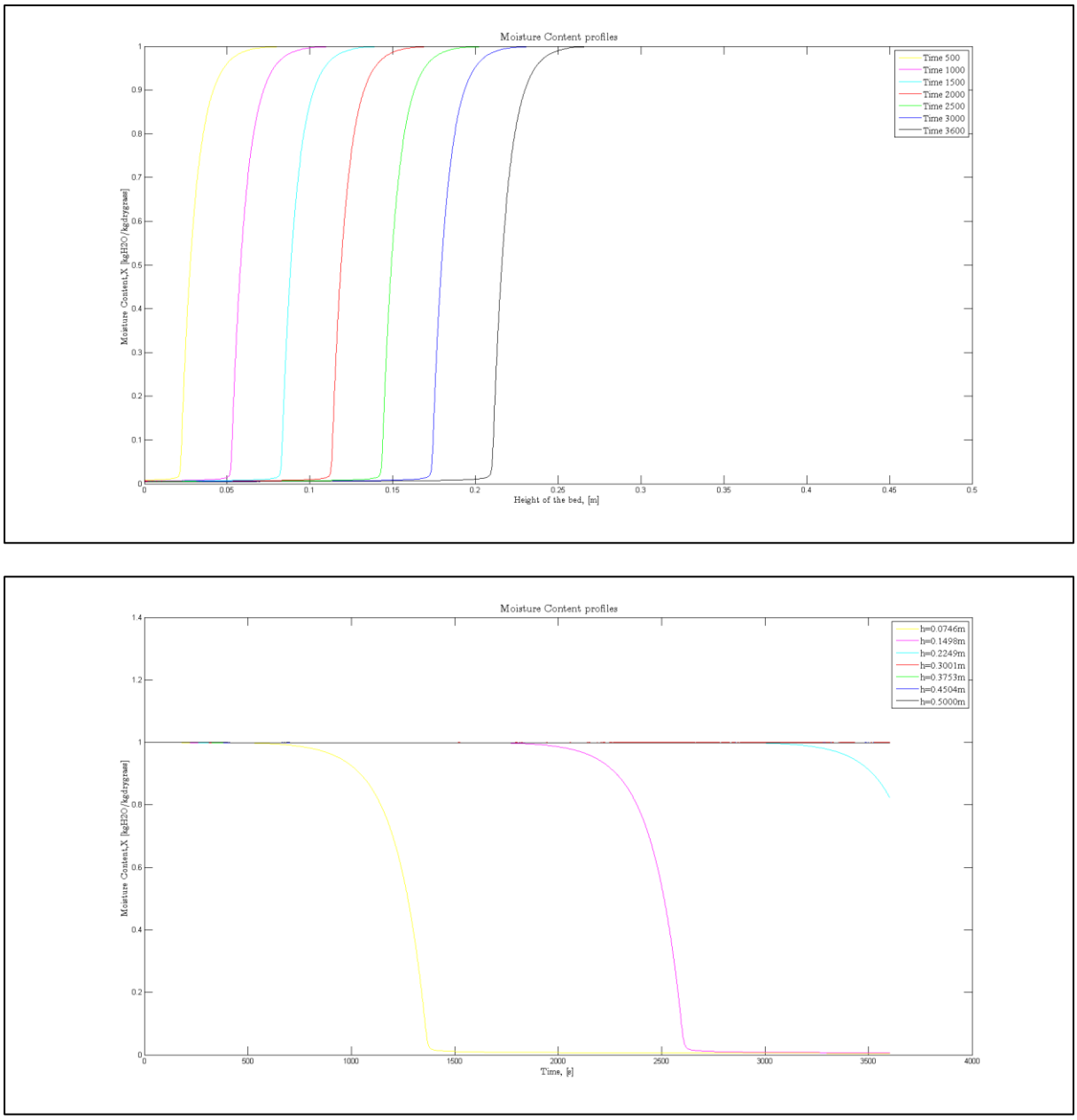

Figure 37: Moisture Content Profiles versus height and time

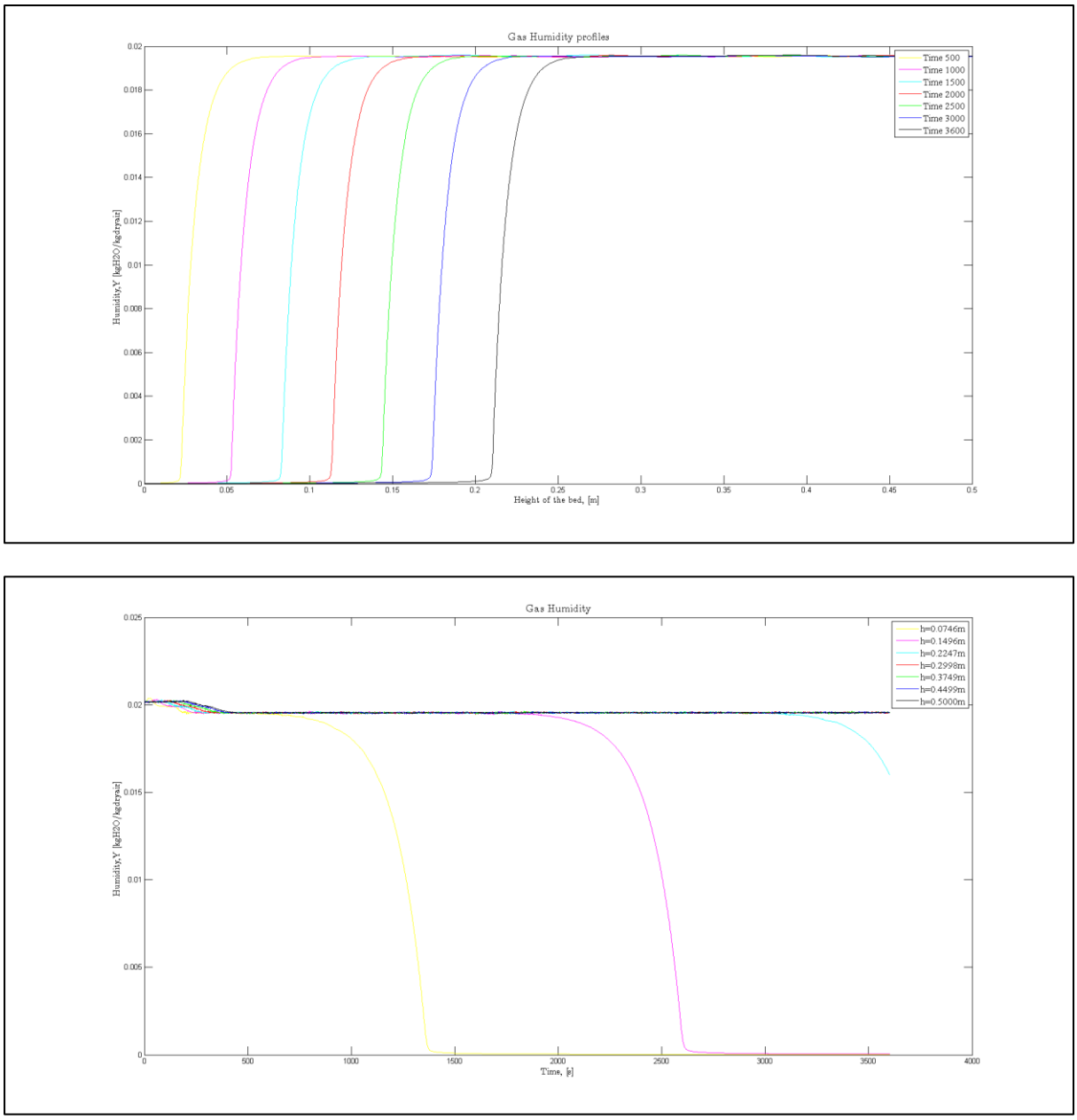

Figure 38: Gas Humidity Profiles versus height and time

4) Flow rate = 90$\frac{\boldsymbol{Nl}}{\boldsymbol{min}}$, Tg = 90℃, Ns=2500, ode23 and drying time = 60 minutes

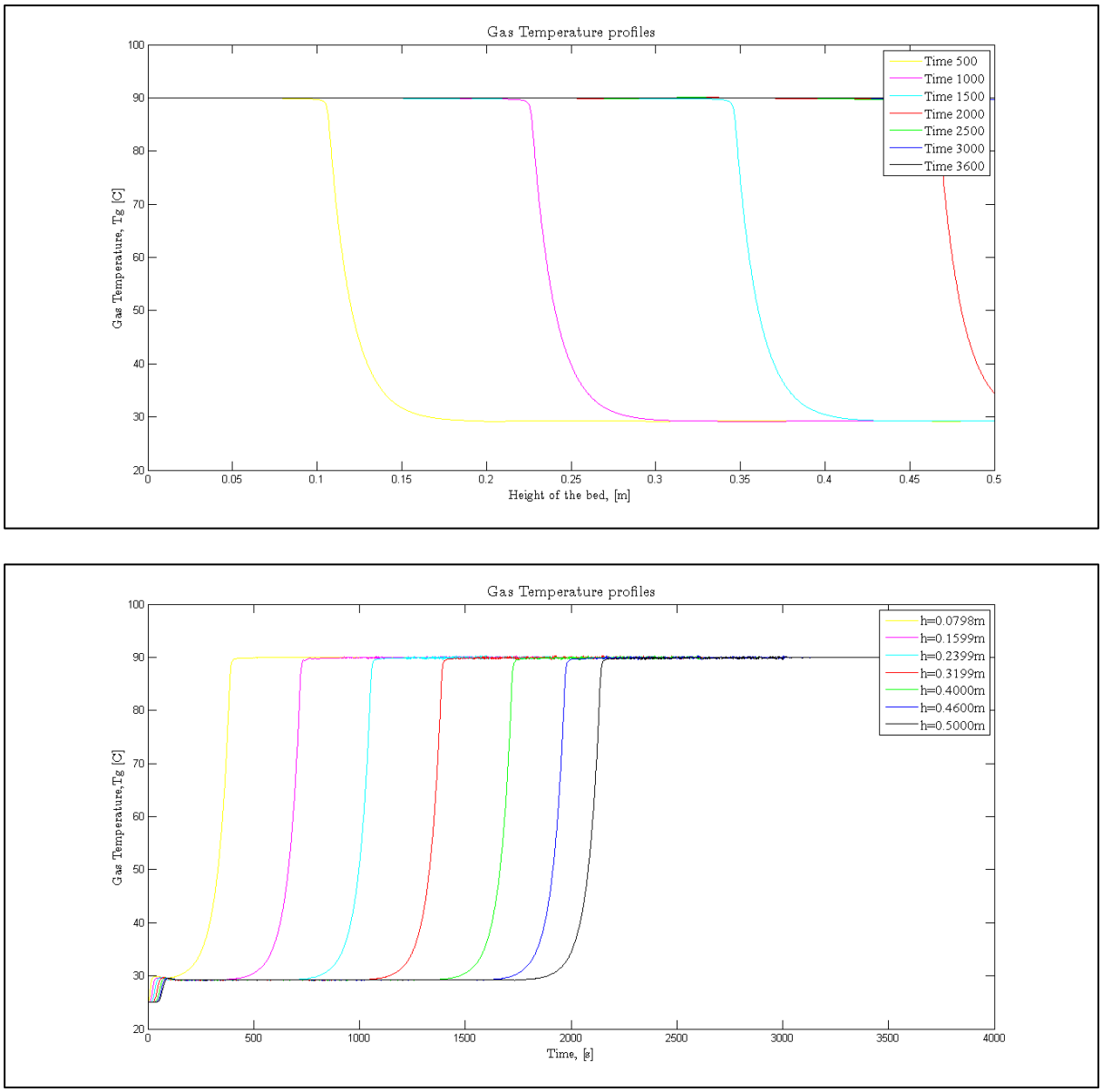

Figure 39: Gas Temperature Profiles versus height and time

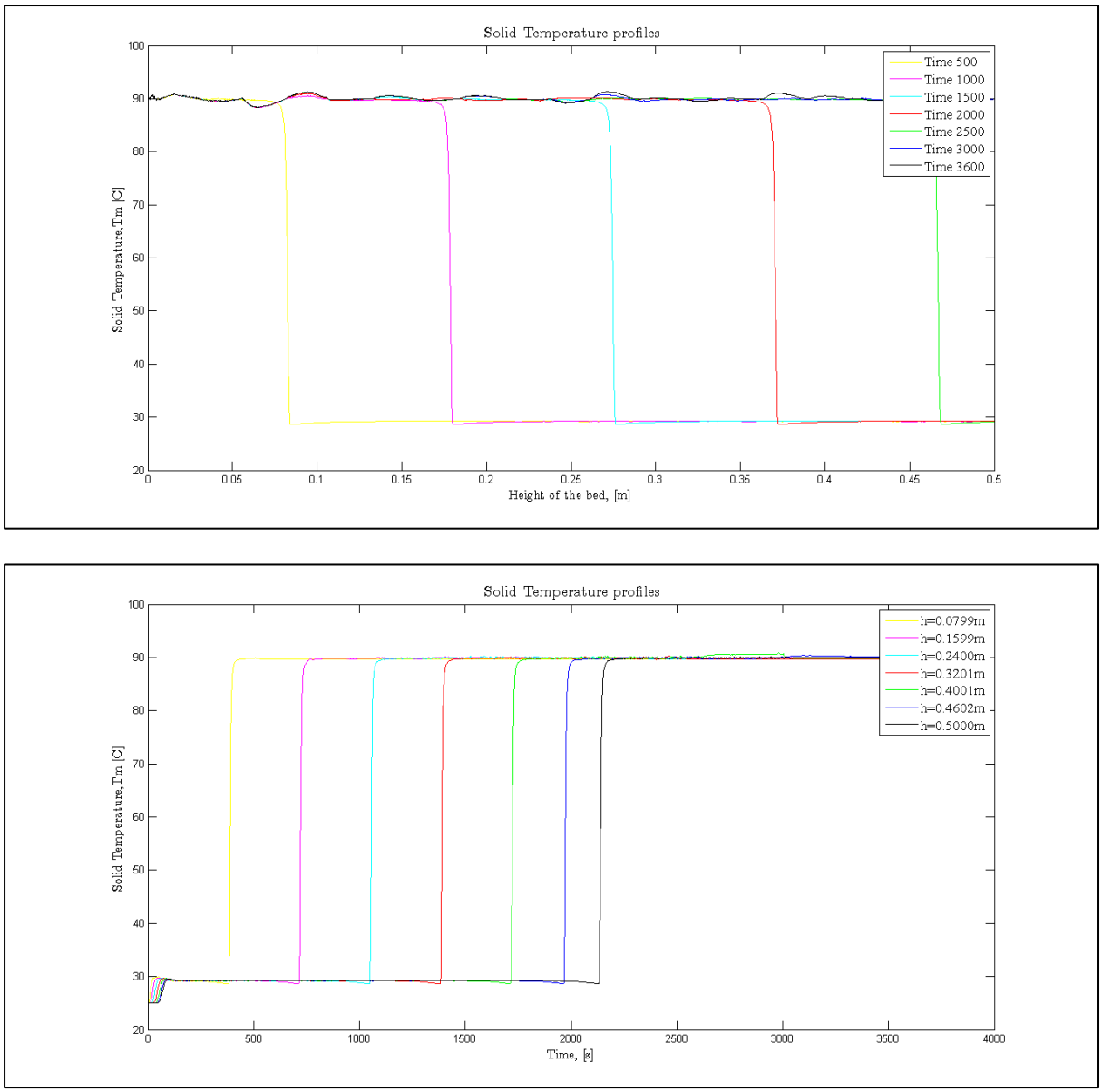

Figure 40: Solid Temperature Profiles versus height and time

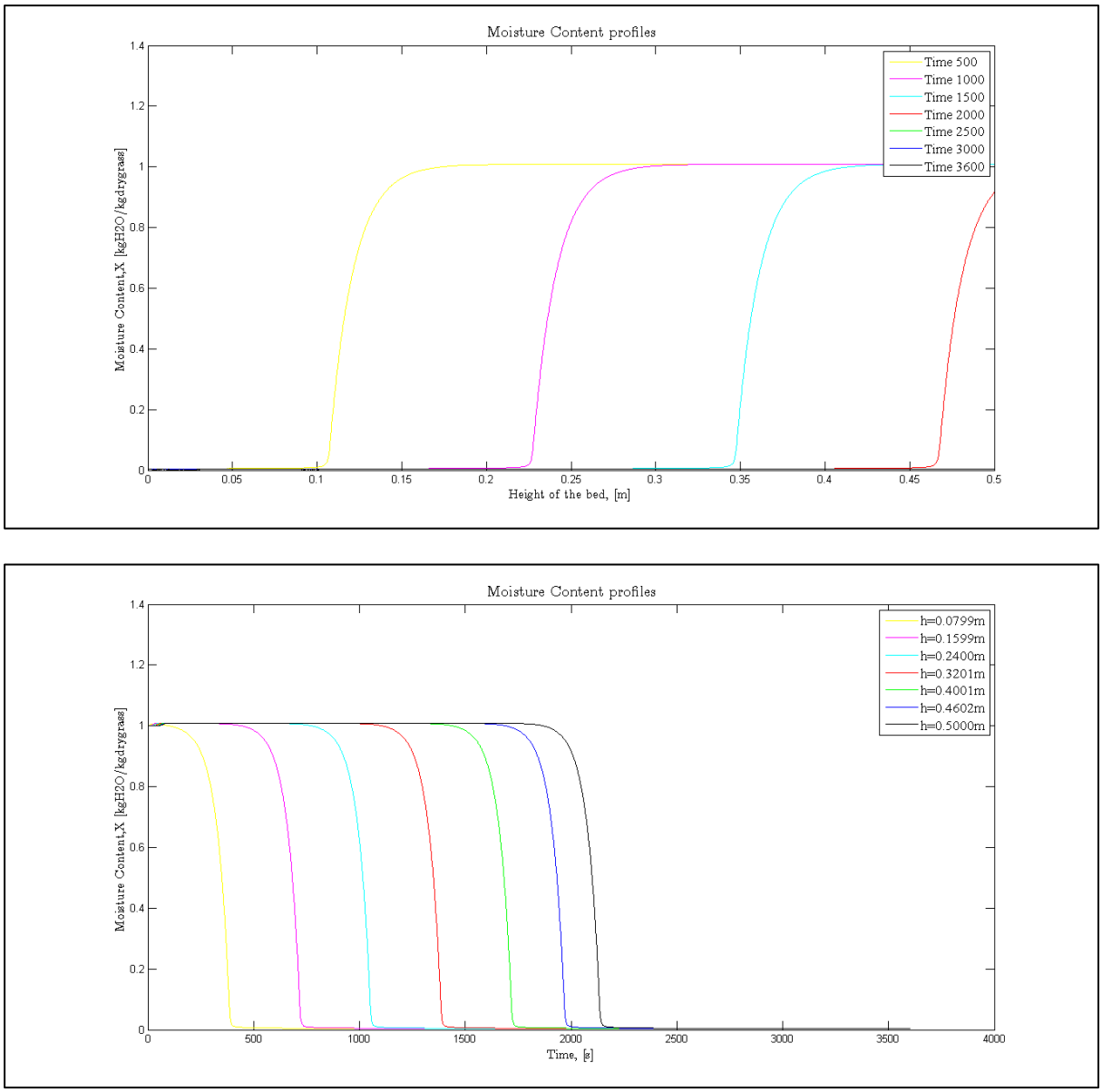

Figure 41: Moisture Content Profiles versus height and time

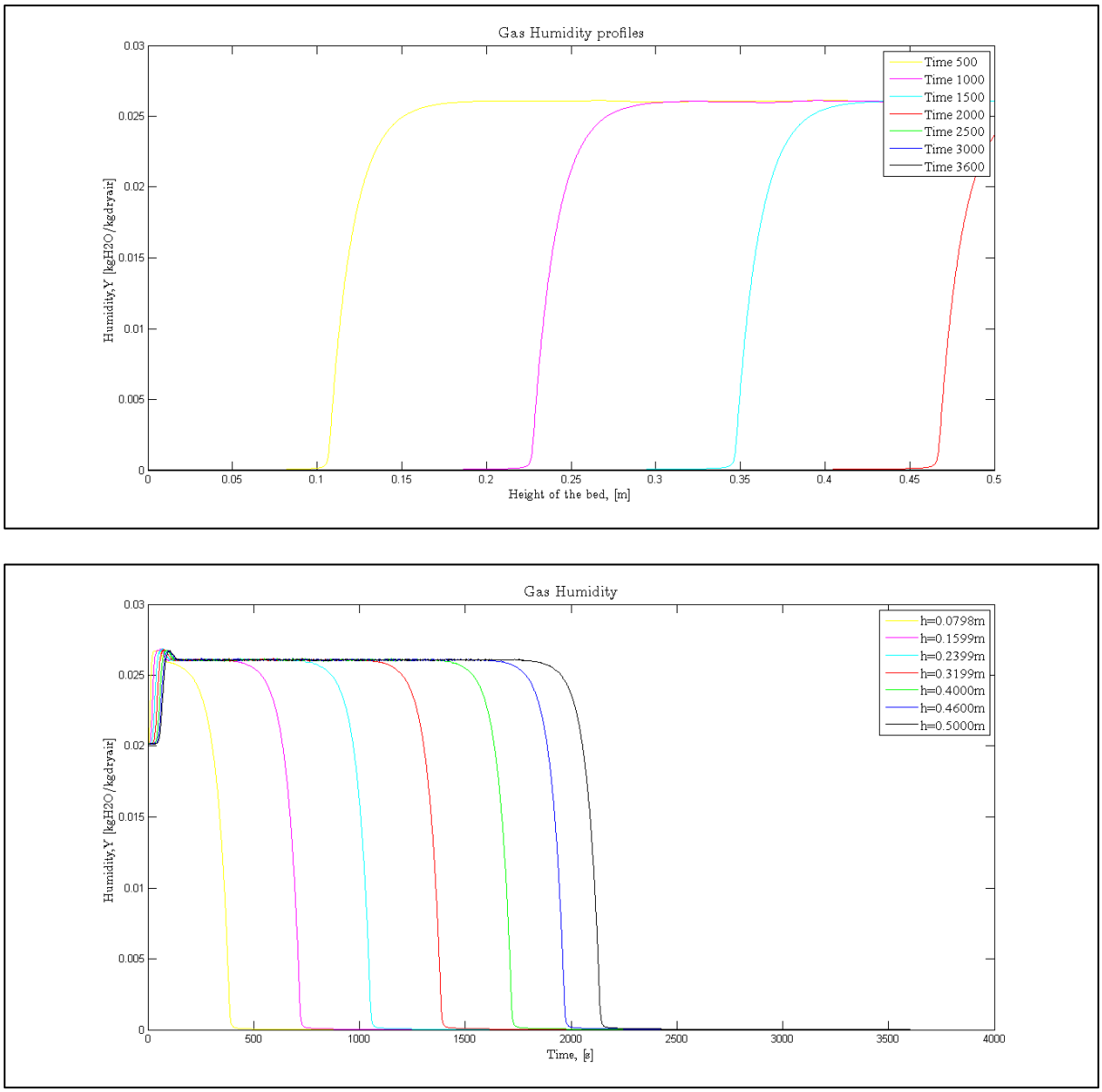

Figure 42: Gas Humidity Profiles versus height and time